TRIBOLOGICAL PERFORMANCE OF ADVANCED POLYMERIC COATINGS UNDER EXTREME OPERATING CONDITIONS

A Dissertation

by

PIXIANG LAN

Submitted to the Office of Graduate and Professional Studies of
Texas A&M University
in partial fulfillment of the requirements for the degree of

DOCTOR OF PHILOSOPHY

Chair of Committee,	Andreas A. Polycarpou
Committee Members,	Luis San Andrés
	Hong Liang
	Jonathan Felts
	Mohammad Naraghi
Head of Department,	Andreas A. Polycarpou

December 2017

Major Subject: Mechanical Engineering

ABSTRACT

Polymers and their composites have favorable tribological performance such as low coefficient of friction (COF) and good corrosion resistance, when working as bearing materials. The present work is studying the tribological performance of thin (~ 10s of microns) high-bearing polymeric coatings under extreme working conditions, including high temperature, cryogenic temperature, high contact pressure, high chamber pressure, starved lubrication, and abrasive wear. This work is an important contribution in proving the concept of application of thin polymeric coatings in environments such as dry sliding bearing, valve sealing surfaces, hydrodynamic bearings and drilling application under different extreme working conditions. Three groups of polymers, namely Polytetrafluoroethylene(PTFE)-based, Polyether ether ketone (PEEK)-based, and Aromatic Thermosetting coPolyesters(ATSP)-based coatings were extensively studied. Out of the three groups of polymers, ATSP-based coating showed the most desirable tribological performance: ‘zero wear’ at different temperature from -160°C to 260°C with dry sliding, extremely low wear coefficient (4.15×10^{-8} mm^3/Nm) under starved lubrication condition, stable coefficient of friction (COF) and low wear rate under sand abrasive condition, and extreme low COF for oil and gas drilling application.

Traditionally, the friction force between two solids is attributed to adhesion and deformation effects; where the adhesion force involves the shearing between the real

contact surfaces and deformation is due to the hard material's asperities plowing on the softer material. This work proposes a phenomenological model of friction for viscoelastic materials by using the viscosity and elasticity parameters acquired by nano-indentation measurements at elevated temperatures. Substituting the viscosity and elastic modulus terms, the model showed reasonable COF for the coatings up to temperatures that were lower than the glass transition temperature.

ACKNOWLEDGEMENTS

I would like to thank my committee chair, Dr. Andreas A. Polycarpou, for his patient and professional guidance. And I also would like to thank my committee members, Dr. Luis San Andrés, Dr. Hong Liang, Dr. Jonathan Felts and Dr. Mohammad Naraghi, for their help and support throughout this research.

Thanks also go to my friends and colleagues and the department faculty and staff for making my time at Texas A&M University a great experience.

Finally, thanks to my father and my wife for their encouragement; and thanks to my lovely daughter for her company.

CONTRIBUTORS AND FUNDING SOURCES

Contributors

Part 1, faculty committee recognition

This work was supervised by a dissertation committee consisting of Professor Andreas Polycarpou, Luis San Andrés, Hong Liang and Jonathan Felts of the Department of Mechanical Engineering and Professor Mohammad Naraghi of the Department of Aerospace Engineering.

Part 2, student/collaborator contributions

The EDS analysis depicted in Chapter 5 was conducted by Dr. Kyriaki Polychronopoulou, a visiting professor of the Department of Mechanical Engineering.

All other work conducted for the dissertation was completed by the student.

Funding Sources

This work was made possible in part by the Turbomachinery Research Consortium at Texas A&M University under Grant Number 1519x6; and by ExxonMobil Chemical Company, Global R&D, Baytown, Texas, USA, under Grant Number 28-406950-00001.

TABLE OF CONTENTS

Page

LIST OF FIGURES

Page

LIST OF TABLES

Page

1. INTRODUCTION

Recently, applications of polymers for tribological purposes are increasing. Much research has been carried out on the tribology of polymers and their application in various industries [1, 2]. Understanding the tribological performance of the polymers is crucial for their successful applications. The tribology of polymers is very complicated: friction is affected by load, sliding velocity and temperature; wear can arise from abrasion, adhesion and fatigue [3]. Other environmental conditions such as lubricant, environmental composition, surface roughness, and abrasive particles can also affect the tribological performance [4-8]. Thus, it is hard to predict the tribological performance based on simple models, and it is wise to carry out laboratory experimental work which could simulate the actual working conditions before deployed in the field. That is why tribology is largely depending on experimental research.

1.1 Tribology of polymers

Tribology is the science that deals with friction, wear and lubrication of interacting surfaces in relative motion. The friction force between two solids is usually attributed to adhesion and deformation effects; where the adhesion force involves the shearing between the real contact surfaces and deformation is due to the hard material's asperities plowing on the softer material. Due to their low surface energy[3], low shear strength [9] and low elastic modulus [10], polymers usually have low COF when they

are used for tribological applications. Polymers have viscoelasticity, which are time and temperature dependent mechanical parameters. Specifically, the temperature is the flash temperature at the contact area and this flash temperature is related with normal load, sliding speed and the body temperature of the two contacting parts. Thus, the friction of polymers is largely affected by load, sliding velocity, and temperature [3].

The wear of the polymers is attributed to abrasion, adhesion and fatigue. The abrasive wear on the polymers surface occurs due to the asperities of the counter surface, the contaminant abrasive particles and also from the polymeric debris that slid on the counter surface; the hardness of the polymer debris could be increased in the sliding process as a result of repeated plastic deformation, and then the polymeric debris could act as an abrasive particle itself [11, 12]. Adhesive wear is caused by the shearing at the real contact area where the joints break with removal of material due to adhesive forces. Cyclic loads (normal force and friction force) placed on the polymer can cause fatigue of the coating followed by nucleation and propagation of micro-cracks [13], resulting in fatigue wear.

Transfer layers are usually formed on the metal surface when polymers slide against metal [14]. Transfer films develop because of adhesion and interlocking of the fragments of material into metal asperities [15]. The transfer film affects the wear performance: transfer film is responsible for the gradual transition from a transient wear behavior to steady state wear behavior; wear occurs by the loss of material before transfer to the counter surface and the loss of transfer film by peeling from the counter

surface [3, 15, 16]. From a qualitative standpoint, sliding conditions such as velocity, load, atmosphere, and temperature are expected to affect the transfer film formation and destruction [15]. Polycarpou and coworkers found that the surface condition of the counter surface would affect the formation of the transfer layer [17], and with the addition of liquid lubricant, it would wash away the polymer wear debris and hinder the formation of the transfer layer on the metal counter surface [18].

1.2 Bulk polymers and their composites

In general, polymers are in bulk form or coating format when they are used for tribological applications. Polymers in bulk format have been widely used, such as the top layer for thrust tilting pad bearings, washers, bushing and so forth. Usually, polymers in pure form (referred to as unfilled polymers) may have high COF, high wear rate and poor mechanical properties, so they do not satisfy the tribologcial application needs. Thus researchers have great interest in producing composites or blended polymers by adding different fillers and reinforcements in the polymers [12, 14, 17, 19-24], improving significantly their mechanical, thermal or tribological properties. Take compressor industry for example: different polymers in bulk format were employed as potential compressor bearing materials [14, 22, 23]. In reference [23] four unfilled polymers and six blended polymers were tested using pin-on-disk configuration, simulating realistic air conditioning compressor conditions: dry sliding, 2.4 m/s sliding speed; 0.14 MPa nominal constant pressure for the unfilled materials, and 7.0 MPa

constant pressure for the blended materials; and 0.172 MPa refrigerant chamber pressure. Under the same experimental conditions in reference [23], reference [14, 22] explored blends of ATSP with PTFE with different weight ratios of 75/25 (C1), 50/50 (C2), 25/75 (C3), and also pure ATSP and pure PTFE. Among the polymers tested in [14, 22, 23], unfilled polymers have much higher wear rates; all other nine filled polymers' wear rates and coefficient of friction (COF) are summarized in **Figure 1**.

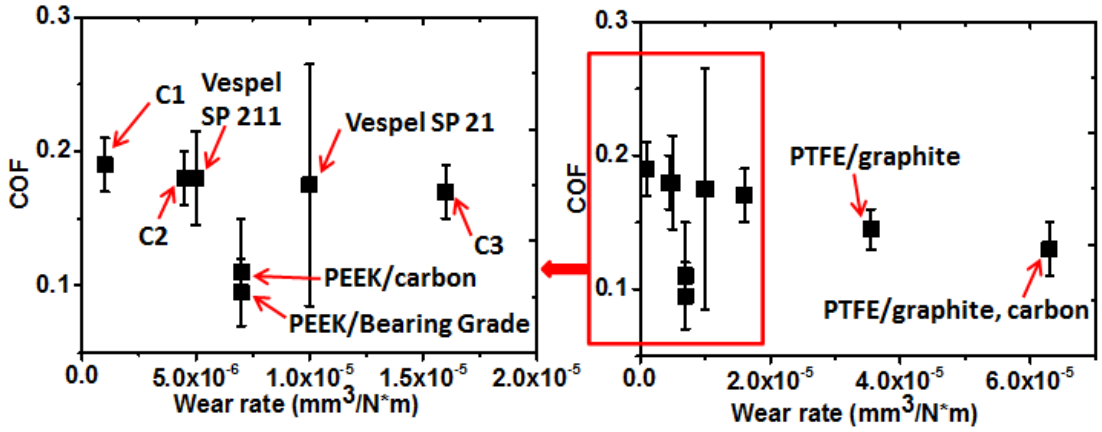

Figure 1 COF vs. Wear rate of bulk polymers sliding with cast iron

From the experiments shown above, the blended polymers tested have good tribological properties that can be tailored to meet specific application needs. Other work also showed great tribological performance of bulk format of polymer composites: low COF and low wear. Sawyer and other researchers found an ultra-low wear rate for PEEK/PTFE composites as low as in the order of 10^{-9} mm^3/Nm[25, 26] and they

optimized the particle size and shape of the Nano-fillers for the bulk polymer Nano-composites [27, 28]. Friedrich and co-workers explored the counter surface topography, orientation of the carbon fiber and temperature effects on the tribological performance of different bulk polymer composites [29-31].

However, polymers in bulk form have shortcomings such as low load capability (7 MPa for some PTFE blends) [23], low dimension precision because of low stiffness and high thermal expansion; high surface temperature when sliding because thick polymers work as heat insulation and heat is not easy to escape; and cold creep. To maintain polymers' advantages and minimize the drawbacks of bulk polymers, thin polymer coatings are an excellent solution. Moreover， thin polymer coatings would have less cost because of their easy depositions method and less material needed.

1.3 Coatings of polymers and their composites

In general, coatings can be classified as either "hard" or "soft" coatings and polymer-based coatings belong to the "soft" coatings. The widely used wear model (or Archard wear model is:

$$F_1 = A_1 * \eta_1 * \left(\frac{v_1}{h_1}\right) \boldsymbol{V = k * \frac{F}{H}} \quad (1)$$

Where *V* is the wear volume, *k* is an empirical wear coefficient, *F* is the normal load and *H* is the hardness of softer material between the tribo-pair. Using the Archard wear model, we would expect hard coatings such as diamond-like carbon (DLC), Ti–N and

WC/C synthesized through physical vapor deposition (PVD) techniques are effective in preventing both abrasive and adhesive wear of metal sliding contacts [32]. However the load carrying capacity of hard coatings may be lower than soft coatings as shown in reference [5], in which DLC coating has a significantly lower scuffing load and higher COF compared with a PTFE-based coating under simulated unidirectional sliding swash plate compressor environment. In addition, hard coatings (DLC) are more sensitive with the environment conditions [5]; and hard coatings are relatively expensive and exhibit difficulties in coating them on substrates with low surface energy or high roughness [32]. Some metallic alloys with different preparation methods can decrease wear rate and COF [33-35]; however, the tribological performance improvement is not very sufficient for extremely low wear and COF applications. Thus alternative solutions such as inexpensive soft polymer coatings need to be explored.

Polymer coatings are widely used as tibological protective coatings, such as erosion/corrosion resistance coatings for automobile [36], , transparent protective coating for touch panel screens and optical applications [37-39], hydrophobic coatings for moisture repellent and dirt resistance[40-42]， bio-implant materials like artificial joints [43, 44], bearing materials for compressor bearings [4-6, 18, 32, 45] or thrust pad bearings [46, 47]. Most of the researchers have been using Nano/Micro indentation/ scratch or moderate conditions such as low PV (pressure times velocity) and low temperature to investigate these polymer coatings' tribological performance [10, 37-44, 46, 48-52]. The extreme tribological performances of the thin polymer coatings have

been mostly focused under compressor applications [4-6, 18, 32, 45] but other applications rarely reported[47] to the best of my knowledge. Thus, it's very necessary to explore the thin polymer coatings for broader applications.

1.4 Objective and research outline

This work is dedicated to study the tribological performance of advanced thin polymeric coatings under extreme working conditions as shown in **Figure 2** of the master chart for this work: high temperature, high load, starved lubrication, abrasive wear, cryogenic temperatures and high chamber pressures. After the extreme tribology experiment, mechanical, chemical and morphology characterization will be carried out in and outside of the wear tracks to explain and understand the coatings' tribological performance. These technologies include Nano/Micro-indentation, Nano/Micro- scratch, SEM/EDS, XPS, optical microscope and profilometer. Despite the tests and characterization, this work proposes a new model to predict the friction for viscoelastic polymers.

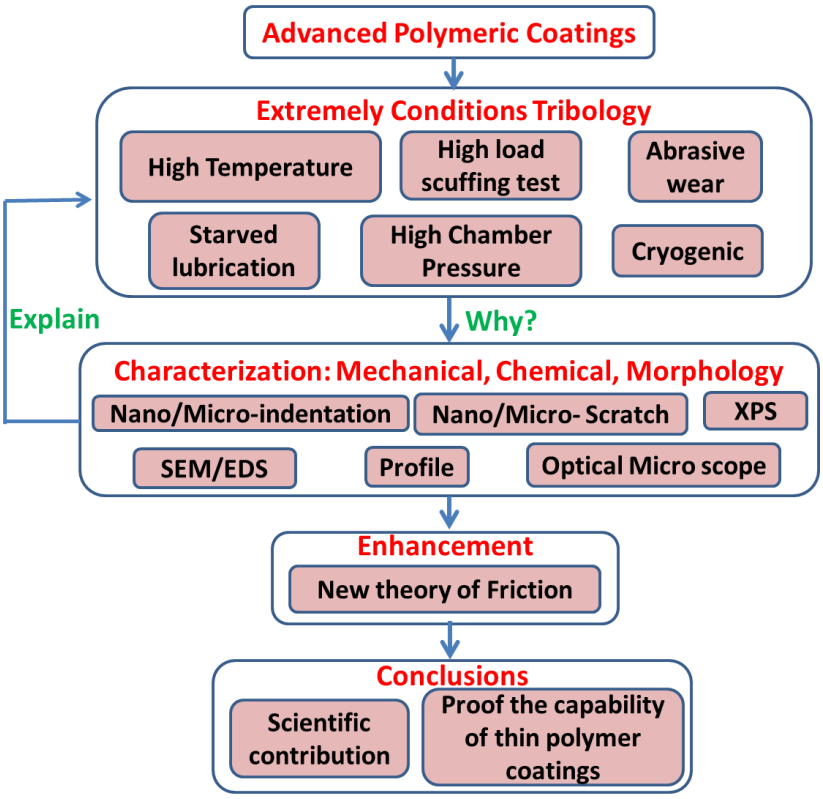

Figure 2 Flow chart of current study

Chapter 2 and 3 explore the temperature tolerance of the ATSP based and PEEK based coatings from -160°C to 260°C in ball-on-disk dry sliding conditions. These tests give the COF trend, wear performance and wear mechanism of the coatings corresponding with the temperature in a broad range of 420°C.

Chapter 4 extensively investigates three different types of coatings (PTFE based, PEEK based and ATSP based) on two different substrate materials with boundary lubrication conditions, simulating extreme working conditions that the tilting pad bearing may encounter. The load capability of the coatings was studied by scuffing tests

and the COF and wear performance were studied by constant load experiments with different durations.

As a further study of chapter 4, Chapter 5 takes the abrasive wear in to account for thin polymeric coatings (PEEK based and ATSP based) used in bearing applications. The experiments were carried out by submerging the samples in lubricant that had 2 wt. % of silica sand. The results showed ATSP-based coating had better wear resistance compared with bare substrate.

Based on the study from chapter 2 to chapter 5, the ATSP based coating showed excellent tribological performance in conditions such as high temperature, high load and abrasive conditions. Chapter 6 puts the ATSP coating in an ultimate challenge, depositing the coating on drilling string for oil and gas drilling application, which has the extreme conditions such as high load, high temperature, high environment pressure and extreme abrasive wear.

Chapter 7 proposed a friction model for viscoelastic polymer coatings. The viscous and elastic parameters at 23°C, 100°C, 180°C and 260°C of the polymer coatings (ATSP based and PEEK based) were measured by high temperature nanoindentation. Inserting the viscous and elastic parameters to the friction model, the model showed good prediction COF compared with the real tests carried out in chapter 2.

The present work has the scientific contribution such as the wear mechanism and friction model for polymer coatings. Also, this work is a strong proof of application of thin polymeric coatings in environments such as hydrodynamic bearings, valve sealing

surface, etc. under different extreme working conditions. And good examples of the extreme working conditions including: extreme temperature range from cryogenic to high temperature dry sliding in space application; the main thrust bearings in the Electrical Submersible Pumps (ESPs) in oil wells once there is a leakage for the protector (seal) section and drilling string of oil and gas drilling application, where the relative surfaces need to endure high temperature, high load, high speed, high environment pressure, and extreme abrasion wear. The following chapters are going to discuss each special extreme working condition in detail.

2. TRIBOLOGICAL PERFORMANCE OF ATSP-BASED AND PEEK-BASED COATINGS AT ELEVATED TEMPERATURE IN DRY CONDITION[1]

The bearing systems in Electrical Submersible Pumps (ESPs) require high temperature and high wear resistance materials, which can improve the running life of ESPs and reduce the maintenance cost for oil wells. In space application, the bearings also need to endure high temperature conditions. This chapter reports on the tribological performance of high-bearing ATSP coatings, which were electrostatically spray-coated. ATSP coatings were tested under a sphere-on-disk configuration from room temperature to 260°C. ATSP coatings showed "zero" wear under moderate load conditions (5N, 110 MPa) and all temperatures and under higher loading conditions (10N, 139 MPa) and room temperature. Scanning electron microscopy analysis indicated that the wear of the coating was mainly from burnishing of the asperity peaks of the coating. At the higher load and temperature (10N, 260°C), the coating failed due to cracks formed by elastic fatigue. For comparison, a commercial thermoplastic PEEK based coating was also tested under the same conditions. Unlike ATSP, PEEK based coating showed abrasive wear grooves and adhesive wear debris under its glass transition temperature. At

[1] Reprinted with permission from "Unlubricated tribological performance of aromatic thermosetting polyester (ATSP) coatings under different temperature conditions." by Lan, P., Meyer, J.L., Economy, J. and Polycarpou, A.A., Tribology Letters,61.1 (2016): pp. 10, Copyright 2016 by Springer.

temperatures higher than its glass transition temperature, PEEK based coating showed adhesive wear and plastic deformation.

2.1 Introduction

Polymers, especially blended high-bearing polymers are important tribological materials for many reasons; they exhibit low friction, moderate wear resistance, good corrosion resistance, self-lubricating properties, low noise emission and are inexpensive to produce[19]. Among all polymers, PTFE is one of the most widely used because of its chemical inertness, very low friction and considerable thermal stability[19, 53]. However, PTFE shows creep and high wear rate in pure form. Similarly, almost all other unblended polymers have some sort of limitations. Pure PEEK exhibits very low scuffing resistance and a large wear rate during reciprocating sliding wear[12]; pure ATSP coating has a high coefficient of friction, high wear rate[24]. Thus researchers have great interest to produce composites or blended polymers to improve their tribological performance.

The ATSP material was invented in the mid-1990s as the cured product of cross-linked aromatic polyester oligomers of various branching and molecular weight configurations[54]. Since then tribological performance of ATSP-PTFE composites was undertaken by several researchers either in bulk or coating form, showing that the composite materials were superior to pure ATSP and pure PTFE. Demas et al. [14, 22]

used a pin-on-disk experimental configuration to investigate the tribological behavior of a wide range of bulk compositions using blends of ATSP with PTFE in an air conditioning compressor environment. They found that ATSP-PTFE bulk composites exhibited low friction and low wear; greater amounts of ATSP used in the blend led to lower wear and the amount of ATSP did not significantly alter the friction coefficient [14]. In a different study, by using sphere-on-disk experiments, Zhang et al. also showed low wear and low friction of ATSP coatings with fluoro-additives applied as a third-body solid lubricant [24]. Huang et al. developed blends of ultrahigh molecular weight polyethylene (UHMWPE) with ATSP. They showed that the UHMWPE/ATSP blend with poly (ethylene-co-acrylic acid) PEA exhibited lower wear rate than UHMWPE; by adding PEA, the interaction between UHMWPE and ATSP was effectively enhanced [55].

Polymers' temperature tolerance is a concern in tribological applications, because the working field temperature could be very high. For example, commercial Electrical Submersible Pump (ESP) systems are rated up to 220˚C, which is based on last 80 years' experience in oil wells, geothermal and steam assisted gravity drain applications[56]. Prior tribological studies with ATSP were conducted under low temperature conditions. In this study, experiments were carried out from room temperature to 260°C using a high temperature tribometer with a sphere-on-disk experimental configuration. The ATSP coating's tribological performance and wear mechanism at different temperatures were studied in detail. As a comparison, a

commercial thermoplastic PEEK/PTFE coating was tested under the same experiment conditions.

2.2 Experimental

2.2.1 High Temperature Tribometer (HTT)

The HTT is a specialized tribometer, as shown in **Figure 3(a)**, with a sphere or pin-on-disk configuration (**Figure 3(b)**) and can perform experiments at temperatures up to 1000°C. It has unidirectional and oscillatory motion; rotational speeds up to1000 rpm and oscillation frequencies up to 5 Hertz. The sample diameter can be up to 95 mm. The force transducer record in situ normal and friction forces (the normal force and friction force as a function of time (that can be converted to displacement)), which is used to calculate the in situ friction coefficient.

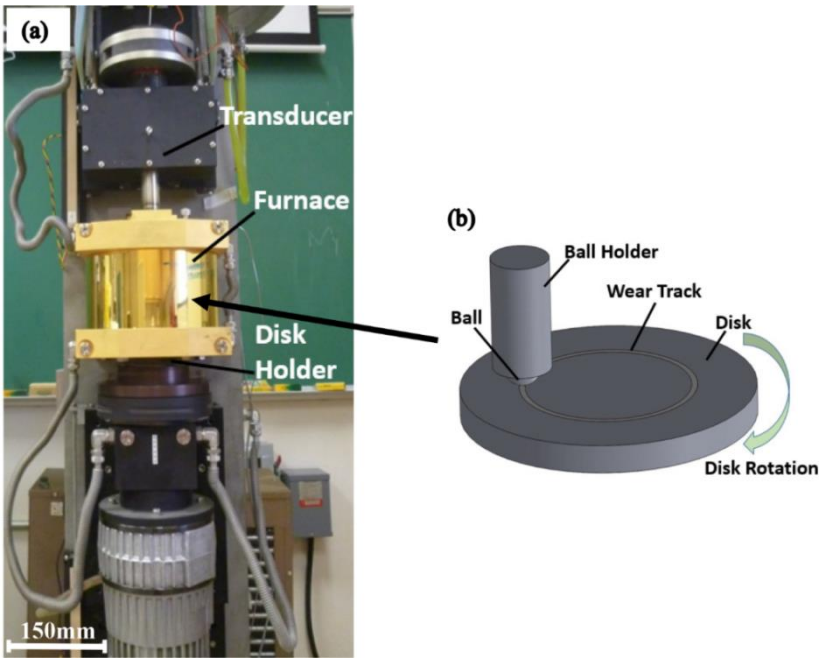

Figure 3 High Temperature Tribometer（HTT） (a) Picture of HTT, (b) Schematic of ball-on-disk experimental configuration

2.2.2 Samples

Two oligomeric systems, namely C2 and A1, which (respectively) have carboxylic acid and acetoxy functional end groups, are used as the precursors for the ATSP coating used in this study. A detailed description of the synthesis of ATSP powders can be found in Economy et al.[57]. Oligomer C2 was synthesized by melt condensation at 270°C using a molar feed ratio of trimesic acid (TMA): isophthalic acid (IPA): 4-aceotxybenzoic acid (ABA): hydroquinone diacetate (HQDA) of 1:4:6:4. Oligomer A1 was similarly synthesize using a molar feed ratio of 2:2:2:7. Example chemical structures for crosslinkable oligomers C2 and A1 are shown in **Figure 4**.

Oligomer products were solids at room temperature and were ground in a Col-Int Tech laboratory grinder. Ground material was sieved via Retsch sieve-shaker and powder that passed through a 38 um screen was utilized. A weight ratio of 1.08:1 for C2:A1 was used and powders were mixed mixed with 5 wt% DuPont Zonyl MP1100 as PTFE lubricating phase. The blended powder was sprayed onto the sand blasted 6 mm thick (and 75 mm diameter) gray cast iron (G2 Durabar) disks using electrostatic spray deposition (ESD). The coating was then cured at 270°C for 30 minutes with convective air. The final thickness of ATSP coatings is 40μm. For comparison, a 35μm thick PEEK based (1704 PEEK/PTFE®) coating was deposited on cast iron by an authorized applicator (Southwest Impreglon). Note that the PEEK based coating used here is a dispersion coating; where it is dried after spraying the dispersion, then followed by a melting process at 371-399°C. Photographs of the disks after coating deposition are shown in **Figure 5**.

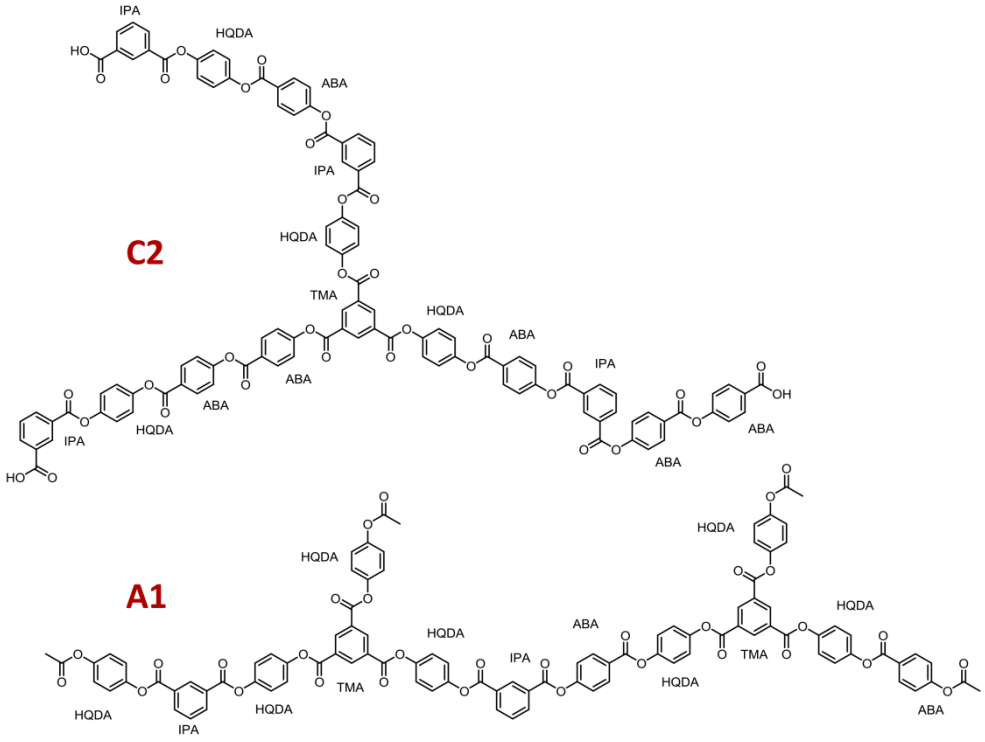

Figure 4 Example chemical structures for cross-linkable oligomers C2 and A1

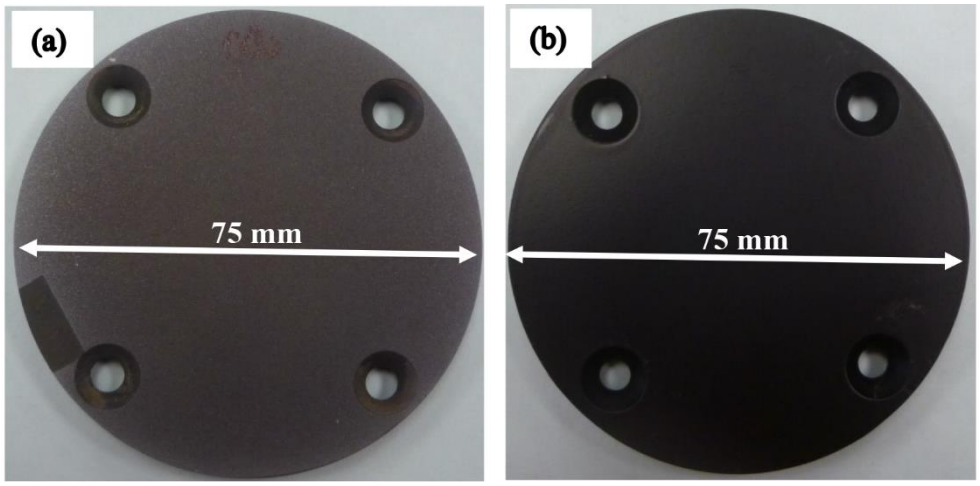

Figure 5 Photographs of coatings on cast iron disks, (a) ATSP, (b) 1704 PEEK/PTFE®

In ESP system, usually, the counter surface material of tilting pad bearing is 4130 steel collar. However, 4130 steel balls were not readily available; we chose 1018 carbon steel balls which have similar carbon content as 4130 steel balls. 6.35 mm diameter hardened 1018 carbon steel balls were used as the counter surface for testing the coatings. The 1018 carbon steel balls were 1000 grade, which had roughness about Ra 0.2μm and hardness of C60. Before each experiment, the coatings were immersed in isopropyl alcohol, and the steel balls were immersed in acetone, and the glass containers were placed in an ultrasonic cleaner for 10 minutes at 50ºC.

2.2.3 Experimental design

As shown in **Table 1**, four sets of experiments were designed for both ATSP and PEEK BASED coatings: room temperature (23ºC), 100ºC, 180ºC and 260ºC under 5 N normal load (corresponding to an approximate initial Hertzian contact pressure of 110 MPa for room temperature), 0.139 m/s sliding speed and 500 m dry sliding distance. To better understand the wear resistance and wear mechanism, higher severity experiments at 10 N (139 MPa for room temperature) were conducted at room temperature and 260ºC with different sliding distances. The elastic modulus and Poisson's ratio used for the calculation of contact pressure for ATSP/PTFE (ATSP Innovations) and PEEK/PTFE[10] were 3.2 GPa and 0.4, respectively.

Table 1 Experiment conditions for high temperature (sliding velocity 0.139 m/s)

Coating	Temperature (ºC)	Normal force (N)	Contact pressure (MPa)	Sliding distance (m)
ATSP based	23, 100, 180, 260	5	110 (room temperature)	500
	23	10	139 (room temperature)	700
	260	10	---	250, 428
PEEK based	23, 100, 180, 260	5	110 (room temperature)	500
	23, 260	10	139 (room temperature)	500

2.2.4 Scanning Electron Microscopy (SEM) and wear analysis

SEM (Tescan VEGA) was used to measure the thickness of the coatings (cross section analysis). The roughness of the coatings was measured using a profilometer (KLA –Tencor). After the tribological experiments on the HTT, a JEOL JSM-7500F SEM was used to study the morphology inside and outside the wear tracks to better understand the wear mechanisms of the coatings. The Tescan SEM was used for the analysis of the wear scar on the steel ball. The profilometer was also used to measure the exact profile across the wear track to obtain the wear rate; the microscope camera in the profilometer was used to determine start and end points of the wear track and 4 different wear scans was performed at 4 different positions to get an average wear data for each

wear experiment. The wear volume and wear rate were obtained using the following equations:

$$Wear\ Volume = \int_{r1}^{r2} 2\,\pi \bullet r \bullet h \bullet dr = \sum 2\,\pi \bullet r \bullet h \bullet \Delta r \qquad (2)$$

$$Specific\ wear\ rate = \frac{Wear\ Volume}{Normal\ Force\ \bullet Distance} \qquad (3)$$

Where r_1 and r_2 is the inner and outer radii of the wear track, and h is the exact/measured wear depth, as shown in **Figure 6**.

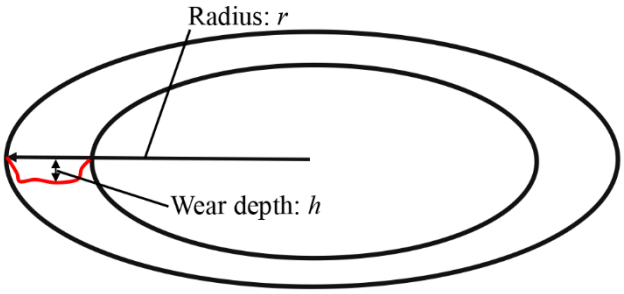

Figure 6 Schematic of wear calculation

2.3 Results and Discussion

2.3.1 Roughness and coating thickness

The roughness and thicknesses of the coatings and substrates are summarized in **Table 2**. The roughness of the steel ball was obtained from the manufacturer's specification. PEEK based coating's roughness is lower than the sand blasted substrate

while ATSP's coating roughness is higher than the sand blasted substrate. The scan length for the roughness measurements was 5 mm. No attempt was made to reduce the roughness of the ATSP coating, which is however possible. This roughness is due to PTFE having a relatively high contact with the oligomer melt combined with the relatively fine particle sizes involved. As the oligomer contacts the PTFE (average particle size of 4 μm [58]), its flow and connection with other oligomer particles can be obstructed due to the high contact angle and high viscosity of the oligomers; thus the higher roughness. The cross section SEM scans of ATSP coating and PEEK based coating are shown in **Figure 7**, showing that both coatings exhibit a somewhat non uniform surface, as well as the average thickness values.

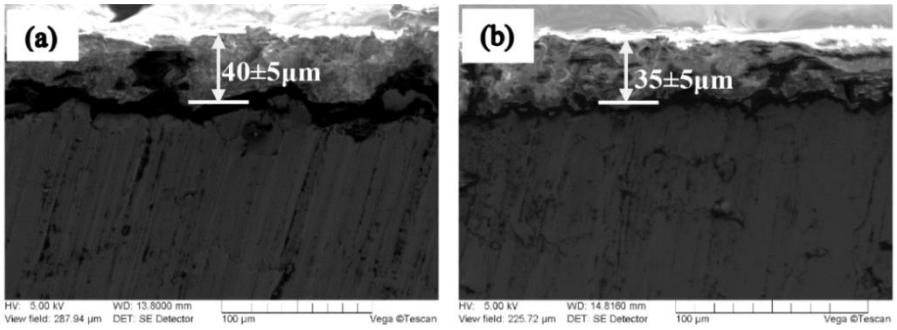

Figure 7 Cross section SEM images of (a) ATSP, (b) PEEK based coatings

2.3.2 Tribological experiments

2.3.2.1 Intermediate loading conditions (5N/110MPa)

Figure 8 shows the in situ COF of the ATSP coating under different temperatures. As the temperature increased, the COF decreased from 0.21 at 23ºC, 0.15 at 100ºC to 0.11 at 180ºC, and when the temperature increased to 260ºC, the COF had no big change compared with in 180 ºC, as depicted in **Figure 8(b)**. The decreasing trend of the COF is attributed to the softening of the polymeric coating (ATSP and 5% PTFE) with increasing temperature, in agreement with Refs. [59, 60]. Since 260ºC is in the range of ATSP's glass transition temperature, the COF stopped to decrease at 260ºC can be attributed to a larger contacting area between the ATSP coating and the steel ball.

Table 2 Roughness and mechanical properties

Surfaces	Rq (μm)	Thickness
ATSP (95%C2A1+5%PTFE)	5.8	40±5
1704 PEEK/PTFE®	1.6	35±5
Cast iron disk before sand blast	0.4	−
Cast iron disk after sand blast	3	−
1018 middle carbon steel ball	~0.2 (1000 grade)	−

The wear scans of the ATSP coating after 5N normal load under different temperatures are shown in **Figure 9**, showing no observable wear. As seen in the wear

scans, the coating was originally rough and there is no evidence of measurable wear, thus under these conditions the ATSP coating exhibited “zero wear” behavior. Next, a higher load/contact pressure (10N) was used to understand ATSP coating’s wear and failure mechanisms.

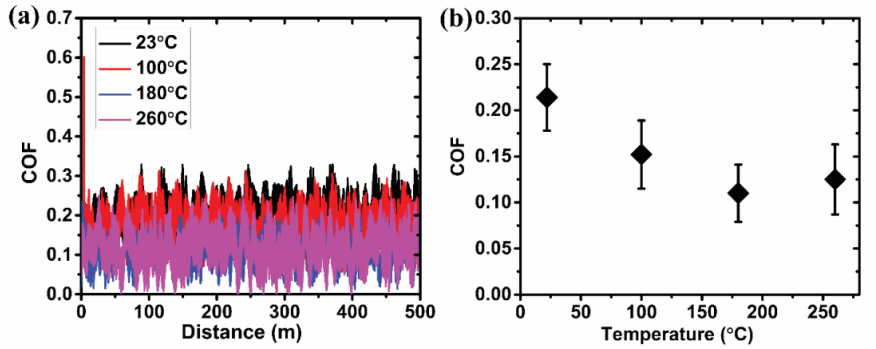

Figure 8 ATSP 5N load experiments (a) in situ COF, (b) average COF versus temperature

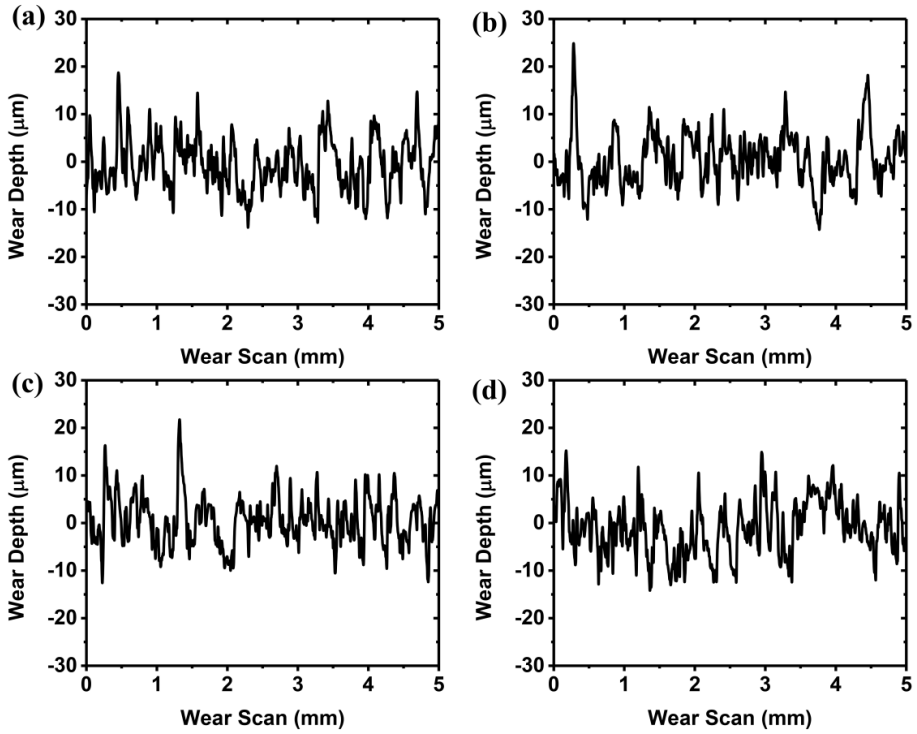

Figure 9 ATSP 5N wear scans (between 2.5mm to 3.0mm) showing no observable wear: (a) 23ºC, (b) 100ºC, (c) 180ºC, (d) 260ºC

Figure 10 shows the COF VS wear rate of the PEEK based coating under different temperatures. Similar with the ATSP coating, PEEK based coating's COF decreased with increasing temperature, 0.22 at 23ºC, 0.16 at 100ºC, 0.10 at 180ºC and 0.093 at 260ºC. This trend was due to the thermoplastic nature of PEEK based: At higher temperatures, the cooperative motion of polymer chain increases, which faciliates the sliding of the steel ball. However the softening effect was no longer evident when the emperature was higher than 180ºC,which was higher than the glass transition temperature of both PEEK[61] and PTFE[62], resulting in only a small decrease of the

COF at 260ºC when compared with 180ºC. This corresponds to the region above the glass transition temperature of PEEK (>143°C), wherein the mobility of chains allows PEEK to rapidly undergo volume relaxation [63] without a qualitative change in mechanism between the glass transition (T_g) and the melting temperature (T_m).

The wear scans of the PEEK based coating after 5N normal load and different temperature experiments are shown in **Figure 11**. The wear of the PEEK based coating was evident, compared to ATSP. As shown in **Figure 10**, when the temperature increased from room temperature to 180ºC, both the wear rate and the COF decreased, corresponding with increasing temperature. When the temperature increased from 180ºC to 260ºC, although the COF decreased sligtly, the wear rate inceresed significantly, from 2.5×10^{-6} mm^3/Nm to 1.4×10^{-5} mm^3/Nm.

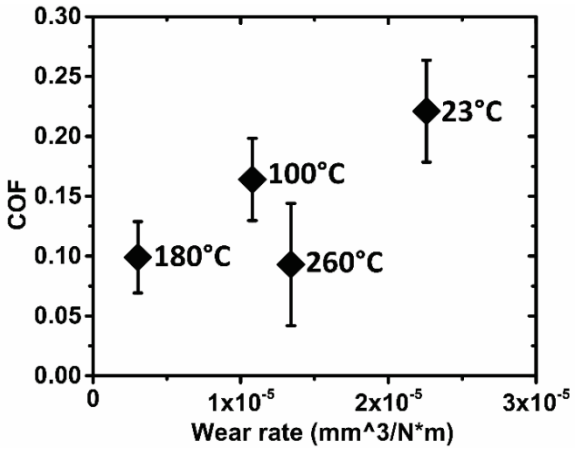

Figure 10 PEEK based 5N load experiments, average COF VS wear rate

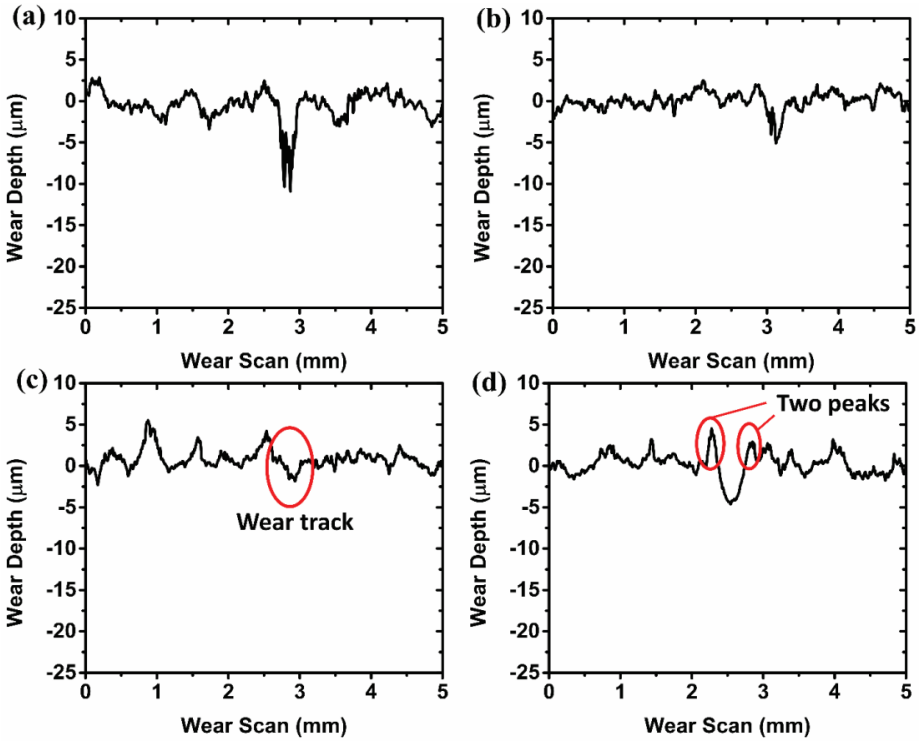

Figure 11 PEEK based 5N wear scans (between 2.5mm to 3.0mm) showing wear: (a) 23ºC, (b) 100ºC, (c) 180ºC, (d) 260ºC

Shown in **Figure 12(a)** is the surface topographical image of the wear scan for PEEK based coating tested at 180ºC, which exhibited the lowest wear rate in these four temperature conditions. The reason for the lower wear is because 180ºC is slightly higher than T_g, and the physical state was viscoelastic but strong enough to sustain the 5N normal load. Observed with this was a transfer layer formed on the surface of the steel ball, as shown in the SEM image in **Figure 12(b)**. This transfer layer helps to decrease the COF and wear rate [18]. While at 260ºC, the PEEK based while also in the viscoelastic state, had softened below the abilityto sustain the 5N normal load; the

material was deformed forming a groove on the boundaries of the wear track, as shown in **Figure 11(d)**.

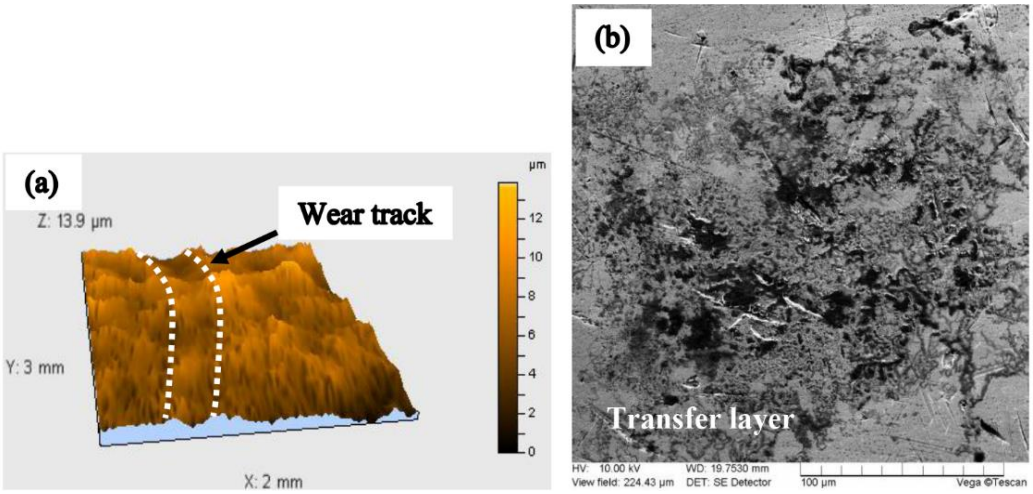

Figure 12 PEEK based 5N, 180ºC experiment (a) 3-D profile showing the wear track, (b) SEM of contact area of steel ball

2.3.2.2 Higher loading conditions (10N/139MPa)

Since the lower loading condition did not produce measurable wear for the ATSP coating, higher load (10 N) experiments were carried out at 23ºC for 700 m. Under this load, the COF was stable, as shown in **Figure 13 (a)**, and wear was too low to be discernible with the coating's surface roughness, as shown in the wear scan in **Figure 13(b)**. At 260ºC, the coating showed no observable wear after 250 m sliding distance, and failed at around 400 m sliding distance. This means that at 260ºC, the wear rate is very low since the coating was still in good shape with no observable wear after 250 m

sliding distance (**Figure 13(c)**). Once the coating was penetrated, it failed, as seen in **Figure 13(d)**. As it will be shown next, cracks in the coating cause ATSP's failure. Note also that the COF with higher load was lower than the COF with lower load: under 5N, the COFs were 0.21 for 23ºC and 0.13 for 260ºC experiments; and under 10N, the COF decreased to 0.15 for 23ºC and 0.082 for 260ºC experiments. This trend of COF decreasing with increasing load was also observed in Ref. [64]. In summary, ATSP coating still shows "zero wear" at the higher contact pressure within small sliding distance and it failed in longer distance due to cracks at 260°C.

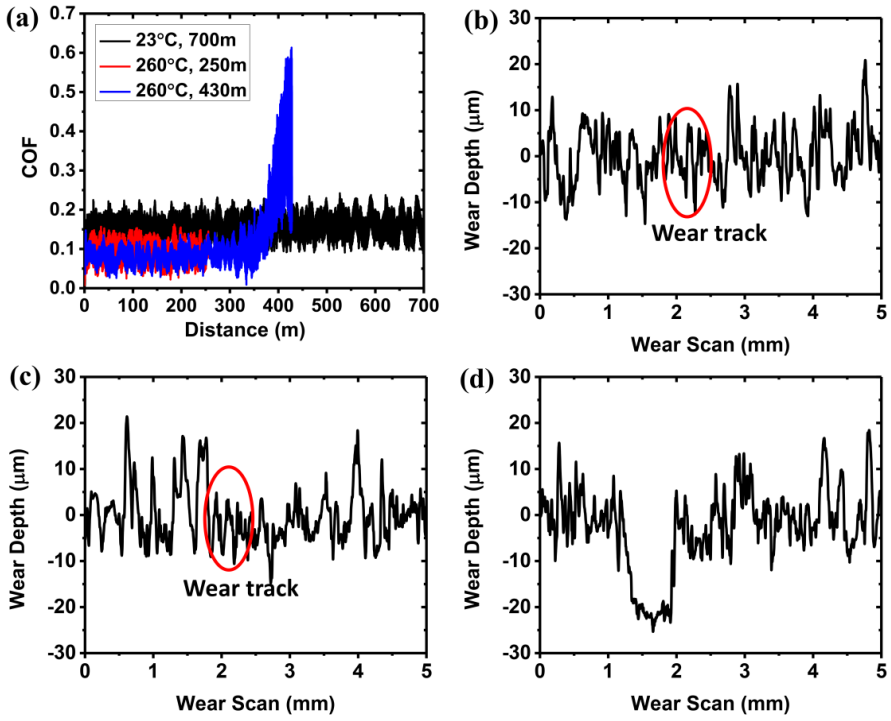

Figure 13 ATSP 10N load experiments, (a) In situ COF, wear scans after (b) 23ºC, 700 m, (c) 260ºC, wear scan of 250 m sliding distance, (d) 260ºC, wear scan after 430 m sliding distance

The in situ COF for the PEEK based tested under 10N (23°C and 260°C) is shown in **Figure 14(a)**. In this case the wear rate was significantly higher compared with the 5N normal load, as shown in **Figure 14(b)**. From the wear scans in **Figure 14(c)** and **(d)**, the wear depth was significant at over 20 μm. As shown in **Figure 14(a)**, the COF at 23°C increased with sliding distance; when the remaining coating became thinner, the contact surface did not fail due to stronger bond between the coating and the substrate. As shown in **Figure 14(d)**, at 260°C and 10N normal load, the wear scar (groove) of the coating was clearer than with 5N normal load. The trend of COF decreasing with increasing load was also observed in the PEEK based coating, as shown in **Figure 14(b)**.

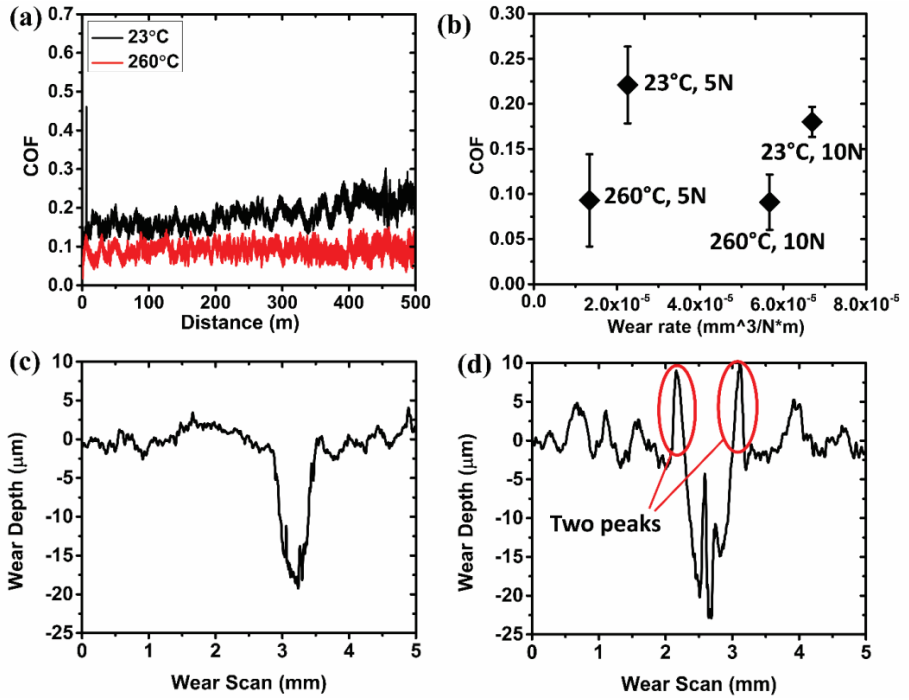

Figure 14 PEEK based experiments, 10 N: (a) in situ COF, (b) average COF Vs wear rate, (c) wear scan, 23ºC, (d) wear scan, 260ºC

2.3.3 SEM analysis

Figure 15(a) and **(b)** show low and high magnification SEM image of the untested ATSP coating. The ATSP coating surface was rough (as reported earlier). This foam-like surface texture is a result of ATSP's chemical and physical interactions occurring between ATSP powders during the curing process after electrostatic spray, and then formed the linkage between larger powder particles. Also, the ATSP coating has a sparse structure, which evolved due to the mechanism described above. The three-dimensional porous structure characteristic of materials showes great elasticity. This kind of pore may play an important role on the entrapment of wear debris during the

sliding process and considerably affect the tribological behavior. PEEK based coating fully melted at 371-399°C, as indicated by the SEM images of the baking process (Ref. [65]), and flowed evenly on the substrate, making the coating uniform, as shown in **Figure 15(c)** and **(d)**.

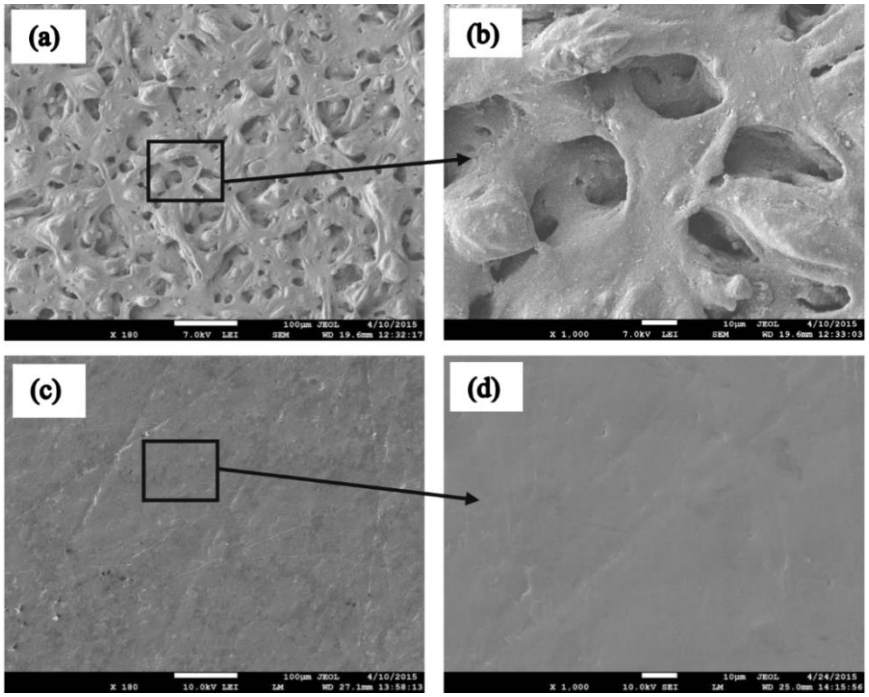

Figure 15 SEM images of untested samples: (a, b) ATSP, (c, d) PEEK based coatings

Figure 16 depicts SEM images after the 5N normal load experiments at different temperatures. The thick arrows shown in the low magnification images indicate the sliding direction. All the low magnification images show that there was "zero coating wear," which is consistent with the wear scans, discussed earlier. In the higher

magnification images, there is observable “burnishing” of the rough asperities of the coating. Because ATSP is a high temperature thermosetting polymer, it resists deformation whether the coating is under low or high temperature; crushing or burnishing of the peaks results from the high contact pressure at the asperity tips. Once burnishing occurs, early in the experiment, the real contact area increases, sustaining the load and thus causing no further wear or burnishing. Despite the high roughness of the coating, wear is insignificant and could not be measured in this work. This is consistent with earlier work where ATSP exhibited extremely low wear rates [24].

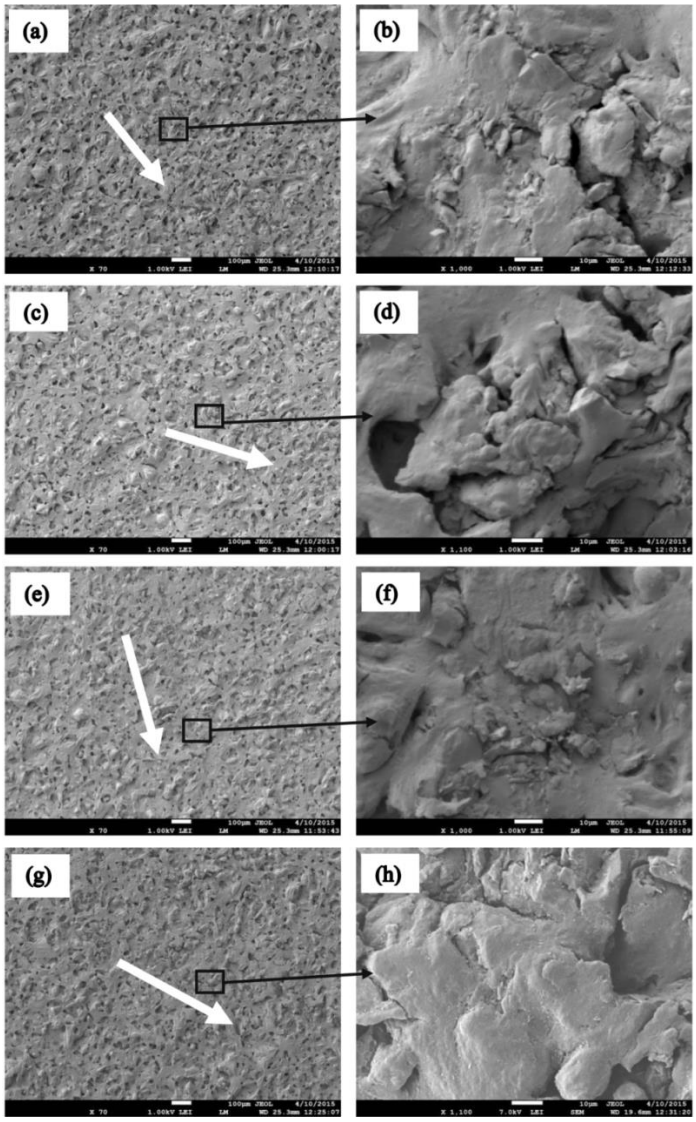

Figure 16 SEM images of ATSP under 5N normal load and different temperatures, (a, b) 23ºC, (c, d) 100ºC, (e, f) 180ºC, (g, h) 260ºC, (thick arrows show the sliding direction)

Under 10N normal load and 23ºC, there was only minor burnishing of the asperity peaks of the ATSP coating, as shown in **Figure 17(a)** and **(b)**, albeit more evident compared with the 5N normal load experiments (**Figure 16**). However, large

cracks across the entire wear track formed at 260ºC with 10N normal force, 250 m sliding distance, as shown in **Figure 17(c)** and **(d)**. These cracks formed because the temperature was in the glass transition range making the coating more vulnerable to high contact pressure; also, cyclic load from the steel ball caused local elastic fatigue [13]; there is a critical contact pressure at which cracks occur in the coating [66] and the 10N normal load was high enough to initiate the cracks which then grew across the wear track. So with 10N load at 260ºC, the coating failed at approximately 400 m sliding distance.

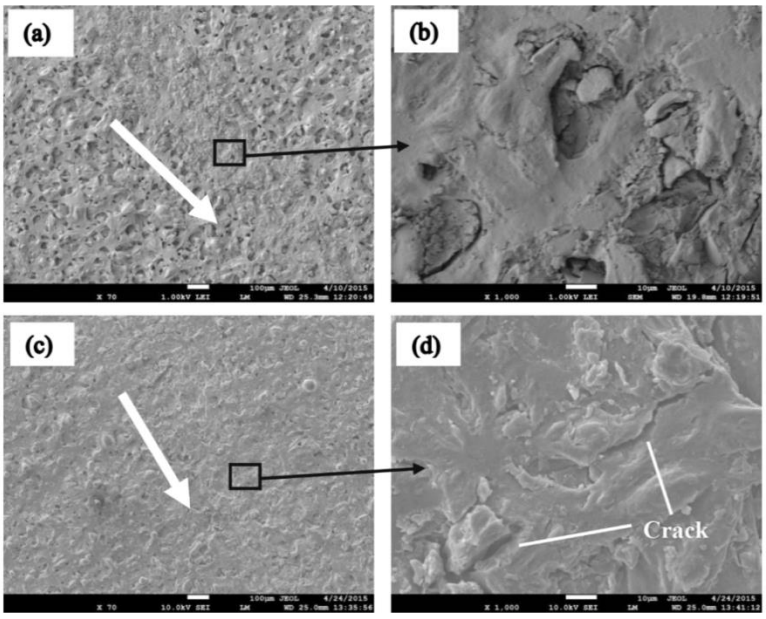

Figure 17 SEM images of ATSP coatings under 10N normal load, (a, b) 23ºC, 700 m, (c, d) 260ºC, 250 m, (thick arrows show the sliding direction)

Figure 18 shows the SEM images of the 5N normal force experiments of PEEK based coatings at different temperatures. At lower temperatures, 23ºC and 100ºC, which is below the glass transition temperature of PEEK, the wear mechanisms of PEEK based coating were mainly abrasion and adhesion, as shown in **Figure 18(a)** and **(b)**, and **Figure 18(c)** and **(d)**.

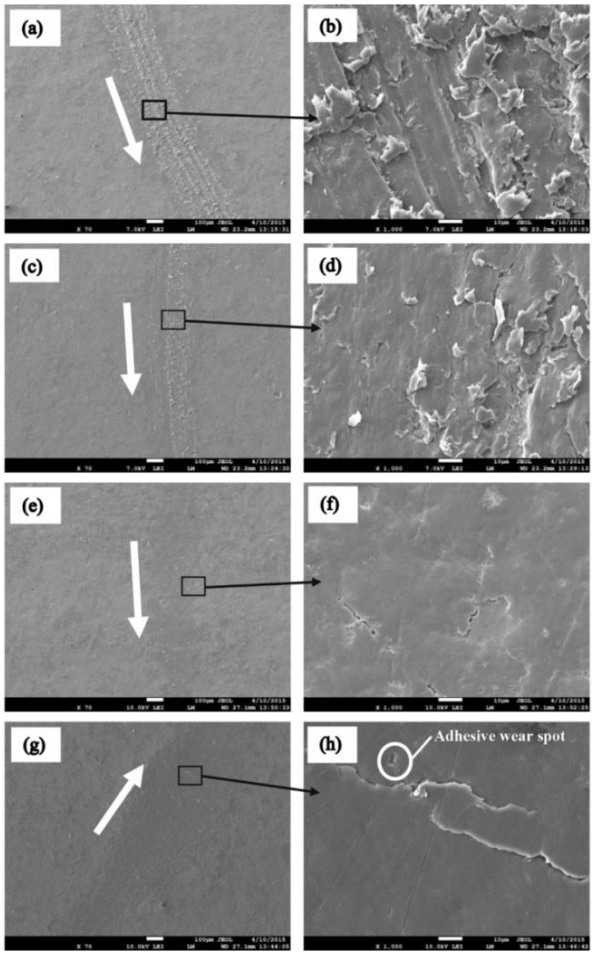

Figure 18 SEM images of PEEK based coatings under 5N normal load (a, b) 23ºC, (c, d) 100ºC, (e, f) 180ºC, (g, h) 260ºC, (thick arrows show the sliding direction)

All presented abrasive wear grooves and adhesive wear are associated with flaky wear debris. The abrasive wear occurred due to the asperities of the steel ball and also from the polymeric debris that slid on the counter surface; the hardness of the polymer debris could be increased in the sliding process as a result of repeated plastic deformation, and then the polymeric debris could act as an abrasive particle itself [11, 12]. While the flaky debris formed by the plastic fatigue of the coating followed by nucleation and propagation of micro-cracks [13], and then with the adhesive force of the steel ball, the debris peeled off the coating [11]. The abrasive wear at 23ºC was more predominant than the abrasive wear at 100ºC. This might be because at 23ºC, the relative hardness of the hardened polymeric debris and the coating could be higher than the relative hardness at 100ºC; so the abrasive wear formed by hardened polymeric debris at 23ºC could be more obvious than at 100ºC.

At 180ºC, which is higher than the glass transition temperature of both PEEK and PTFE, the wear was mainly adhesive wear; plastic deformation and creep should also aid in the removal of the PEEK based coating material from the original surface, as indicated in the wear scan in **Figure 11(c)**. At 180ºC, as shown in **Figure 18(e)** and **(f)**, the lack of an abrasive wear groove combined with the SEM image of the steel ball in **Figure 12(b)**, which shows adhesive or transfer wear, the wear mechanism of the PEEK based at 180ºC is primarily adhesive wear. At 260ºC, there was almost no observable wear debris, but as shown in **Figure 18(g)** and **(h)**, the cracks formed across the wear track due to plastic fatigue of the coating [13]. The adhesive contact with the steel ball

removed some material creating pits. Due to scarce wear debris at 260ºC, plastic deformation and creeping were the main reasons for wearing the PEEK based coating, as also indicated in the wear scan in **Figure 11(d)**. When the load increased to 10N, the wear was more prevalent, as shown in **Figure 19**, with the wear track being wider; but the wear mechanism remained the same. At 23ºC, predominantly abrasive wear with some adhesive wear was observed (**Figure 19(a)** and **(b)**). At 260ºC, primary wear was due to adhesion and deformation of the material (**Figure 19(c)** and **(d)**).

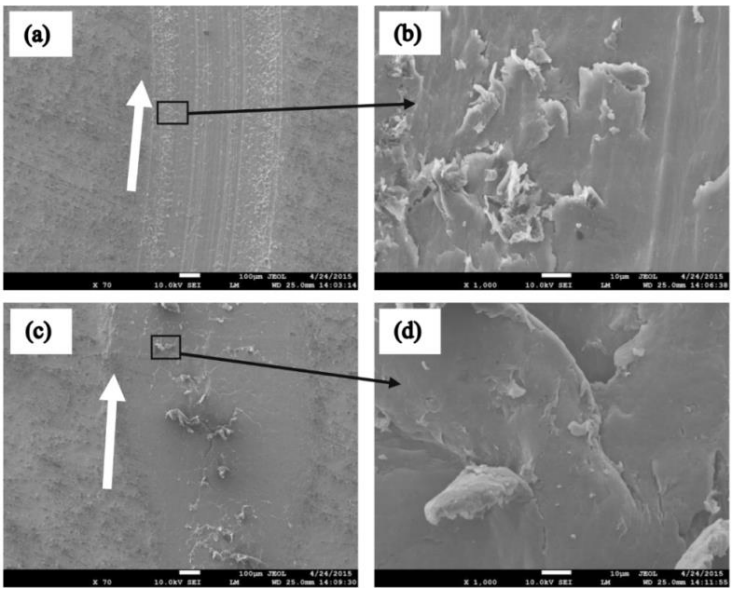

Figure 19 SEM images of PEEK based under 10N normal load, (a,b) 23ºC, 500 m, (c,d) 260ºC, 500 m

2.4 Conclusion

ATSP/PTFE and PEEK based coatings were tribologically tested under different temperature and load conditions using a specialized high temperature tribometer. The results are summarized in **Figure 20**, in the form of the COF vs wear rate of both coatings under different experimental conditions, and the following conclusions could be drawn:

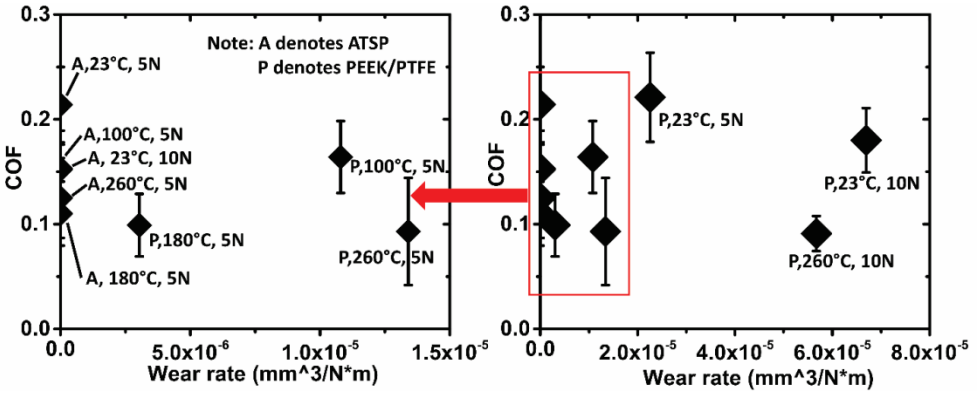

Figure 20 Summary of ATSP/PTFE and PEEK based coating results: average COF Vs wear rate, showing that ATSP/PTFE exhibits "zero wear" while PEEK based shows a higher wear rate

a) ATSP/PTFE exhibited "zero wear" as measured using wear scans under all experimental conditions, except at 260ºC and 10N normal force for 430m sliding distance. SEM analysis showed the wear of the ATSP coatings was mainly from burnishing of the asperity peeks of the coating;

the failure mechanism of the ATSP coating under this case was due to cracks formed by elastic fatigue.

b) For PEEK based coatings, with increasing of the operating temperature, the abrasive wear became less important and the adhesive wear became more predominant. At 180ºC, the coating formed a transfer layer that helped decrease both COF and the wear rate of the coating.

c) For ATSP/PTFE coatings with 5N normal load, the COF decreased first with increasing temperature, from 0.21 at 23ºC to 0.011 at 180ºC, and then increased to 0.12 at 260ºC. For PEEK based coatings, the COF monotonically decreased with increasing temperature, from 0.22 at 23ºC to 0.093 at 260ºC.

d) Both ATSP/PTFE and PEEK based coatings showed that increasing the load/pressure could result in decreasing of the COF. For PEEK based coating, although the COF decreased with higher load, the wear rate increased.

3. TRIBOLOGICAL PERFORMANCE OF ATSP BASED COATINGS UNDER CRYOGENIC CONDITIONS

Thin polymeric coatings are great candidates for extreme temperature dry sliding conditions where oil lubricant and grease are ineffective. Earlier research in chapter 2 demonstrated that ATSP-based coatings with a thickness of approximately 30 μm exhibit excellent wear resistance and low friction coefficient (COF) at high temperatures up to 260°C. In this chapter, the tribological performance of ATSP-based coating under cryogenic environment with temperatures as low as -160°C was investigated by using a ball-on-disk experimental configuration. This report complements the tribological performance map of this coating from cryogenic to high temperature conditions. The experiments showed that under an initial Hertzian contact pressure of 110 MPa (calculated with room temperature parameters), ATSP coatings exhibited near zero (immeasurable) wear and the COF, in general, increased when decreasing temperature, with a peak value at -100°C. Under higher contact pressure of 139 MPa (calculated with room temperature parameters), at -160°C, there was a transition point where the COF dropped notably. Further investigation revealed that this favorable transition is due to the development of a polymer transfer film on the contact point of the steel ball. For comparison, a commercial bearing grade PEEK-based coating was also tested under similar conditions. SEM/EDS was implemented to inspect and explain the coating tribological performance.

3.1 Introduction

Polymers exhibit unique and favorable tribological advantages such as self-lubrication, good wear resistance, low vibration, lightweight, and low cost. Hence, they are feasible substitutes for extreme dry sliding conditions, where traditional liquid lubricants or greases are impractical. For instance, cryogenic temperatures set the limits in many technologies such as space applications, superconductivity, medical diagnostics, cryogenic cooling, and cryogenic liquid storage and transportation [67-74].

For tribological space applications, the extreme cryogenic conditions surrounding the driving mechanisms for the components of satellites and space stations; bearings of lunar rover rotating parts; valves and seals for liquid fuel storage and control of rocket engine, experience harsh conditions. Research agencies, such as the Federal Institute for Materials Research and Testing (BAM) in Germany, and Special Research & Development Bureau of B. Verkin Institute (SR&DB) in Ukraine have promoted cryogenic tribological research to satisfy these technological needs. They designed different types of low temperature tribometers with a pin-on-disk configuration that could experimentally simulate dry sliding or submerged sliding in coolant conditions. They have conducted numerous cryogenic tribological studies for different materials, including polymers and composites, soft solid lubricant coatings, and hard coatings, such as diamond like coatings and TiN [71, 72, 75-83].

Cryogenic tribology research in BAM investigated bulk polymers and composites by using PTFE, PEEK, polyimide, polyamide and epoxy as matrix.

Additionally they investigated different fillers such as carbon fiber, MoS_2, graphite, TiO_2, and bronze at different temperatures, ranging from -269°C to room temperature. Both submerged conditions in a liquid coolant or coolant gas ambient were explored. Findings from their research includes the key role of (a) the transfer layer on the counter metal surface, and (b) the coolant medium, filler content and compositions on the tribological performance of polymeric composites. Also, they reported on the better wear resistance at lower temperatures, as a result of changes in the mechanical properties and reduction of the COF at lower temperatures [67, 72, 77].

Mixing different polymer resins as binder and MoS_2, PTFE and graphite as solid lubricants, the researchers at SR&DB produced various polymeric composites that could be deposited on metallic substrates. They reported that at cryogenic temperatures (-267°C to -53°C) fatigue wear is the dominant wear mechanism. They concluded that such coatings exhibit a better wear resistance at low temperatures, confirming the previous findings of BAM. However, their research concluded that the COF increased when temperature decreased which was contrary to BAM's reported conclusions [80, 82, 83]. This disagreement could be justified by the different testing conditions that they applied. While BAM conducted their tests under submerged conditions, SR&DB applied dry contact sliding conditions. For example, in one of BAM's studies of PTFE matrix composites at -196°C, the COF in helium gas is much higher than in N_2-liquid [77], which could be attributed to the more effective lubrication of liquid nitrogen, compared to gaseous helium.

Sawyer and his colleagues reported cryogenic tribology results of PTFE. They successfully applied an empirical friction formula [84], activation energy of Van der Waals forces and hysteresis loss to explain their friction data. Besides the experimental results, they also used molecular dynamics simulations to study the friction performance of PTFE with different sliding orientations [70, 80, 85, 86].

The earlier cryogenic tribological studies have primarily focused on bulk polymers and composites. Bulk polymers undergo large thermal expansion with strong changes in temperature, because of their high thermal expansion coefficient. This inherent property makes them unsuitable for precision demanding applications that experience serious temperature changes such as space applications. To this effect, hair-thin polymeric coatings on metal-base materials yield good solutions for this drawback. Polymeric coatings with micron-size thickness have minute thermal expansion even with severe temperature differences. Additionally, solid lubricant coatings that were studied by SR&DB [80, 82, 83] were developed more than 15 years ago; hence they do not reflect recent developments and potential of high bearing thin polymeric-based coatings.

Polycarpou and collaborators have been investigating different advanced bearing grade polymeric coatings, including PTFE-, PEEK- and ATSP-based coating. Applications include harsh working conditions, such as oil-less air-conditioning compressors, and tilting pad bearings with three-body abrasive wear in electrical submersible pumps (oil&gas applications), among others [18, 45, 87]. Among the investigated coatings, ATSP-based coatings demonstrated very favorable tribological

performance under room temperature as well elevated (up to 260 °C) temperatures. However, there has been no tribological data of ATSP-based and PEEK-based coatings under cryogenic conditions. This paper presents tribological performance of ATSP-based coating at room temperature, -40°C, -100°C and -160°C obtained by modifying an existing tribometer for cryogenic testing conditions. PEEK-based coatings were tested under identical testing conditions to compare their performance.

3.2 Experimental

3.2.1 Specialized cryogenic tribometer

High Temperature Tribometer (HTT), as shown in **Figure 21(a)**, which was designed for tribological experiments up to 1000 ºC under versatile pin-on-disk configurations, such as ball-on-disk in **Figure 21(b)**, curve pin-on-disk in **Figure 21(d)** and also flat pin-on-disk. The tribometer was modified by implementing an in-house-built cryogenic test stage that expanded the testing temperatures down to -196°C in liquid nitrogen or other higher temperature with ±3°C accuracy. As shown in **Figure 21(c)** of liquid and gas nitrogen pipes for the cryogenic stage, the cooling process of the test chamber was started by injecting nitrogen gas inside the chamber for 10 minutes to evacuate the ambient air and the moisture; then using a control valve, liquid nitrogen was allowed inside the test chamber whose evaporation could absorb heat and reduce the temperature inside the chamber. The chamber temperature was directly related with the

evaporation rate of liquid nitrogen in the evaporator, as shown in **Figure 21(d)**; thus the temperature could be set by adjusting the valve to set the liquid nitrogen flow rate. The modified cryogenic tribometer has the same ability as mentioned in chapter 2: a unidirectional movement, as shown in **Figure 21(b)**, with speed up to1000 rpm; and oscillatory motion, as shown in **Figure 21(d)**, with frequency up to 5 Hz. Force transducers that are connected to the pin holder measure in situ normal and friction forces which yield the in situ coefficient of friction (COF).

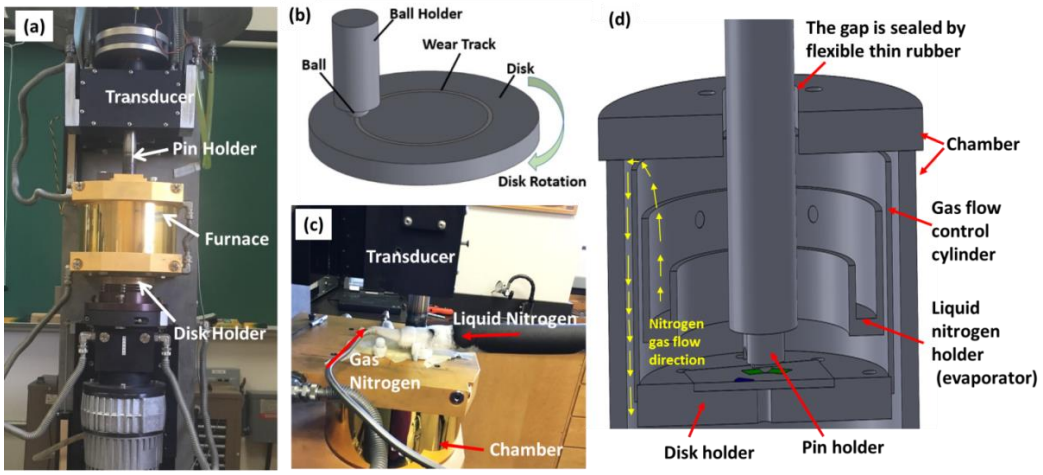

Figure 21 Specialized cryogenic tribometer, (a) Unmodified HTT, (b) ball-on-disk experimental configuration, (c) liquid and gas nitrogen pipes and (d) schematic of cross section for cryogenic experimental stage

3.2.2 Samples

Two oligomeric systems, namely carboxylic acid end-capped oligomer CB2 and acetoxy acid end-capped oligomer AB2, are used as the precursors for the ATSP powder

material and then coating. The following process of producing the coating is the same as described in chapter 2. For comparison, a commercial PEEK/PTFE (1704 PEEK/PTFE®) coating with a similar thickness of 35μm which is also deposited on cast iron disk by an authorized applicator (Southwest Impreglon) was also investigated. Photographs of the coatings on the cast iron disks are shown in **Figure 22**. The surface roughness of ATSP and PEEK/PTFE coatings are 3.1μm and 1.6 μm, respectively, and were measured using a KLA –Tencor profilometer.

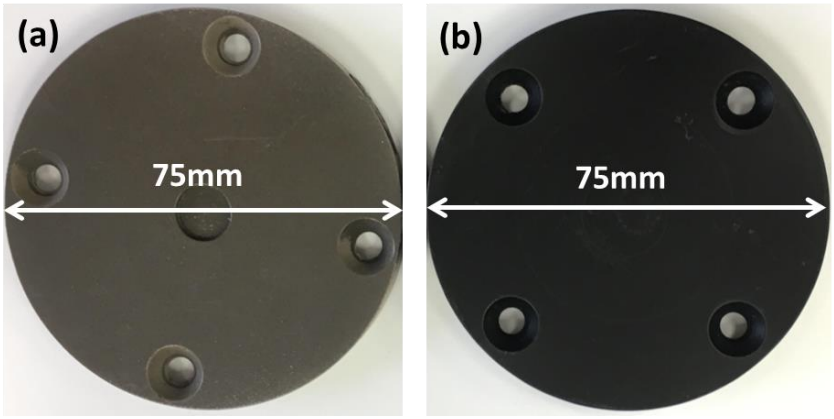

Figure 22 Photographs of coatings on cast iron disks, (a) ATSP, (b) 1704 PEEK/PTFE.

316 stainless steel balls with a diameter of 6.35 mm were used as the counter surface for ball-on-disk experiments. Before each experiment, the coatings and steel balls were immersed in isopropyl alcohol, and acetone, respectively. Using an ultrasonic cleaner for 10 minutes at 50ºC, any artificial contamination was removed from their surfaces. Finally, all samples were dried using a hot air blower.

3.2.3 Experimental methodology

As shown in **Table 3**, ATSP coating experiments were performed at four different temperatures: 23ºC (room temperature, RT), -40ºC, -100ºC and -160ºC; with 0.25m/s sliding speed, test duration of 5000 cycles, and normal load of 5 N, which applied an initial Herzian contact pressure of 110 MPa at RT. The sliding diameter was varied from 20.3 mm to 35.6 mm, thus 5000 cycles or 10000 cycles were applied for the tests and then each position of the coatings had the same times of wear paths and the wear on the coatings would be comparable with each other. To investigate the effect of normal load on the obtained data, experiments were also conducted at 23ºC and -160 ºC with identical sliding velocity and normal load of 10 N for two test durations. To ascertain the repeatability of the obtained data, all the experiments were conducted at least 2 times. Note, the elastic modulus and Poisson's ratio were 3.2 GPa and 0.4 respectively for both ATSP and PEEK/PTFE coatings [10].

Table 3 Experimental conditions for the cryogenic tribological experiments

Coating	Temperature (ºC)	Normal load (N)	Sliding velocity (m/s)	Initial Hertzian contact pressure at RT (MPa)	Sliding cycles
ATSP	23(RT), -40, -100, -160	5	0.25	110	5000
	23(RT), -160	10	0.25	139	5000, 10000
PEEK/PTFE	-40, -160	5	0.25	110	5000

After the tribological experiments, a contact profilometer (KLA –Tencor) was used to perform several scans across the wear tracks to obtain the exact profile of the wear tracks. An SEM (Tescan VEGA) was used to examine the wear track on the polymeric coatings and the 316 SS balls. The EDS analysis was carried out by JEOL JSM-7500F with 10KV voltage.

3.3 Tribological experimental results

Figure 23(a-b) show the in situ COF vs. sliding cycles for the ATSP coatings at different temperatures and at 5 N and 10 N normal load experiments, respectively. As shown in **Figure 23(a)** the COF of the ATSP coatings was stable for the duration of the experiments, taking different values, depending on the temperature. **Figure 23(b)** shows

that the COF values at RT temperature and 10 N normal load are stable and it is lower than its counterpart experiments conducted at 5 N normal load. For the 10 N normal load experiments at -160°C, the initial COF value was similar to the 5 N normal load at -160°C. However, for the 10 N experiments, after some sliding distance, the COF exhibits a sudden transition (reduction), and then increased slightly, as shown in **Figure 23(b)**. For the experiments with relatively stable COF values through the experimental duration, it is postulated that their contact condition did not significantly change during the experiments. For the 10 N normal load at -160°C, the sudden change in the COF could be attributed to transfer film formation during the experiments, as it will be substantiated using SEM.

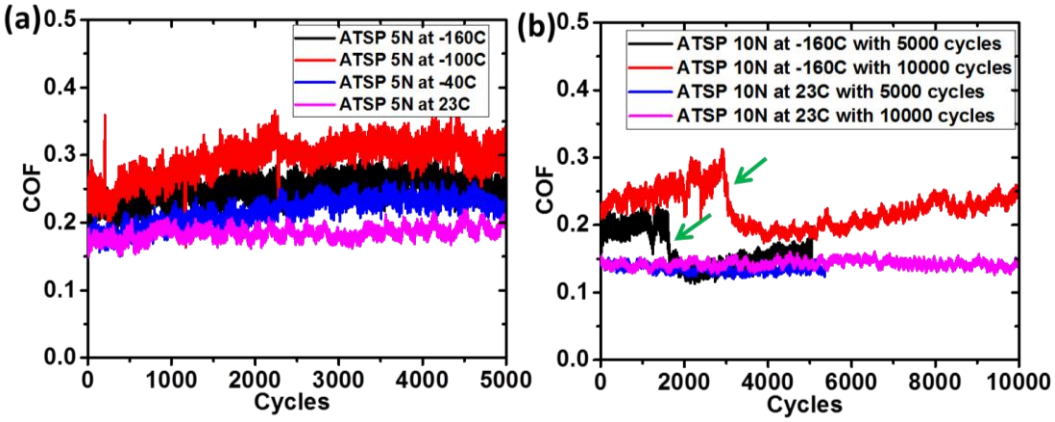

Figure 23 In situ COF vs. cycles at different temperature for ATSP coatings, (a) 5 N and (b) 10 N normal load

Figure 24 presents the COF vs. sliding cycles for PEEK coatings at -40°C and -160°C for a normal load of 5 N. In both cases, the COF was low at the beginning of the experiments (during run in period) but increased substantially after about 2000 cycles. The low COF during the run in period followed by an increasing trend is similar to the COF of polyamide sliding in liquid nitrogen [78], and is due to run-in that the contact surfaces have not reached the steady contact conditions at very beginning.

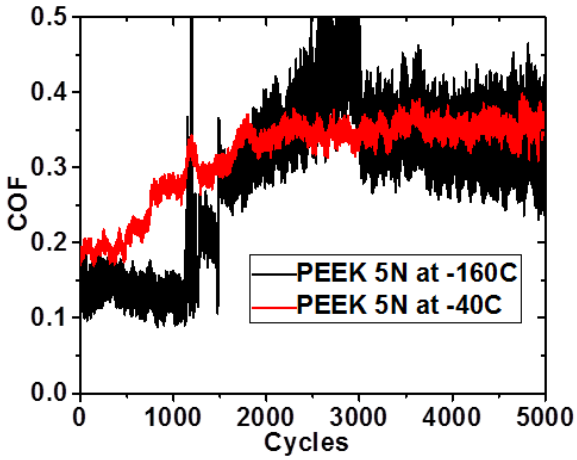

Figure 24 In situ COF vs. cycles with 5 N normal load for PEEK coatings at -40ºC and -160ºC

Figure 25(a) summarizes the COF values obtained for ATSP and PEEK coatings at different loads and temperatures. The reported COF values were the average values from 4000 to 5000 cycles, which exhibited stable sliding states. For the ATSP coatings with 5 N normal load, the COF exhibited a decreasing trend when the temperature increased from -100°C to RT, which was consistent with earlier studies of ATSP

coatings at higher temperature range from RT up to 260°C [88]. When the temperature increased from -160°C to -100°C, the COF increased slightly. Around -100°C, the COF reached a maximum, which was consistent with other data reported for PTFE material in cryogenic conditions that showed a peak in COF value around -60°C [85]. Under the higher 10 N normal load the COF decreases, which was also consistent with other studies at higher temperatures [64, 88]. The PEEK coatings showed 68% and 35% higher COF, compared with the ATSP coatings at -40ºC and -160ºC respectively.

Figure 25(b) shows typical wear scans across the wear tracks of the two coatings after the 5 N normal load at -160°C experiments. Clearly, wear is too small to be measured, compared to the surface roughness, which was also observed in the SEM analysis, similar with other research[78]. For the PEEK coatings, it had a clear wear scar under 5 N normal load at RT and higher temperatures [88], as shown in **Figure 25(c)** of wear scan of PEEK after 5N at RT test. Testing its performance at lower temperatures proved immeasurable wear. This observation could be explained by the decrease in the polymer molecules mobility at low temperatures, which result in an increase of their toughness [89]. Note that ATSP coatings have a noticeably larger roughness, compared to the PEEK coatings.

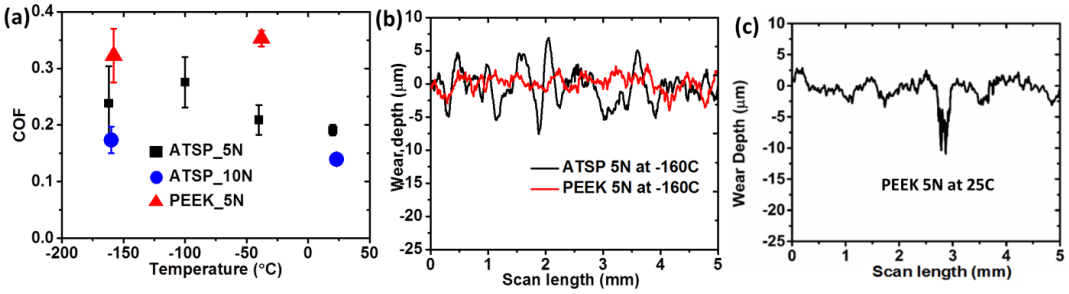

Figure 25 COF and wear after pin-on-disk tests, (a) COF vs. temperature, (b) wear scans after -160°C tests (c) wear scan of PEEK after RT test with 12000 cycles

3.4 SEM analysis

The SEM images of wear tracks of the ATSP coatings after experiments at different temperatures under 5 N normal load are shown in **Figure 26**. At 50X magnification, as shown in **Figure 26(a), (c), (e)** and **(g)**, the wear scar is barely visible that justifies the "zero wear" obtained from wear track scans illustrated in **Figure 25(b)**. Comparing the SEM images at 500X magnifications of the samples tested at RT and cryogenic temperatures, reveals the negligible "zero" wear in the former and visible wear in the latter.

As shown in **Figure 26(d)** and **(h)** at temperatures -40°C and -160°C, respectively, there are micro cracks formed in the wear scars, but no wear or material removal on the peaks of the coating. The micro cracks also happened in other tribological studies under cryogenic conditions [67, 77]. The origin of such micro cracks can be attributed to two major factors. First, is the extremely high contact pressure generated on these peaks. This is shown in **Figure 26(d)**, where the contact spot on the

peak has a radius of about 70 µm, with 5 N normal load, the average contact pressure was 325 MPa, which exceeded twice the compressive strength (160 MPa) of ATSP at RT. Second, there is an increase in the elastic modulus and a decrease in the break point of deformation of polymer materials at the cryogenic temperatures [89]; Thus, rendering the coating more rigid and brittle in these cryogenic conditions. Other locations undergo lower contact pressures that could not initiate or facilitate the propagation of a crack. At a temperature of -100°C, apart from the formation of the micro cracks, another active wear mechanism was material removal due to the sliding contact of the steel ball. The more clear wear scratches in the SEM at -100°C in **Figure 26(f)** was in agreement with the higher COF at this temperature.

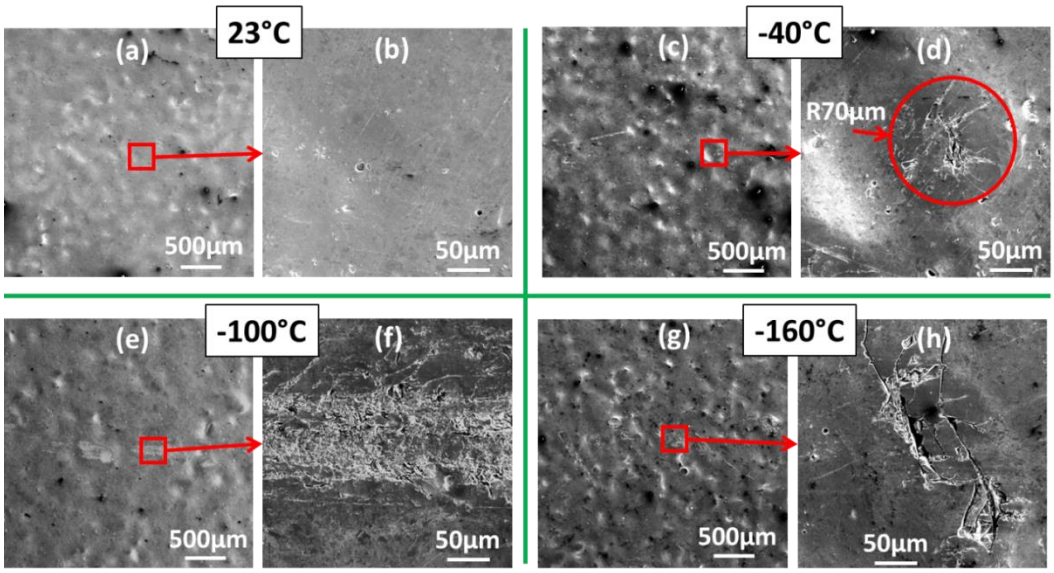

Figure 26 SEM images of the wear tracks of the ATSP coatings after experiments at different temperatures under 5 N normal load: (a, b) 23°C, (c, d) -40°C, (e, f) -100°C, (g, h) -160°C.

Figure 27 shows the SEM imgages of the PEEK coatings after cryogenic tests. Similar to **Figure 25(b)**, a burnishing mark with negligible material ploughing or wear is observable. Propgation of wear cracks on the ATSP coating and their absence on PEEK coating could be ascribed to more uniorm pressure distrubution on the PEEK surface due to its more even topography. This could be seen by comparing the contact area of ATSP coating and PEEK coating at a temperature of -40°C in **Figure 26(d)** and **Figure 27(b)**. In addition, the width of the wear track (deeper color) for PEEK was bigger than that of ATSP at temperature of -40°C; thus PEEK should have lower elastic modulus at the same cryogenic temperature, which made it easier to deform and have bigger width of wear track.

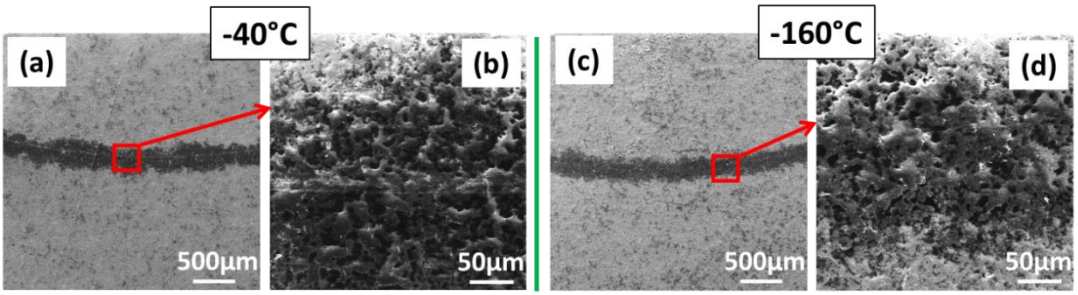

Figure 27 SEM images of the wear tracks of the PEEK coatings after experiments at different temperatures under 5 N normal load: (a, b) -40°C, (c, d) -160°C.

Figure 28 shows the SEM images of the wear tracks of the ATSP coatings after experiments with the higher contact pressure using 10 N normal load. This higher contact pressure caused clear burnishing on the peaks of the coating, as shown in **Figure**

28(b) and **(d)**, while the 5 N force only incurred negligible burnishing at RT as shown in **Figure 26(b)**. The longer duration experiments (10000 cycles), as shown in **Figure 28(d)**, smoothened the contact area, and also produced micro cracks due to the fatigue of material. At temperature of -160°C, the cracks that occurred at RT under 5 N normal load in **Figure 26(h)** were absent in samples tested at -160C with 10 N normal load, as shown in **Figure 28(f)** and **(h)**. One could expect more severe crack propagation at higher loads due to its higher contact pressure. On the other hand an opposing effect of the higher load could be restructuring the already formed cracks and mending the surface by reshaping the topography with high pressure and the interchain transesterification reactions of ATSP material[90]. The mobility of the polymer influences the tribological properties strongly [91]. It is noteworthy that higher contact force resulted in lower COF in the present work, in agreement with the literature [64, 88]. Higher contact pressure causes higher shear stress at the contact surface and thus removal of the polymer more easily [92] and thus can reduce COF. It is clear that the formation of transfer film is related with the mobility of the polymers. The clear transfer layer formed on the steel ball at -160°C with 10 N normal load as shown in **Figure 29(a)**. Nonetheless, there was no visible transfer layer formed with the lower contact pressure of 5 N normal load at same temperature, as shown in **Figure 29(d)**. Thus we can conclude that higher contact pressure on the polymer surface can improve the mobility of polymers.

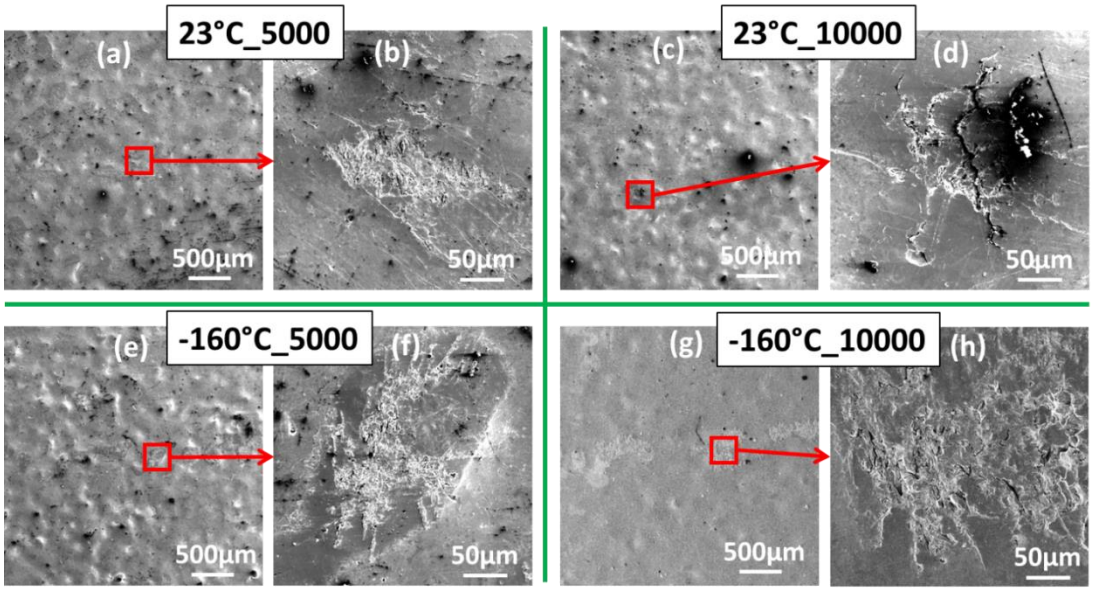

Figure 28 SEM images of the wear tracks of the ATSP coatings after experiments at different temperatures and durations with 10 N normal load: (a, b) 23°C, 5000 cycles, (c, d) 23°C, 10000 cycles, (e, f) -160°C, 5000 cycles, (g, h) -160°C, 10000 cycles.

Plots of in situ COF vs. number of cycles in **Figure 23(b)** show that only the experiments with 10 N normal load at -160°C experienced a sudden decrease of COF during the experiments. This could be explained by the gradual development of a transfer film on the steel balls. To better illustrate this transfer film, **Figure 29** shows the SEM images of wear tracks on the steel balls after 5000 sliding cycles at -160ºC. At normal load of 5 N at -160°C after 5000 cycles, the steel ball did not have a considerable transfer film as shown in **Figure 29(d)**, while a clear transfer film is visible at 10 N normal load at the same temperature as shown in **Figure 29(a)**. The EDS analysis in **Figure 29(b-c)** confirmed that the black film on the steel ball as in **Figure 29(a)** is the polymer transfer film that was full of carbon. This is in agreement with the literature,

that showed higher contact pressures could accelerate the formation of a continuous transfer film [92]. Note that it is common to develop a transfer film on the metal sliding surface for metal vs. polymer tribological pairs at normal temperature [15, 17, 93, 94] and low temperatures [78]. However, the transfer film developing rate is relative to sliding distance [15, 93], thus for other conditions in this study that had no substantial transfer film on the steel balls, extending the test duration might help the formation of a more developed transfer film. For PEEK coating, without transfer film at -160°C with 5N normal load after 5000 cycles as shown in **Figure 29(e)**, its COF was relatively high as indicated in **Figure 24**.

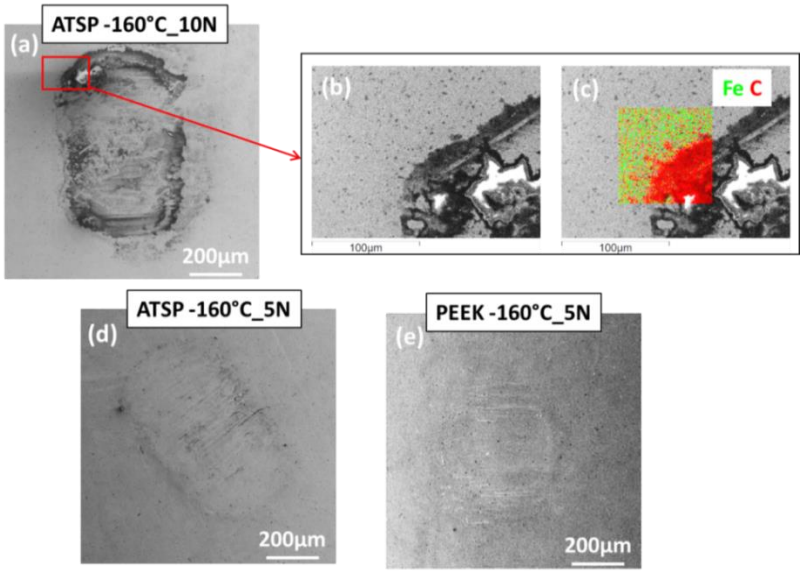

Figure 29 Wear scar on 316 SS balls after experiments under different conditions: (a) ATSP coating at -160°C with 5 N normal load and 5000 cycles, (b) ATSP coating at -160°C with 10 N normal load and 5000 cycles, (c) PEEK coating at -160°C with 5 N normal load and 5000 cycles.

3.5 Conclusion

A cryogenic tribological study was carried out for thin high bearing ATSP and PEEK-based coatings under different temperatures and loading conditions by using an in-house-built cryogenic stage on an existing tribometer. Combined with earlier research [88], this study helped to build up the full map of the tribological performance for ATSP coating from -160°C to 260°C. From the current cryogenic study, the following conclusions could be drawn:

a) For ATSP coatings under medium contact pressure of MPa (5 N normal load), in general, the COF decreased with increased temperature, with a peek value -100°C.
b) Both ATSP and PEEK coatings showed immeasurable wear by using wear scans, obtained using a contact profilometer. PEEK coatings under medium contact pressure showed 68% and 35% higher COF, compared to ATSP at -40ºC and -160ºC, respectively.
c) ATSP coatings developed micro cracks on the peaks of the surface due to the high contact pressure on the peaks caused by cryogenic temperatures.
d) PEEK coatings did not show cracks because of lower contact pressure came from its lower elastic modulus, which makes it easier to deform.
e) Higher contact pressures (10 N normal load) accelerate the development of transfer film that could reduce the COF favorably.

4. ADVANCED POLYMERIC COATINGS FOR TILTING PAD BEARINGS WITH APPLICATION IN THE OIL AND GAS INDUSTRY[2]

After the dry sliding investigation of polymer coatings from cryogenic to high temperature in chapter 2 and chapter 3, this chapter and following chapters investigate the tribological performance in lubricated conditions for the polymer coatings. Under extreme operating working conditions, the oil film in hydrodynamic bearings may get destroyed, resulting in mixed and boundary lubrication conditions; subsequently, the bearing surfaces might seize and cause catastrophic failure, rendering the machine non-operable. To address these extreme working conditions, three advanced coatings are proposed in this chapter: PTFE based, PEEK based and ATSP based coatings. A specialized high pressure tribometer, with a pin-on-disc configuration, combined with boundary/starved lubrication, was utilized to simulate the tilting pad bearing's severe working conditions encountered inside an Electrical Submersible Pump used in the oil and gas industry. Two sets of experiments, scuffing (step load) and constant load wear experiments were carried out. The coatings exhibited excellent performance compared to bare substrate materials. Scuffing experiments showed that all three coatings exhibited

[2] Reprinted with permission from "Advanced polymeric coatings for tilting pad bearings with application in the oil and gas industry." by Lan, P., Meyer, J.L., Vaezian, B. and Polycarpou, A.A., Wear, 354–355(2016): pp. 10-20, Copyright 2016 by Elsevier.

improved scuffing performance and wear experiments showed that the coatings exhibit relatively low coefficient of friction and low wear rate. Among coatings investigated, ATSP coating exhibited the best wear resistance.

4.1 Introduction

Hydrodynamic bearings are commonly used due to their high speed, high load capabilities and low friction [95]. Full film lubrication is expected for a hydrodynamic bearing, however severe working conditions could be encountered, such as during start and stop, lack of lubricant, elevated temperature and high load conditions. These severe conditions are likely to penetrate the oil film, resulting in mixed and boundary lubrication conditions [46, 96]. White metal is dimensionally stable and easy to repair, and is widely used in hydrodynamic bearings (e.g., Babbitt). On the other hand white metal has a low melting point, which restricts its maximum life (combination of speed and load) [97]. Under severe working conditions, direct contact between the white metal and the rotating shaft or runner could yield frictional heat, leading to severe adhesive wear and burn damage of the white metal surface, with the possibility of catastrophic failure [46].

In many industries there is a need for more compact machines working under higher power densities, and thus resulting in severe working hydrodynamic bearing conditions [98]. Recent advances in subsea and deep-sea exploration require the

development of next generation of interface materials, working under aggressive operating conditions, including higher temperatures, higher pressures and limited liquid lubrication. For example, in the case ESPs in oil wells, which typically have 10 years or longer productive life [99], replacing of the ESP is a time consuming and expensive procedure, associate with oil production loss [100]. The thrust bearing in ESP's seal chamber and electrical motor could fail because of excessive load, vibration and high temperature [101, 102]. So it is important to research and implement new bearing materials, which could sustain higher loads and higher temperatures, and potentially extend ESPs service life and reduce maintenance costs.

PTFE exhibits outstanding properties such as low coefficient of friction, high ductility, broad working temperature, anti-seizure properties and inertness to chemicals. These properties make PTFE an efficient substitute for white metal in tilting-pad thrust bearings [98, 103, 104]. Using laboratory experiments and finite-element analysis, Glavatskih and other researchers examined the application of PTFE-faced hydrodynamic thrust bearings [105-108] and found that PTFE composites have good thermal insulation so that pad thermal crowning is reduced. This allowed them to operate with lower power loss, and slightly higher collar temperatures, compared with similar Babbitt bearings. Besides these advantage, PTFE based composites showed much better wear resistance compared to Babbitt [46, 109]. The PTFE composites on the PTFE-faced pad are in bulk form, with a thickness of over 1 mm. However, the polymer has a much higher thermal expansion, and thus the thick polymer is not able to be applied in high

precision conditions, such as journal bearings which need to retain the dimension very well. These problems could be addressed if the polymer is in a thin layer coating on a metal substrate, in which case dimensional stability and conventional bearing clearances are retained[110]. Also, using thermo-elasto-hydrodynamic (TEHD) analysis of thrust bearings with PTFE-faced pads, Fillon showed that a decrease of the PTFE layer would help increase the oil film thickness and decrease oil film maximum temperature [98].

Despite the published research on the application of polymer materials on hydrodynamic bearings, the literature is scarce for thin polymeric-based coatings in hydrodynamic bearings. Since PTFE and other polymer materials show cold creep and high wear rate in pure format, researchers have tried to improve their tribological performance by adding different fillers and reinforcements in pure polymers [14, 17, 20, 21, 24, 46, 109, 111]. PTFE-based, PEEK-based and ATSP-based bulk materials as well as thin (10's of micron thick) coatings were shown to improve the tribological performance in air-conditioning and refrigeration compressors [14, 24, 32]. In this work, three different metal-backed thin coatings, which all include PTFE, were procured and tested under conditions of thrust tilting-pad bearing, which worked as a presentative of hydrodynamic bearings. The tribological performance of these coatings was investigated under boundary lubricated pin-on-disc experimental conditions, simulating extreme working conditions of the tilting pad thrust bearing in ESPs. Because for thin coatings, their resistance to abrasive particles and high temperature in ESPs are also critical, we will explore these harsher working conditions in our future research.

4.2 Experimental

4.2.1 High pressure tribometer (HPT) and experiment configuration

Figure 30 (a) shows a photograph of the HPT, and the simulated pin-on-disc configuration is depicted in **Figure 30** (b). It has the following capabilities: closed loop normal load control up to 4,500 N; environmental chamber pressure control from 0.0014 MPa to 1.72 MPa; closed loop temperature control from -10°C to 120 °C; measures in situ friction force, normal force, and near contact temperature; and performs unidirectional and oscillatory experiments. Hydrodynamic bearings are most prone to failure during transient operating conditions, especially at the stop/start stage [109, 112]. Shown in **Figure 30** (c) is a schematic of a tilting pad thrust bearing, under extreme working conditions such as high load, stop/start, and lack of lubrication or vibration, in which case the tilting pad and the runner contact each other.

The boundary lubricated pin-on-disc experimental configuration simulates these severe conditions. The disc is made out of the bearing pad material and the pin from the collar material. The disc was mounted on the upper rotating spindle and the pin was fixed on the pin holder, which is directly attached on a 6-degrees-of-freedom force transducer. Normal load and rotation of the disc were input parameters to test the tribological performance of the disc and pin.

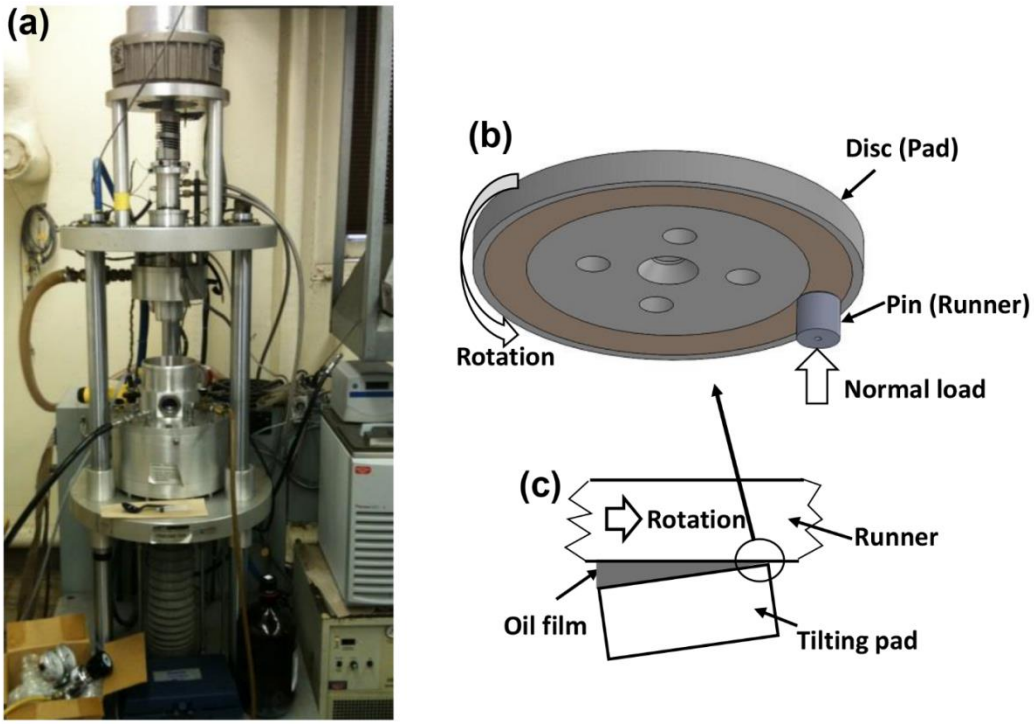

Figure 30 HPT and experiment configuration, (a) photograph of the HPT, (b) schematic of pin-on-disc configuration, (c) thrust tilting pad bearing.

4.2.2 Samples

Three commonly used tilt pad body materials were selected as disc substrates, namely 304 stainless steel, copper chrome C18200 (denoted as C182), and tin bronze C93200 (denoted as C932). 4130 steel was selected as the collar material, which was made to the counter pin material. Three coatings, namely ATSP based, PEEK based and PTFE based were deposited on the pad body materials C182 and C932. The coatings were not coated on the stainless steel substrate because stainless steel showed the worst performance when tested against 4130 steel.

Two types of oligomeric system, namely CB2 and AB2, which have carboxylic end groups and acetoxy end groups, are the precursors of ATSP. The coating composition is the same as in Chapter 3. ESD method was applied to spray the blended powder on the sand blasted C182 and C932 disks. Then the disks were cured under 270°C for 30 minutes in an oven with convective air. The final thickness of the ATSP coating was around 40μm.

PEEK based coatings (1704 PEEK/PTFE®) and PTFE based coatings (DuPont TEFLON® 958G-414) were deposited on C182 and C932 by two authorized applicators from Southwest Impreglon, Inc. and Orion Industries, respectively. For certain both of these coating contain PTFE, but their detailed compositions were unknown, as they are proprietary. Photographs of the substrate disks and coatings are shown in **Figure 31**. Also, shown in the C932 disc image is a 6.35 mm diameter 4130 steel pin that was used as the counter surface. On the backside of the pin, there is a small hole for insertion of a miniature thermocouple to measure the near contact temperature (NCT) about 2 mm below the sliding surface. Before each experiment, the coated discs were immersed into isopropyl alcohol and the metal samples were immersed in acetone in glass containers, then the glass containers were placed in an ultrasonic cleaner for 10 minutes at 50ºC temperature.

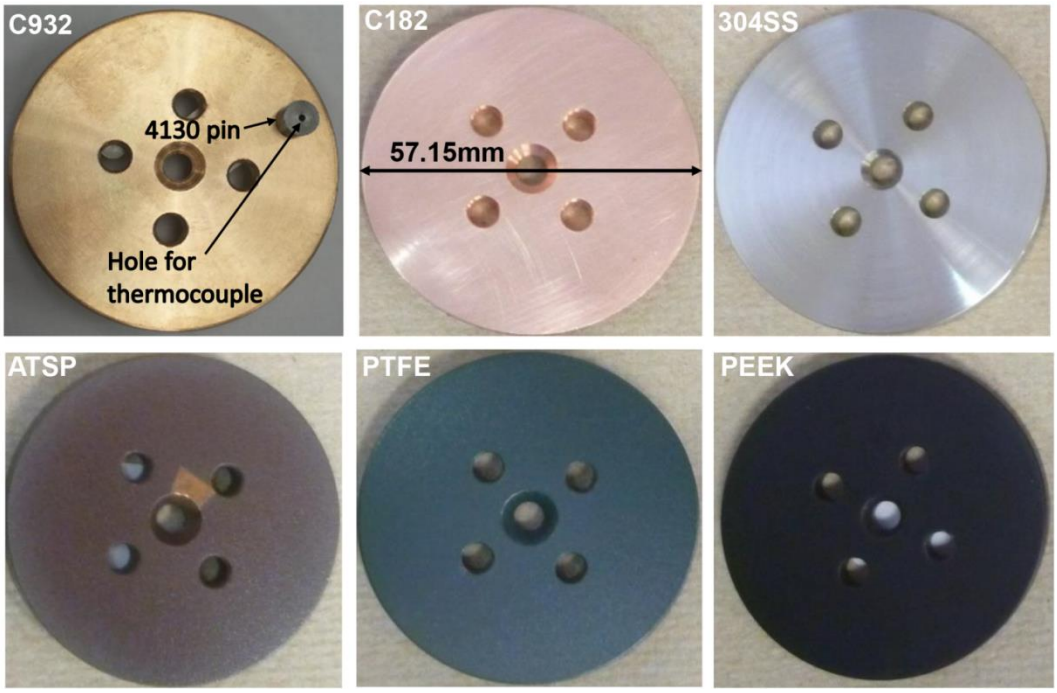

Figure 31 Photographs of the substrate materials and coatings.

The properties of the coatings and surfaces involved in this research are summarized in **Table 4**. All coatings' surfaces are rougher than the substrate material with ATSP coating having the highest roughness. Hardness was measured by Nano-mechanical test instrument (Hysitron TI Premier) with a high load Berkovich probe.

Table 4 Materials and coatings properties.

Materials	Rq(μm)	Hardness (GPa)	Thickness(μm)
ATSP (95%CB2AB2+5%PTFE)	3.3	0.25	40±5
PEEK based (1704 PEEK/PTFE®)	1.9	0.28	50±5
PTFE based (DuPont 958G-414®)	2.0	0.29	30±5
304 Stainless steel	0.3	3.46	___
Chrome Copper C18200	0.6	2.01	___
Tin-Bronze C93200	0.7	1.22	___
4130 Steel (Pin)	0.16	2.48	___

4.2.3 Experimental design

As shown in **Table 5**, there were two sets of experiments: load-to-failure or scuffing experiments and constant load wear experiments. All experiments were performed under ambient pressure, room temperature (23°C) and boundary lubrication conditions. Boundary lubrication was achieved using 25 mg of ISO 46 grade mineral oil applied on the pin surface before every experiment. Scuffing experiments were performed to determine the maximum critical load that the interface can sustain before catastrophic failure [113]. The constant load experiments were performed to study the wear resistance, wear mechanisms and measure the coefficient of friction (COF) and wear rate. A nominal contact pressure of 4.7 MPa was applied every one minute for the

scuffing experiments and 13 MPa of contact pressure was applied for the constant load experiments. A scuffing experiment is terminated when scuffing occurred, as seen by a sharp increase of the COF and/or a sharp increase in the NCT. For constant load experiments, different sliding distances were carried out. The shortest experiments were 4.3 Km (30 min at 2.4 m/s sliding velocity) to study the run in performance of bare materials and coatings. Longer experiments of 25.9 Km (180 min at 2.4 m/s) were performed to study the long-term durability of the coatings. The best performing coating, as far as wear is concerned (ATSP on C932), was also tested for longer experiments to determine its long-term limit/life: Three stages of sliding distance: 0 to 25.9 Km, 25.9 Km to 77.8 Km, and 77.8 Km to 155.5 Km. These experiments were also used to verify the durability of ATSP coating and to study the wear performance under different sliding distances/speeds. The sliding speed was 2.4 m/s except for stage 3 (77.8Km to 155.5Km) of ATSP on C932, which was 3.6 m/s.

Table 5 Experimental conditions at room temperature and boundary lubrication.

Experiment type	Load (MPa)	Distance (Km)	Speed
Scuffing	4.7 /min	To scuffing	2.4 m/s (1000 rpm)
Wear	13	4.3 Km, 25.9 Km,77.8 Km (ATSP on C932), 155.5 Km (ATSP on C932)	2.4 m/s (1000 rpm) 3.6 m/s (1500 rpm) for ATSP on C932 from 77.8 Km to 155.5 Km

After the tribological experiments on the HPT, the cross section profiles of the wear tracks were measured using long scans on a contact profilometer. From the wear track profiles, the wear volume and wear rate was then readily calculated. An optical microscope and a scanning electron microscope (SEM) were used to measure the surface morphologies inside and outside the wear tracks to understand the wear mechanisms of the coatings.

4.3 Tribological results and discussion

4.3.1 Scuffing experiments

Figure 32 shows the in situ normal load, in situ COF, in situ NCT and the wear scans of the scuffing experiments for the three different coatings on C182 substrate material, as well as the experiment using bare C182 substrate material. The sliding speed was 2.4 m/s and the load was increasing 140 N every one minute, which was 4.7 MPa per minute (see **Table 5**). Experiments would be terminated when scuffing occurred manifested by a sharp increase of the COF and/or a sharp increase of the NCT. In all cases, except PEEK coating on C182, an increasing of the COF with scuffing was observed. Note that for PEEK coating on C182, even when the contact force reached 2600 N (86.7 MPa) and the NCT reached more than 300°C, the COF was still stable. This is likely due to the coating material acting as a third-body solid lubricant. For PEEK coating, when the sliding distance was around 2200 m, the NCT decreased

sharply due to the coating being almost penetrated and the pin contacting the substrate material. Before the pin contacted the substrate material, the polymer coating worked as a heat insulator and the frictional heat flowed slowly to the disk. When the coating was penetrated, the heat went from the pin to the disk quickly and the NCT dropped quickly. ATSP coating on C182 also showed this NCT drop phenomenon.

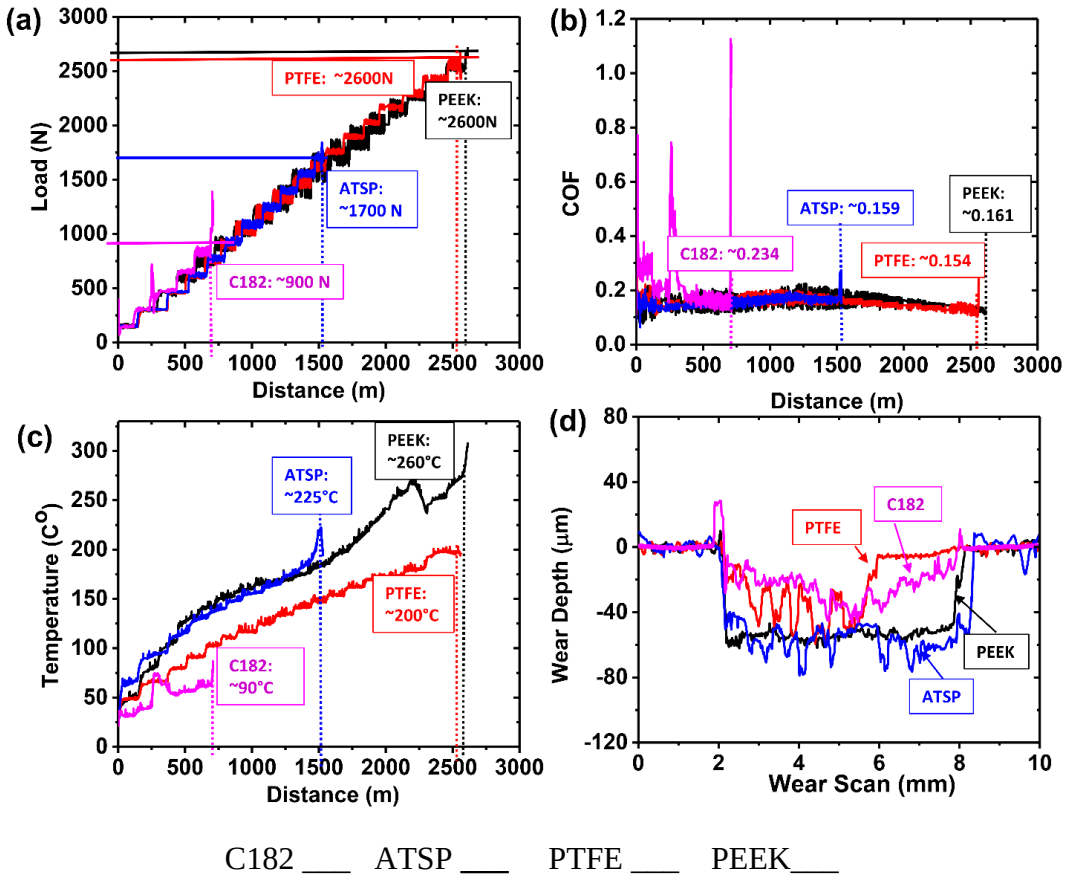

Figure 32 In situ scuffing experiments and wear scans of coatings on C182 and bare C182. (a) Scuffing load vs. sliding distance, (b) COF vs. sliding distance, (c) NCT vs. sliding distance, (d) disc wear scans.

Figure 33 shows a summary of all the scuffing experiments. Bare tin bronze C932 showed the highest scuffing load of 1700 N (56.7MPa) among the three bare materials. Actually for C932, it had the deepest average wear depth (81.4μm) among all experiments after scuffing. And C932's scuffing load was determined by the sharp increase of the temperature instead of sharp increase of COF; this was because the COF was always low and relatively stable due to the loose texture of this material. Bare 304 SS failed almost immediately against 4130 steel counter-surface with a scuffing load of 150 N (5 MPa). Since 304 SS / 4130 steel is not a good contact pair in this experiment setup, the 304 SS was not coated with any coatings in this research. All three coatings improved the scuffing load of the substrate materials. Coatings on C182 improved the scuffing load of C182, from C182's 900 N to ATSP's 1700 N, PEEK's 2300 N and PTFE's 2600 N. Coatings on C932 improved the scuffing load of C932, from C932's 1700 N to ATSP's 1850 N, PEEK's 2500 N and PTFE's 2450 N. This improvement is very important since these were thin films that once stressed significantly they were prone to delamination. Also, all coating's scuffing loads were much higher than the highest average working pressure of 3.5 MPa, calculated from a commercial thrust tilting pad bearing's maximum load and its pads surface area [114]. From this point of view, all coatings were a good choice for the application and their bonding strength to the substrate was acceptable. It should also be mentioned that ATSP, compared to PEEK and PTFE coatings showed a lower scuffing load, albeit significantly higher than the nominal operating pressure, due to delamination from the substrate material.

Improvement of the adhesion bonding of ATSP coatings to the substrates would alleviate this issue.

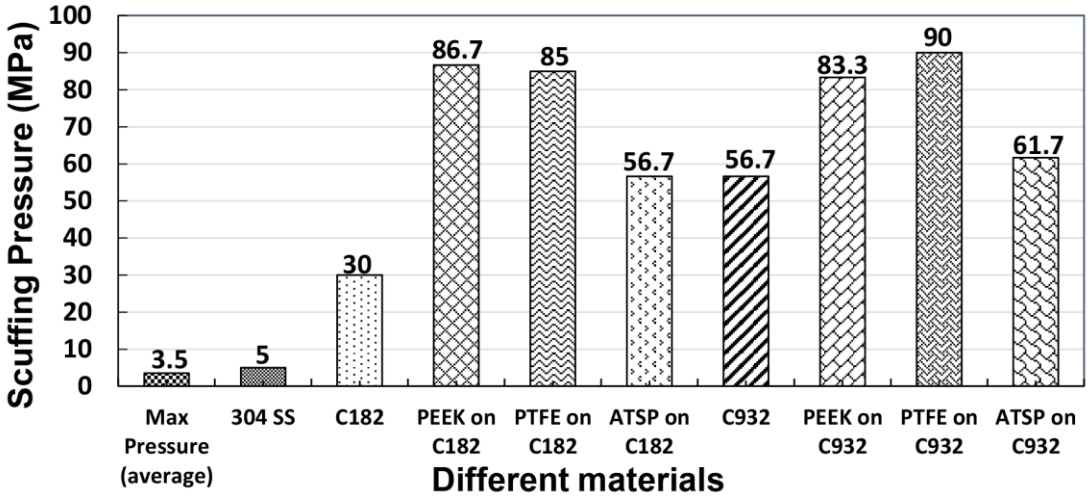

Figure 33 Scuffing pressure of different coatings and substrates.

4.3.2 Wear experiments: 4.3 Km sliding distance (30 min)

Figure 34 shows in situ 4.3 Km sliding distance constant load wear experiments at room temperature of the three coatings on C182 and C932, as well as the behavior of bare materials C182 and C932. From **Figure 34** (a-c), bare C182 showed the highest COF and deepest wear scar, compared to the coatings on C182. For bare C182, its COF and temperature were increasing with sliding distance, which is indicative of the diminishing effects of the minimal lubricant at the interface. Because of the self-lubrication property of the coatings, their COF and temperature were not increasing with sliding distance. Also, note that although bare C182 had the highest COF, it had the

lowest NCT due to the heat generated by friction between the contacting surfaces could be transferred to the disk easily, without polymer coatings acting as heat insulator. From **Figure 34** (c), the ATSP coating was the roughest, and it exhibited almost zero wear, showing only mild polishing on top of its peaks.

For the coatings on C932 substrate, their in situ performance and wear scans, as shown in **Figure 34** (d-f), had almost the same pattern as for the coatings on C182. Bare C932 had the highest COF but it had the lowest average wear depth, even though there was a deep wear grove (around 20 μm) for bare C932, as shown in **Figure 34** (f).

Figure 35 shows microscopic images of the wear tracks on the disks and counter pins for coatings on C932 after 4.3 Km sliding distance. Both PEEK and PTFE coatings showed abrasive wear grooves. For ATSP, because of its high roughness, the wear of the coating was mild polishing on top of its peaks.

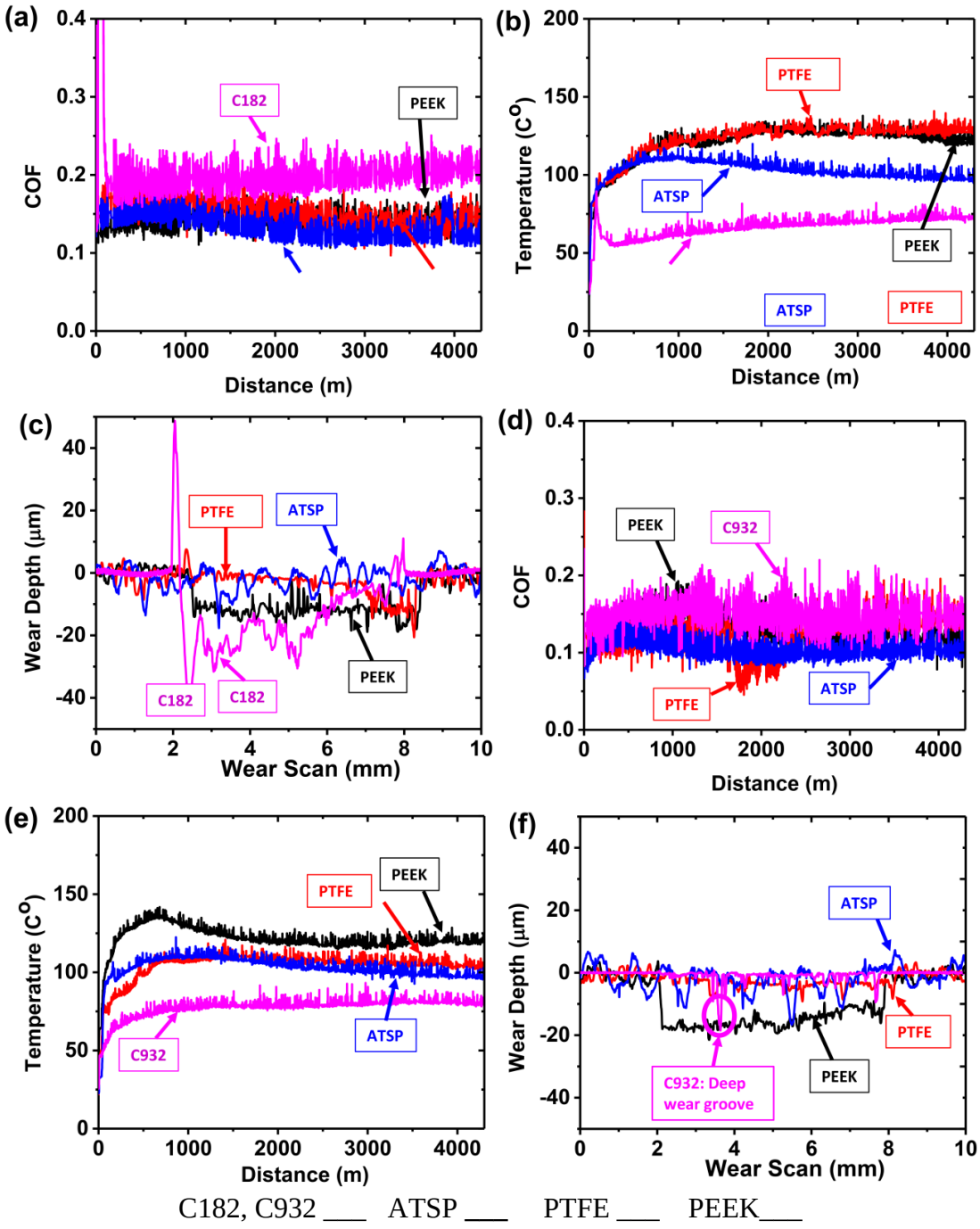

Figure 34 In situ 4.3 Km wear experiments. (a, b, c) in situ COF, NCT and wear scans of coatings on C182 and bare C182, (d, e, f) in situ COF, NCT and wear scans of coatings on C932 and bare C932.

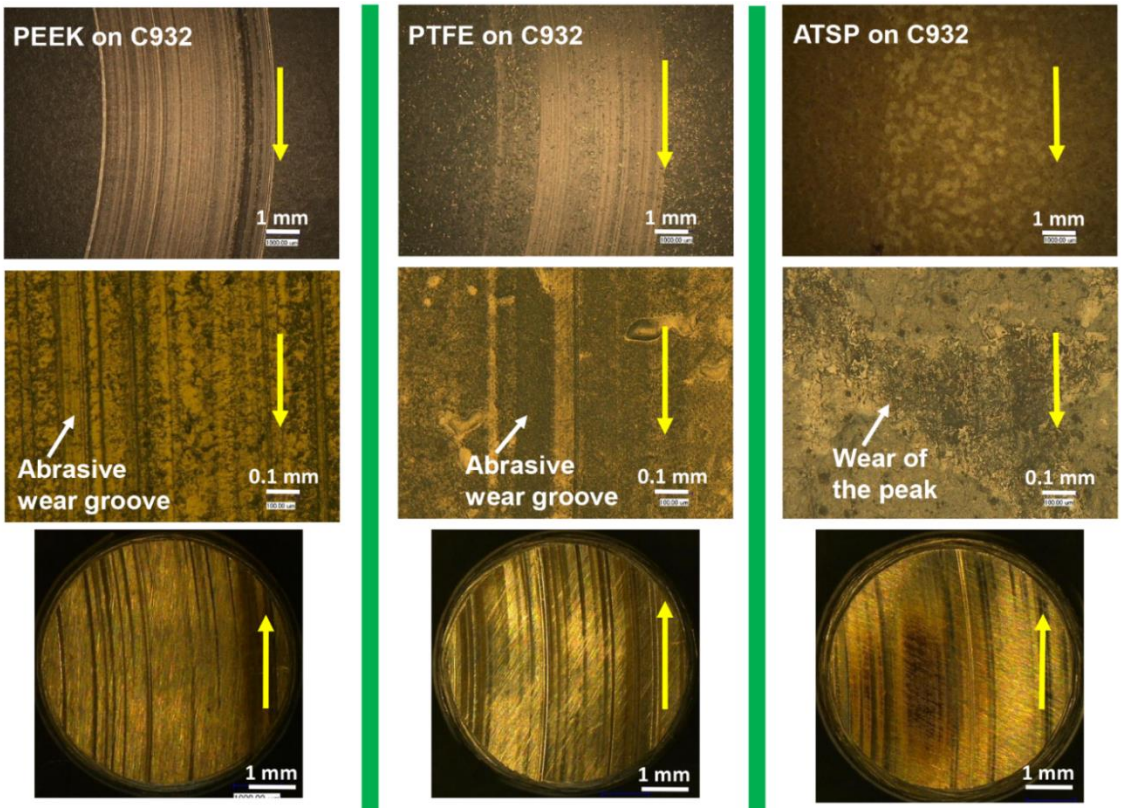

Figure 35 Microscopic images of wear tracks on disks and pins after 4.3 Km experiments on C932 substrate (top images: low magnification, disks; middle images: higher magnification, disks; bottom images: pins).

Figure 36 shows a summary of the COF vs. wear rate of the different coatings and substrate experiments. The labels with no underline indicate coatings on C182 substrate and bare C182 substrate. The labels with underline indicate coatings on C932 substrate and bare C932 substrate. For coatings on C182, ATSP coating exhibited the best performance, with the lowest COF of 0.136 and the lowest wear rate of 1.7×10^{-6} mm^3/Nm. PTFE had better wear resistance than PEEK, but PTFE's COF was slightly higher than PEEK's COF. For coatings on C932 and bare C932 substrate, bare C932 has

the lowest wear rate but highest COF and also deep wear groove, as indicated in **Figure 34** (f); ATSP coating also had the best performance among three coatings, with the lowest COF of 0.108 and the lowest wear rate of $1.4x10^{-6}$ mm^3/Nm; PTFE coating exhibited intermediate performance and PEEK coating had the highest COF and wear rate. Comparing the same coating on different substrates, their COF and wear rate were different due to the substrate's hardness influence, as well as the substrate/coating/lubricant interaction. The elastic deformation and compatibility of the coatings on harder substrate C182 appears to cause worse tribological performance compared to the coatings of softer substrate C932.

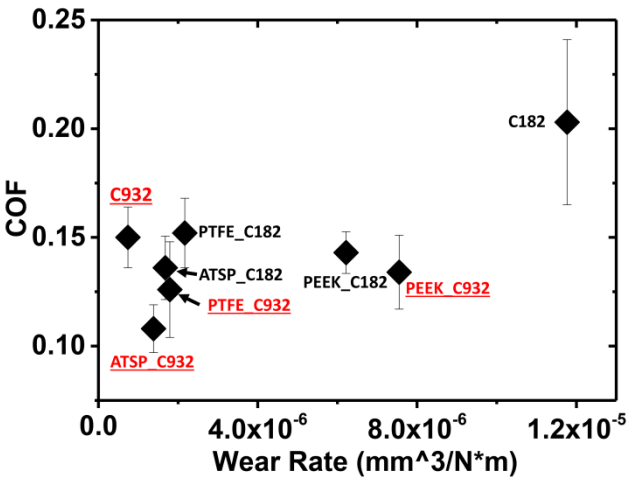

Figure 36 COF vs. wear rate of different coatings and substrates for 4.3 Km wear experiments

4.3.3 Durability experiments

4.3.3.1 25.9 Km sliding distance (3 hours) experiments

Figure 37 shows constant load experimental results for 25.9 Km sliding (180,000 cycles) of the three coatings on C182 and C932 substrate materials. Each 3-hour experiment was conducted by three 1-hour long experiments, and 25 mg of lubricant was added at the beginning of the experiment and after the second hour. **Figure 37** (a-c) show the in situ COF, NCT and wear scans of the three coatings on C182 substrate. ATSP coating showed the lowest wear, with mild polishing of its asperity peaks, PEEK had the highest wear and PTFE exhibited intermediate wear. For the PEEK coating after about 11 Km sliding distance, there was large vibration on its COF, due to the loss of the coating material and lubricant, resulting in severe lubrication condition. **Figure 37** (d-f) shows in situ COF, temperature and wear scans of the coatings on C932. As with C182, ATSP exhibited the best performance with almost zero wear, PEEK exhibited the worse performance and PTFE showed intermediate wear performance.

Figure 38 shows microscopic images of the wear tracks on both the disks and pins on C932 after 25.9 Km sliding, which had the same wear pattern as 4.3 Km sliding. Both PEEK and PTFE coatings showed abrasive wear groove and the wear of ATSP coating was mainly polishing of the asperity peaks.

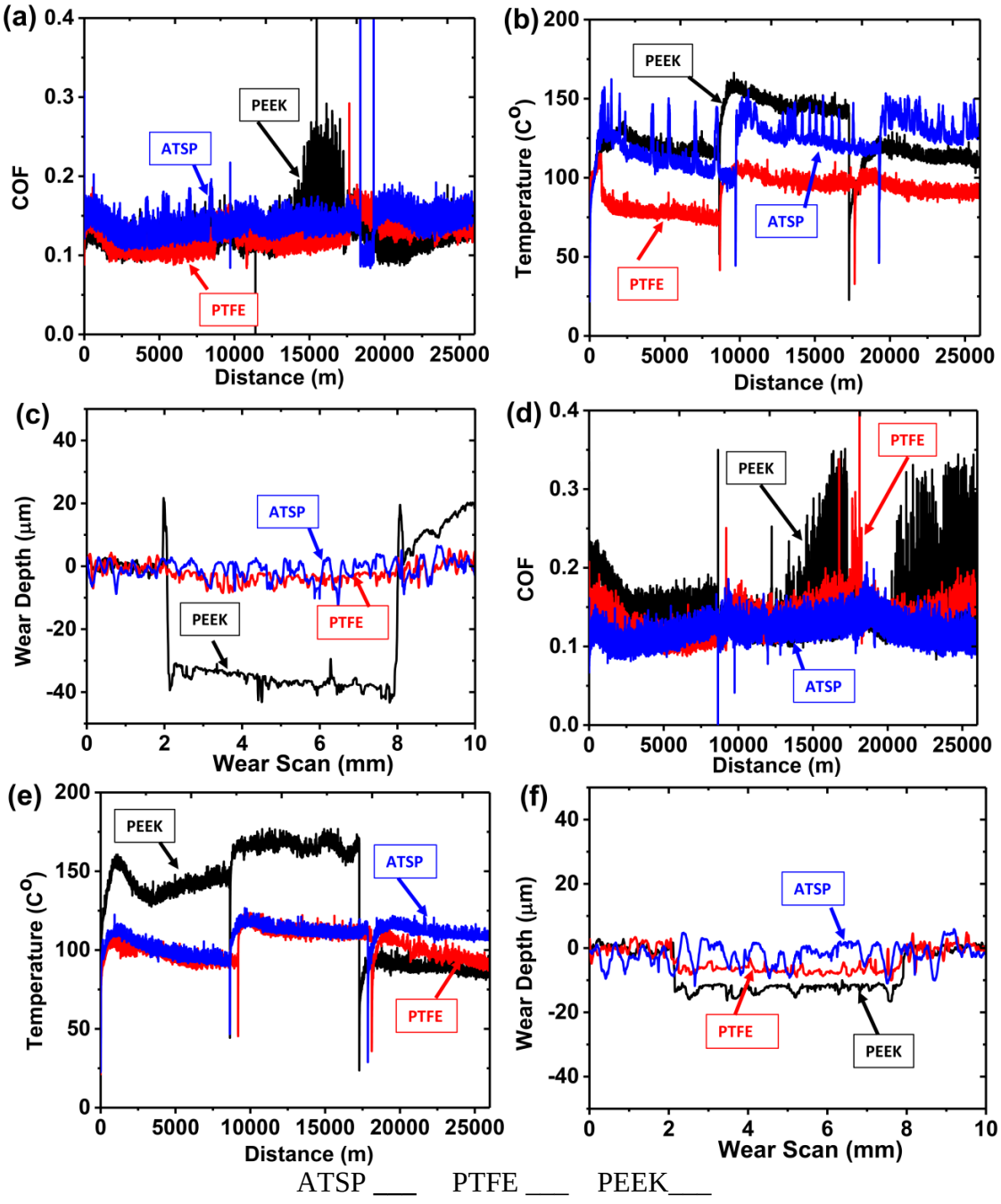

Figure 37 In situ 25.9 Km durability experiments. (a, b, c) in situ COF, NCT and wear scans of coatings on C182, (d, e, f) in situ COF, NCT and wear scans of coatings on C932.

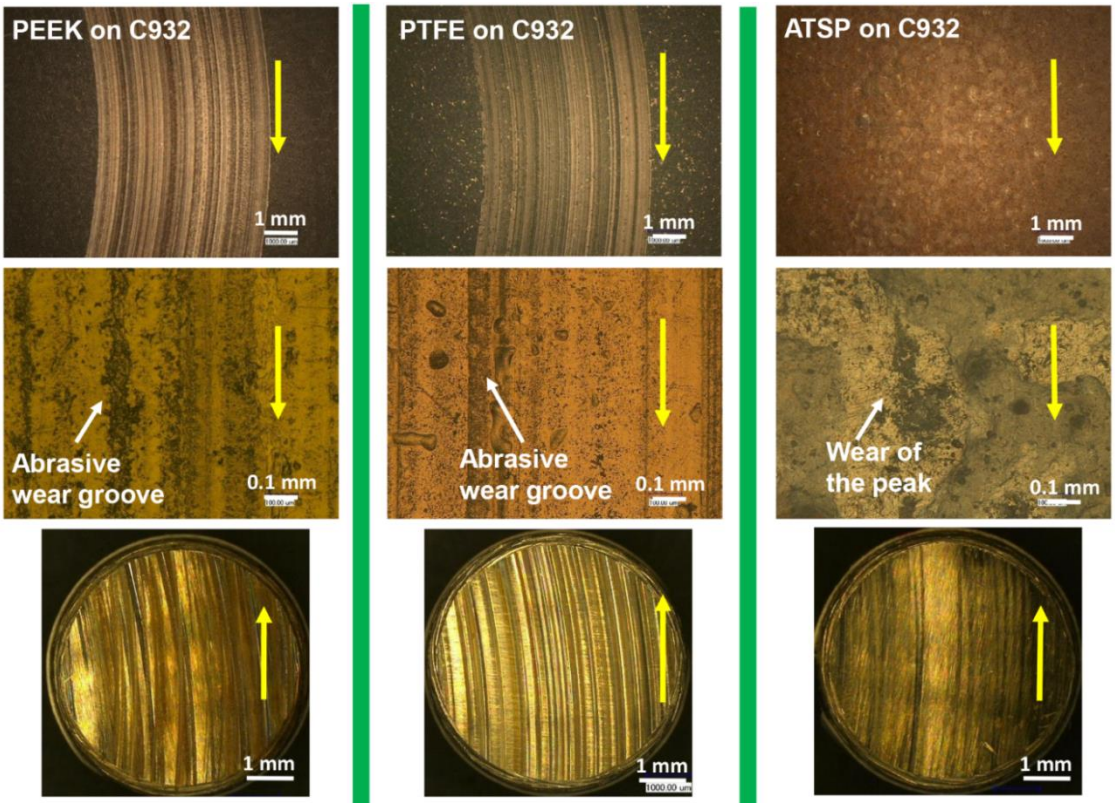

Figure 38 Microscopic images of wear tracks on disks and pins after 25.9 Km sliding distance experiments on C932 (top images: low magnification, disks; middle images: higher magnification, disks; bottom images: pins).

4.3.3.1 Life experiments: 77.8 Km and 155.5 Km sliding distance

Since ATSP coating on both substrates showed excellent wear resistance under 4.3 Km wear and 25.6 Km durability experiments, additional lifelong experiments were performed to determine whether this coating could sustain its superior performance over the life of the device. For this purpose, we chose ATSP on C932 substrate and performed 77.8 Km and 155.5 Km sliding experiments. The sliding speed was 2.4 m/s

except for stage 3 (77.8 Km to 155.5 Km), which had a sliding speed of 3.6 m/s. 25 mg of lubricant was added at the beginning of the experiment and every two hours during the experiment. The wear depth of the coating increased slightly with increasing sliding distance, however, even after a sliding distance of 155.5 Km (corresponding to more than 1.08 million cycles), the wear was still mild polishing of the asperity peaks, as indicated in **Figure 39**.

Figure 40 is a summary of the COF vs. wear rate for the different coatings on C182 and C932 for different sliding distances. Except for the 77.8 Km and the 155.5 Km experiments, all other experiments are for durability (25.9 Km) experiments. The labels with no underline indicate coatings on C182 substrates and the labels with underline indicate coatings on C932 substrates.

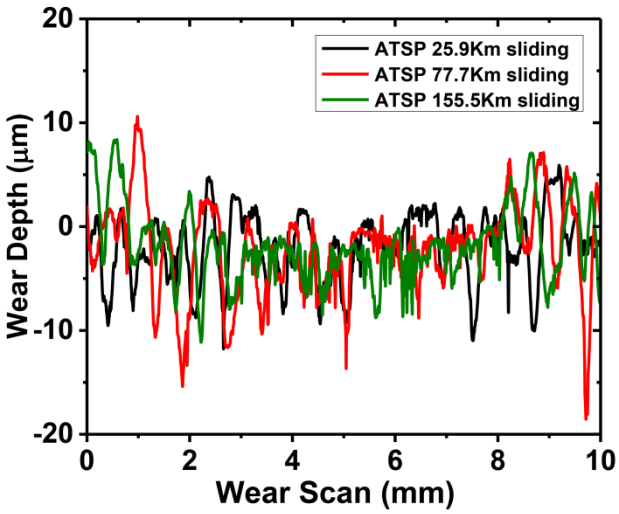

Figure 39 Wear tracks of ATSP on C932 after different sliding distance experiments.

Considering the durability experiments (25.9 Km) with C182 substrate, ATSP coating had the highest COF of 0.14 and the lowest wear rate of $1.06x10^{-7}$ mm^3/Nm. Both PTFE and PEEK had the same COF, with PTFE exhibiting better wear resistance than PEEK. For the case of coatings on C932 substrate, ATSP coating exhibited the overall best performance, with the lowest COF of 0.12 and the lowest wear rate of $2.25x10^{-7}$ mm^3/Nm. PTFE coating showed intermediate performance and PEEK coating the worst performance. The COF and the wear rate of 25.9 Km sliding experiments were different compared to the COF and wear rate of the short 4.3 Km sliding experiments. For the 4.3 Km sliding distance, the lubricant was abundant, compared to the subsequent time, as the lubricant became less effective because of the centrifugal action and absorption of the lubricant by the wear debris. During the first 4.3 Km sliding distance, the coatings went through a run-in period, and the wear rate was higher than the following stable period, with higher contact area and lower contact pressure. Both ATSP and PTFE coatings exhibited a better wear resistance on C182 substrate than on C932 substrate for the durability 25.9Km experiments.

For the lifelong 155.5 Km sliding distance experiments of ATSP on C932, the wear rate was the lowest measured at $4.15x10^{-8}$ mm^3/Nm. Such low value is also seen with very thin advanced diamond like carbon coatings [115] and very hard CrN coatings [116]. The average COF increased slightly with increasing sliding distance, being 0.121 for the first 25.9 Km, 0.130 for the 77.8 Km (7.4% increase) and 0.137 for the 155.5 Km

experiment (5.4% increase). On the other hand, the wear rate decreased with increasing sliding distance.

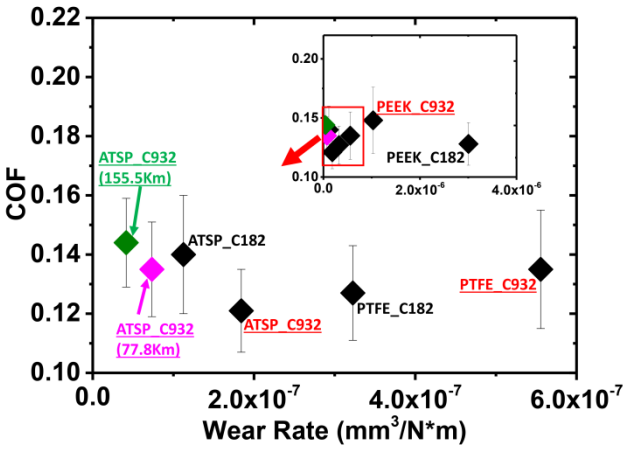

Figure 40 COF vs. wear rate of different coatings and different sliding distances.

4.3.4 SEM analysis

Optical images in **Figure 35** and **Figure 38** could not show the detailed morphology after the wear experiments, and SEM was carried out to analyze the wear mechanisms of the coatings, as shown in **Figure 41** (for the coatings on C182 substrate after 25.9 Km sliding distance). **Figure 41(a-c)** show the wear tracks of the ATSP coating, which is mainly adhesive wear on top of the coated asperity peaks. Rougher and porous surface is seen on top of the peaks after the wear experiments, under higher magnification. The lubricant could disturb the wear debris adhere to the coating and impede formation of transfer layer on the counter steel pin's surface. Note that these

pores could work as lubricant reservoirs, which would continually supply lubricant that helped reduce the COF and wear. The wear of PEEK coating was due to both abrasive and adhesive wear, as shown in **Figure 41(d-f)**. The abrasive wear debris came from the plowing of the steel pin asperities, thus observing the flaky wear debris just beside the abrasive wear groove. While the adhesive wear formed by the plastic fatigue of the material, then flowed by micro-crack nucleation and propagation [13], with the adhesive of the steel pin, the debris came off the coating [11].

The wear mechanism of PTFE coating was similar to that of the PEEK coating. The wear of PTFE coating also included abrasive and adhesive wear mechanisms. The difference was that the wear debris of the PTFE coating was much smaller than the PEEK coating. This difference could explain the difference of wear rate between PTFE and PEEK coatings. PEEK coating had larger wear debris, resulting in higher speed of material loss; while PTFE coating had smaller wear debris, resulting in lower wear rate.

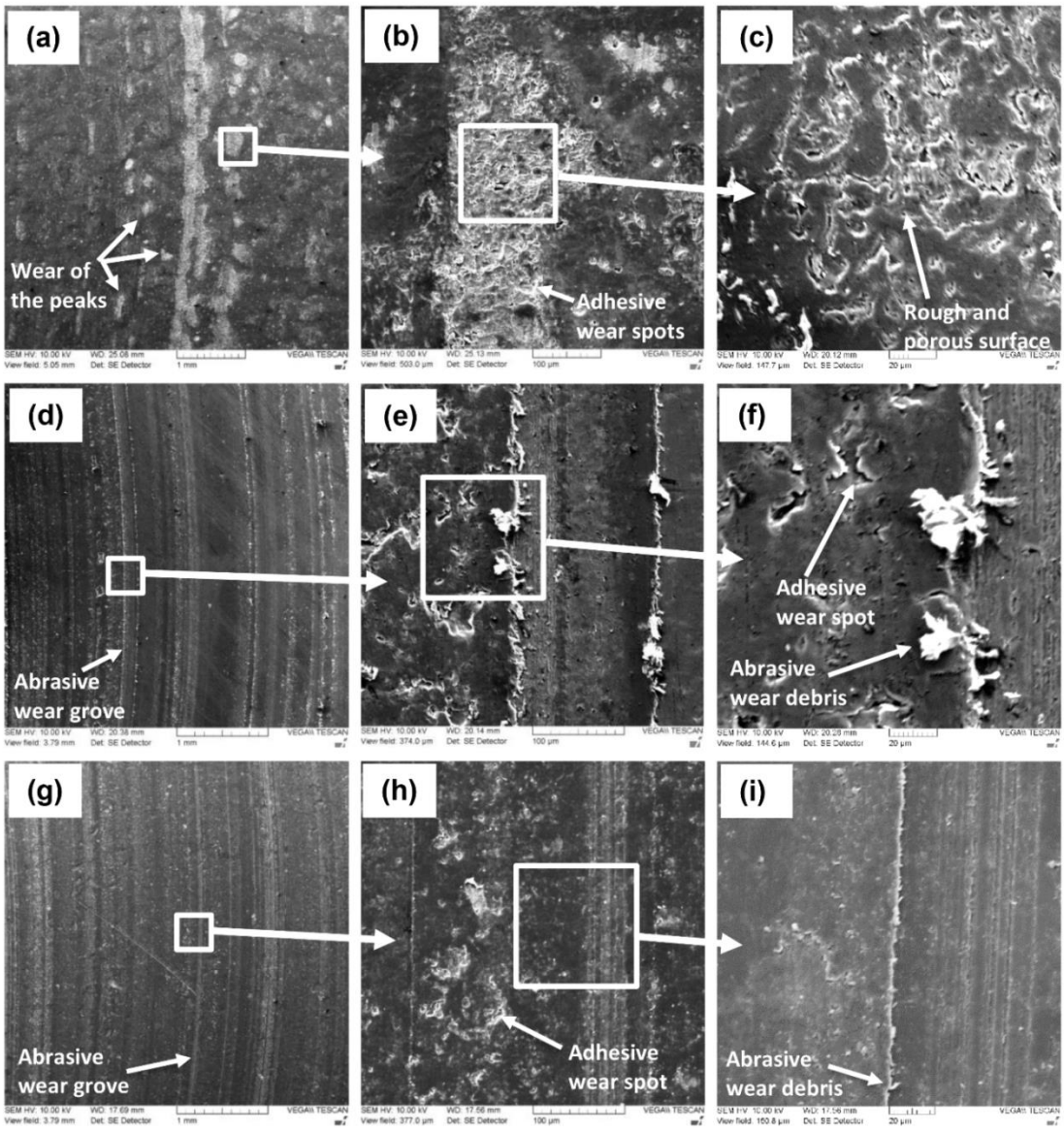

Figure 41 SEM of coatings on C182 after 25.9 Km sliding distance, (a, b, c) ATSP, (d, e, f) PEEK, (g, h, i) PTFE.

4.4 Conclusion

Experimental results using a specialized tribometer simulating tilting pad thrust bearing contact conditions using three advanced polymeric-based coatings (PEEK-based, PTFE-based and ATSP-based) have shown excellent performance, compared to bare substrate materials. The ATSP coatings showed excellent bearing performance and could be used on the pads of thrust tilting pad bearings. Specifically,

a) Load-to-failure scuffing experiments showed that all coatings improve the scuffing resistance compared to the substrate materials. In all cases, the scuffing pressure was significantly higher than the tilting pad bearing's highest average working pressure.

b) Based on the short (4.3 Km sliding distance) wear experiments, among the three coatings on two different substrates, ATSP coating exhibited the best performance, with the lowest COF and lowest wear rate. PTFE coating exhibited intermediate wear resistance and PEEK coating the highest wear rate.

c) Based on the durability (25.9 Km) wear experiments, ATSP showed the best wear resistance, with a wear rate of 1.06×10^{-7} mm3/Nm (C182 substrate). For life experiments (155.5 Km) of ATSP on C932, the coating showed an extremely low wear rate of 4.15×10^{-8} mm^3/Nm.

d) SEM analysis showed that ATSP's minimal wear is because of mild adhesive burnishing wear of the asperity tips and the formation of porous

surfaces which was good for improving the lubrication condition. PEEK and PTFE coatings' wear came from both abrasive and adhesive wear.

5. SAND ABRASIVE WEAR OF ADVANCED POLYMERIC COATINGS[3]

ATSP based coatings exhibit extremely low wear rates ($4.15x10^{-8}$ mm^3/Nm) under boundary lubrication simulating tilting pad bearings in harsh conditions in chapter 4. It is acknowledged that coatings' resistance to abrasive particles encountered in the bearing is also critical; the abrasive wear resistance of ATSP-based coatings and PEEK based coatings are studied in this chapter using an accelerated wear experimental configuration with submerged lubrication and 2% weight of sand. The coatings' performance is compared with bare substrate (C18200chromium copper) material. The results demonstrate that ATSP based coatings have good abrasive wear resistance and very stable COF because of their elastic deformation and a black tribo-layer that forms on the surface. ATSP based coatings exhibit higher wear rate after adding the sand, while the wear rate of PEEK based coating decreased with sand compared with no sand condition due to sand working as solid lubricant. The abrasive wear mechanism of ATSP was studied by varying the duration of experiments between 3,420 m and 13,680 m, different sand size particles and different pin materials; SEM, micro-scratch testing and X-ray photoelectron spectroscopy (XPS) were used to verify the wear mechanisms.

[3] Reprinted with permission from "Three-body abrasive wear by (silica) sand of advanced polymeric coatings for tilting pad bearings" by Lan, P., Polychronopoulou, K., Zhang, Y. and Polycarpou, A.A., Wear, 382–383(2017): pp. 40-50, Copyright 2017 by Elsevier.

5.1 Introduction

Hydrodynamic bearings such as tilting pad bearings are widely used due to their low COF and high load capability [95]. Under severe conditions, such as elevated temperatures and higher loads, where loss of lubricant can take place, the lubrication condition of the hydrodynamic bearing may get destroyed and reduced to mixed and boundary lubrication conditions [46, 96]. Under such conditions, traditional pad bearing material (Babbitt metal) is not able to sustain significant contact. Polymeric materials are good candidates for bearing systems due to their good resistance to temperature, corrosion, galling and seizure, tolerance to small misalignments, low friction during contact, moderate wear resistance, self-lubricating properties, low noise emission and low production cost [19, 45, 46, 97, 103, 104, 106-109, 117]. As soft material, the wear resistance of polymers is a concern; in order to improve the wear resistance but sustain low COF for polymers, different strategies have been tried, among them the addition of different fillers/reinforcements [5-8, 14, 87, 88] and developing new polymer composites [54]. As for the application format in bearing system of polymers, they can be used as bulk material or in coating format. PTFE and PEEK-based polymers in bulk format are widely used as plain bearing materials [45, 97, 103, 104, 118-120] due to their aforementioned advantages. However, bulk polymers cannot be applied for precision conditions, such as in the case of journal bearings, because they are subjected to deflection (large deformation) with temperature change due to high thermal expansion.

In addition, polymers present high thermal resistance because of the low thermal conductivity that is combined with high thickness of the bulk polymer [87].

These disadvantages can be overcome by applying thin polymer coatings, in which appropriate dimensions and thermal stability can be retained[98, 121]. Extremely low wear resistance ($4.15x10^{-8}$ mm^3/Nm) of ATSP based coatings has been reported under boundary lubrication simulating tilting pad bearing in harsh conditions [87]. It was acknowledged that these polymer coatings' resistance to abrasive wear encountered in plain bearings is critical, as the thin coating might be penetrated and wear-out by the hard particles. In this work, we selected two advanced coatings (ATSP based and PEEK based coatings) to be tested under severe sand abrasive conditions.

Abrasive wear relates to cutting or plowing of the surface by harder particles or asperities [3] and mainly has forms of two-body abrasion, three-body abrasion or a combination of the two [8]. Researchers applied different experimental protocols to evaluate abrasive wear resistance. Two-body wear tests are performed by sliding polymer samples on sand paper [7, 122]. Three-body abrasive wear tests are usually carried out by sliding a wheel or ball on the polymer test sample and applying the abrasive particles between the contacting surfaces [117, 123-126]; the abrasive particles can be applied in dry [123] or wet (slurry) [117, 124-126] conditions and the particle size varies from few microns to hundreds of microns. Researchers have been using standard or simplified methods to investigate the micro scale abrasive resistance of polymers, such as applying low sliding speeds and small sand size particles [117, 124-

126]. However, in real applications such as the tilting pad bearings in ESPs in oil wells, the working conditions of the polymer coatings is much more severe, with sliding speed more than 15 m/s and various abrasive particle sizes. In this work, contaminated lubricant was used, mainly composed of sand (#140), the particle size of which ranges from less than one micron to 300 microns, and ISO 46 mineral lubricant, which are typical for this application. In order to potentially simulate the severe sand contaminated conditions such as in ESPs, a sliding speed of 1.9 m/s was applied.

5.2 Experimental

5.2.1 Ultra-High Pressure Tribometer (UHPT) and experimental configuration

Figure 42(a) shows a photograph of the UHPT with a pin-on-disc configuration. Detailed description of the UHPT can be found elsewhere [127]. Basically, normal loads up to 1,120 N can be achieved, whereas an environmental chamber can operate in pressures up to 13.8 MPa. Unidirectional and oscillatory experiments can also be performed using the UHPT whereas friction, normal load and near contact temperature can be measured in situ. As shown in **Figure 42(b)**, the normal load is applied from the pin side; the pin holder is connected with a 6-axis (three forces and three torques) transducer. The disk is mounted on the disk holder that is rotated by an electric motor. Both disk and pin are being submerged in lubricant with/without sand inside a cylindrical container, as shown **Figure 42(c)**. The mixing and dispersion of the sand

particles with the lubricant is being assisted by the rotational movement of the disk itself. This results in the formation of the sand contaminated lubricant that simulate the extremely abrasive conditions of tilting pad bearings.

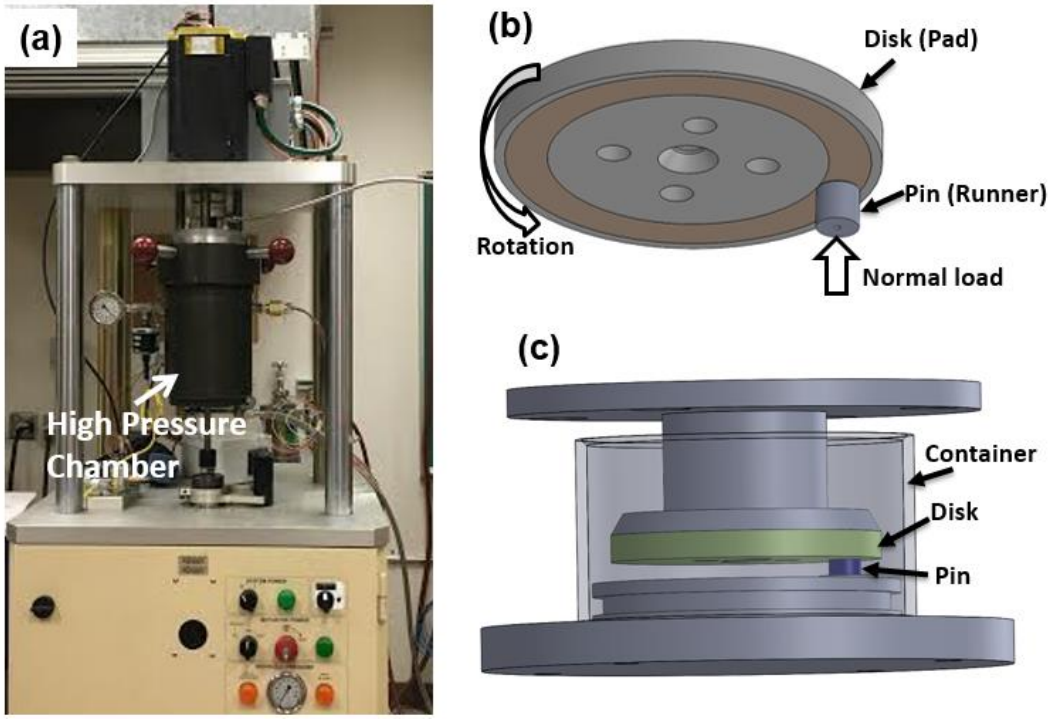

Figure 42 UHPT and experiment configuration, (a) picture of the UHPT, schematics of (b) pin-on-disk configuration, and (c) contact interface container.

5.2.2 Materials

ATSP coatings with same composition as in chapter 3 and 4 were deposited using ESD method by spraying a blended powder (95wt.% of ATSP and 5wt.% of PTFE) on the sand blasted C18200 disks, then the disks were cured at 270°C for 30

minutes in a furnace with convective air. The PEEK based coating (1704 PEEK/PTFE®) was deposited on C18200 by an authorized applicator (Southwest Impreglon, Inc.).

4130 steel and C93200 bronze pins with a diameter of 6.35 mm were used as counter surface for the pin-on-disk experiments. Sand abrasive wear experiments were performed using 2 wt. % sand #140 that was added into an ISO 46 mineral oil to form the so-called contaminated lubricant. Before each experiment, ATSP coating was immersed with isopropyl alcohol and the metal samples were immersed in acetone and placed in an ultrasonic cleaner for 10 minutes at 50ºC temperature.

The relevant properties of the samples used in this study including the two coatings, the substrate C18200 and the counter pins are summarized in **Table 6**. The roughness was measured using a Tencor P6 profilometer and the hardness of the coatings was obtained by micro-indentation; the hardness of the steel and thickness of the coatings were provided by the vendors.

Table 6 Roughness, Hardness and Thickness of the coatings and substrate materials.

Surfaces	Rq(μm)	Hardness(GPa)	Thickness (μm)
ATSP (95%CB2AB2+5%PTFE) disk	3.3	0.25±0.02	30±5
PEEK (1704 PEEK/PTFE®) disk	1.9	0.28±0.4	35±5
Chrome copper C18200 disk	0.6	HRB 70	___
4130 steel pin	0.16	HRB 97	___
Bronze C93200 pin	0.5	HRB 27	___

An optical image and particle size distribution of the commercially available sand #140, are shown in **Figure 43**. The largest sand size is up to 0.3 mm and the size distribution was achieved by a sieve set. In general, the size distribution of the sand used in the experiments was similar of the sand size in the Gulf of Mexico coast[128].

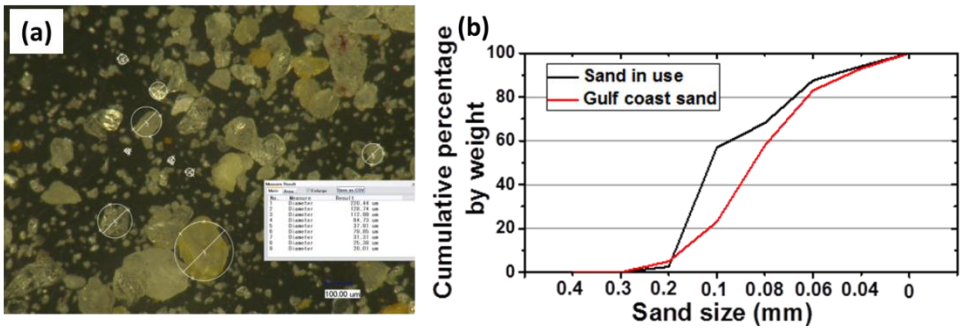

Figure 43 #140 sand used in this study, (a) optical microscope image (b) size distribution.

5.2.3 Experimental methodology

5.2.3.1 Tribological evaluation studies

Experiments were carried out following the protocols shown in **Table 7**. Three disk surfaces, namely ATSP coating, PEEK coating and bare C18200 substrate were selected to investigate the role of the coatings and to compare different coatings' tribological performance (ATSP vs. PEEK). To study the effect of abrasive sand, experiments in the presence and absence of sand were performed. Smaller sand size (<53 microns) that was sieved out from #140 sand (which included sand from less than one micron to 300 microns) and different sliding duration (30 min, 80 min and 120 min) were used in the experiments to study the wear mechanisms of ATSP coatings. In the sand abrasive experiments of ATSP coatings, there was a black layer formed on top of the wear scar of the ATSP coating as shown in **Figure 44(c)**. To verify if the black layer is from the high-carbon-containing 4130 steel or not, a brass pin with no carbon content was also used for the experiments. The sliding speed was 1.9 m/s (average wear track diameter: 36.3 mm) with a nominal contact pressure of 6 MPa (180 N normal force).

Table 7 Experimental conditions of abrasive experiments.

Coating/Pin	Distance, m Duration, min	Sand size	Speed, m/s /rpm	Pressure, MPa/Load, N
ATSP based vs. 4130 pin	3,420/(30), 9,120/(80), 13,680/(120)	a: #140; b: <53μm	1.9/1,000	6/ 180
PEEK based vs. 4130 pin	3,420/(30)	#140	1.9/1,000	6/180
Bare C18200 vs. 4130 pin	3,420/(30), 6,840/(60)	#140	1.9/1,000	6/180
ATSP disk vs. C93200 pin	9,120/(80)	#140	1.9/1,000	6/180

Figure 44 shows the sand abrasive wear experimental setup. The 2 wt. % sand was added in a place of about the same distance off the center, whereas the pin was placed in the same off center distance but at the opposite side. Once the disk was submerged and contacted with the pin, its rotation would help to mix the sand with the lubricant. Comparison of **Figure 44(b)** and **(d)**, shows that the lubricant was clear before the experiment and then became dark colored at the end of the experiment. A black layer was also formed on the wear track in the case of the ATSP coating, as shown in **Figure 44(c)**.

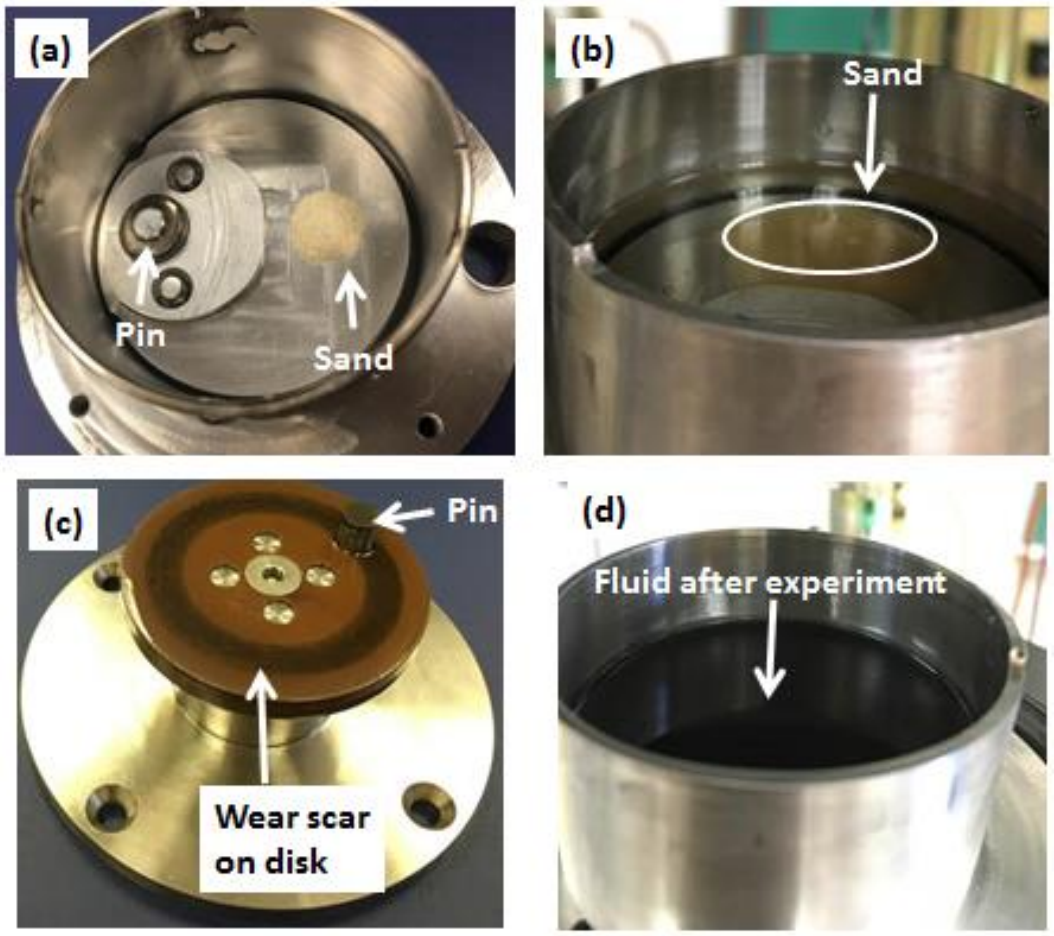

Figure 44 Sand abrasive wear experimental configuration. (a) sand position without fluid, (b) clear lubricant with sand, (c) pin and disk after experiment, (d) lubricant fluid after the experiment.

5.2.3.2 Surface characterization after the tribological tests

After the UHPT tribological experiments, a Tencor profilometer (P-6) was used to obtain 12 mm long wear scans which cover the 6.35 mm cross section/width of the wear tracks, so as to make possible the calculation of the wear volume and wear rate. To understand the wear mechanisms of the coatings, different analytical tools were

employed, namely optical microscopy, SEM and X-ray XPS. SEM (VEGA II LSH) at an operating voltage of 10 KV was used to obtain the microphotographs. XPS studies were performed inside and outside of the wear tracks by using an Omicron ESCA system equipped with a monochromatic MgKα X-ray source (1253.6 eV) and operated at 300 W. Samples were analyzed under vacuum ($P < 10^{-8}$ Torr), whereas survey scans and high-resolution scans were collected using pass energies of 40 eV, respectively. Binding energies were referred to the C 1s binding energy at 284.6 eV. Prior to XPS measurements, the samples were ultrasonically cleaned to suppress outgassing inside the XPS chamber. In addition, micro scratch experiments were performed using a Hysitron TI-950 Premier to investigate the wear mechanisms of the coatings.

5.3 Tribological performance and wear mechanisms

5.3.1 ATSP and sand abrasive wear mechanism

Figure 45 shows the sand abrasive experimental results of ATSP coatings along with the bare C18200 material. In the absence of sand, the COF (**Figure 45(a)**) for the case of ATSP coating and bare C18200 was stable and both disk surfaces and pins exhibited zero wear under submerged conditions. It is clear that in the case with and without sand, the COF of ATSP is higher than in the case of bare C18200 (referred to as C182 in the figure); this is because the ATSP coating had a much higher roughness than the bare C18200 substrate surface (see **Table 7**). After adding the sand, the COF of bare

C18200 increased by 473% compared to the no sand condition (0.011 to 0.063); while the increase for ATSP coating case was only 39% (0.083 to 0.115). More important is that the COF of ATSP coating was more stable than the case of bare C18200. The wear rate of ATSP ($6.1x10^{-7}$ mm^3/Nm) was much lower than that of C18200 ($1.3x10^{-6}$ mm^3/Nm) in sand contaminated conditions. The unstable COF condition of bare C18200 is expected to cause excessive vibration for the bearing system and accelerate the failure of the device.

To investigate the wear mechanism of sand abrasion on the ATSP coating, experiments with different durations (30 min, 80 min and 120 min, corresponding to 3,420, 9,120, and 13,680 m) were carried out, as also shown in **Figure 45(a)**. The wear scans of the disks and pins are shown in **Figure 46**. As shown in **Figure 46(c, d)**, after the 120 min experiment, deep wear scratches were observed on the ATSP-coated disk and high peaks on the pin. In general, it is anticipated that the harder material would wear out the softer material; but in the present study, the steel pin had a relative high wear rate (as shown in **Figure 45(b)**) and formed these high peaks.

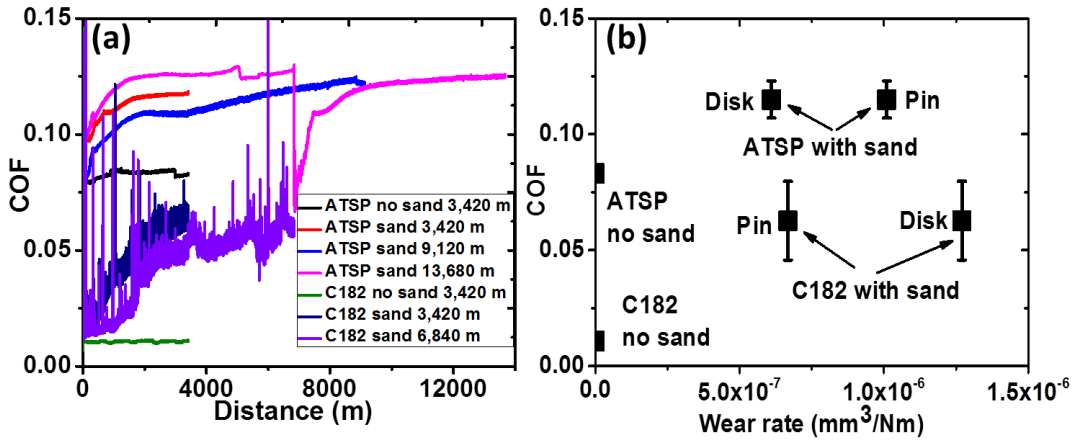

Figure 45 Sand abrasive wear experiments: (a) In situ COF vs. distance, (b) COF vs. wear rate.

From the optical microphotographs following the experiments at different durations, as shown in **Figure 47**, we can obtain information about the wear mechanism of the ATSP coatings. There were two stages of the wear: (A) sand particles randomly scratch the ATSP coating; and (B) continued wear grooves formed on the ATSP coating. Stage (A): sand particles randomly trapped between the sliding surfaces at the first stage. It is reasonably anticipated that small particles of sand would cause shallow scratches, with large particles of sand cutting through the thin film ATSP coating. This is illustrated in **Figure 47**, where the microphotograph of ATSP coating after 80 min (9,120 m) sliding is presented. It is noticed that the scratches do not follow the wear track cycle. The width of the abrasive scratches is from few microns to more than 100 μm, but only the scratch with the largest width penetrated the substrate material. **Figure**

48 shows the SEM images after the 80 min sliding experiment, which clearly shows the different size of abrasive wear scratches.

Stage (B): as shown in **Figure 44(c)**, there was a black layer formed on top of the ATSP coating; it is anticipated that this black layer, along with the ATSP's elastic deformation, would protect the ATSP coating from severe wear. For the 4130 steel pin, its wear caused by a combination of two-body and three-body abrasive wear because some of the hard particles were readily penetrated and be held by the polymeric surface[3]. Since the two-body wear rate is much higher than the three-body wear [129], the wear rate of 4130 steel became much higher than the wear rate of ATSP coating, shown in **Figure 45(b)**. However, in the places where deep scratches formed in stage A, there were absent of ATSP coating that could hold and press the sand on the steel pin. Then those places on the pin would have less wear and form the peaks; at the end, the peaks would in return cause abrasive wear on ATSP coating and form the continued scratches all the way along the wear track, as shown in the microphotograph of ATSP after 120 min (13,680m) sliding in **Figure 46(g)**. For the bare C18200 substrate, the wear was more consistent, with the wear increasing with test duration, as shown in **Figure 46(e, f)** and **Figure 49**.

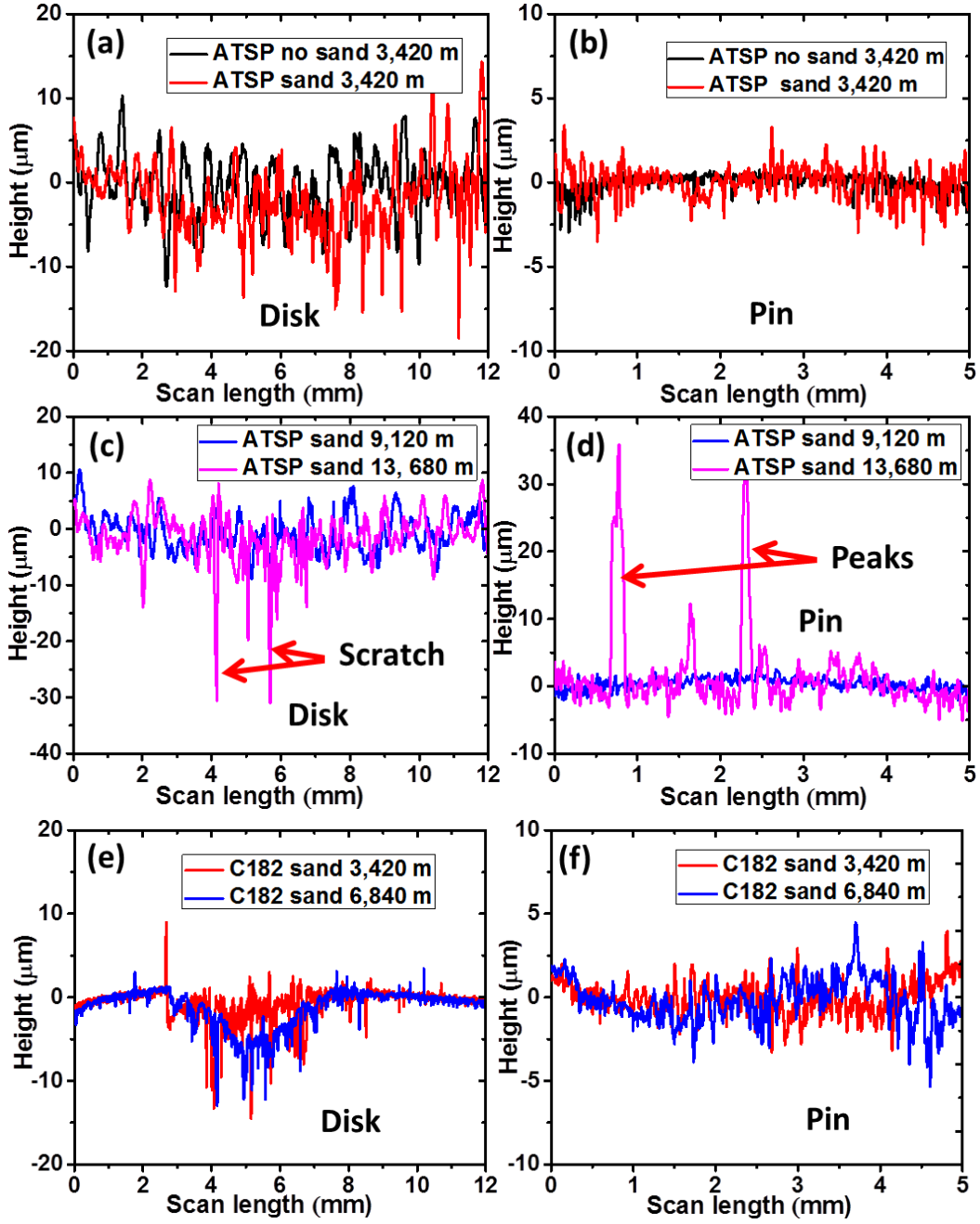

Figure 46 Wear scans of tested samples with different sliding distances and different surface materials after sand abrasive wear. (a, b) 3,420 m tests of ATSP coating with/without sand, (c, d) 9,120 m and 13,680 m tests of ATSP coating with sand, (e, f) 3,420 m and 6,840 m tests of bare CC18200 with sand.

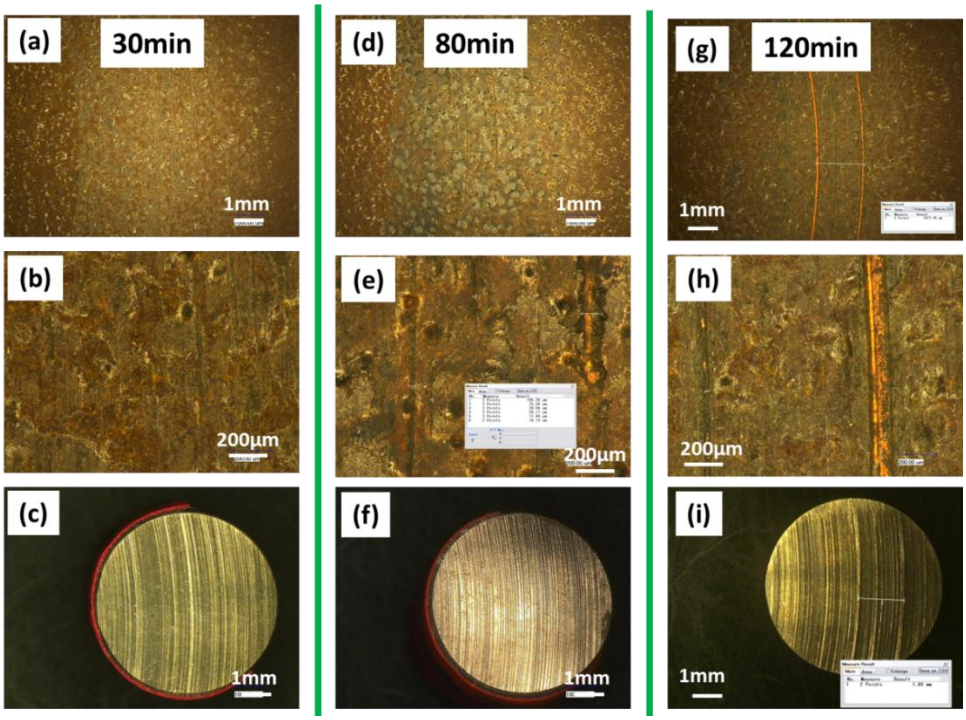

Figure 47 Optical microscopy images of ATSP coating (a, b, d, e, g, h) and pins (c, f, i) after different duration of sand abrasive wear experiments, (a, b, c) 30 min (3,420 m), (d, e, f) 80 min (9,120 m), (g, h, i) 120 min (13,680 m).

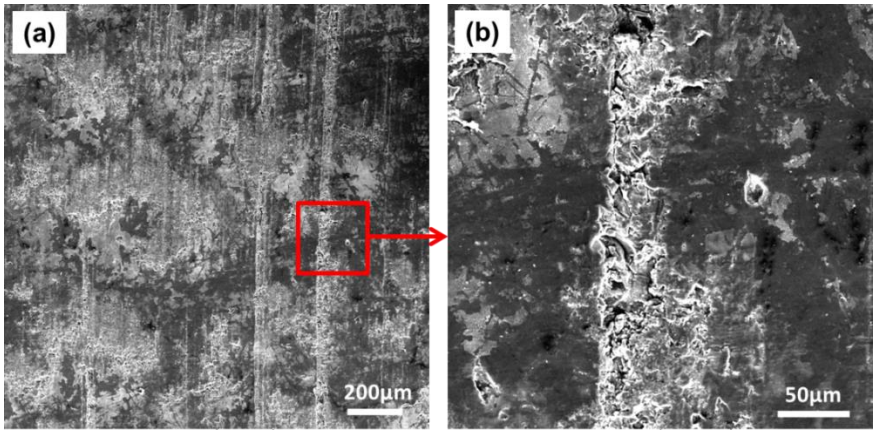

Figure 48 Different magnification SEM images of ATSP coating (a) low, and (b) high magnification, after 80 min (9,120m) sand abrasive wear experiment.

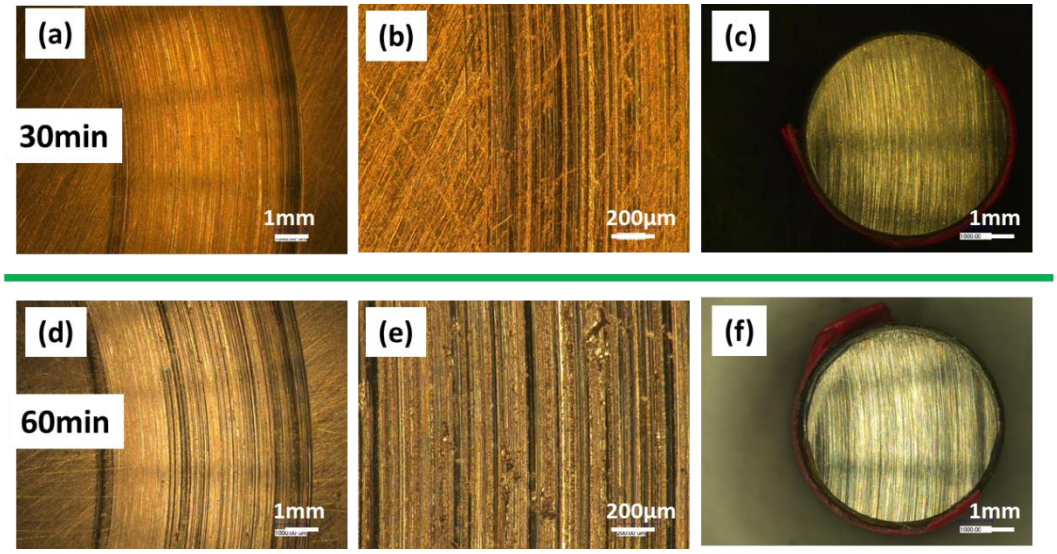

Figure 49 Optical microscopy images of bare substrate C18200 (a,c,d,e,) and pins (c,f) after sand abrasive wear experiment for 30 min (3,420 m) (a, b, c) and 60 min (6,840 m) (d, e, f).

5.3.2 Verification of ATSP sand abrasive wear mechanism

To verify the wear mechanism mentioned above, a 120 min (13,680m) experiment with sieved smaller sand (0-53µm) was carried out. In addition, to identify whether the origin of the black layer was from the carbon steel 4130 steel pin (0.27-0.34 wt. % carbon) or not, a C93200 pin ("zero" carbon) was used for the sand abrasive experiments. The wear scans and optical images are shown in **Figure 50**. Using the sand with 0-53µm particle size, there were no obvious cut through scratches, as indicated in **Figure 51**. The experiment with the no carbon C93200 pin also showed a black layer on the ATSP surface; this means the black layer was the result of a tribo-chemical reaction

taking place on the sliding interface and not carbon originating from the 4130 carbon steel.

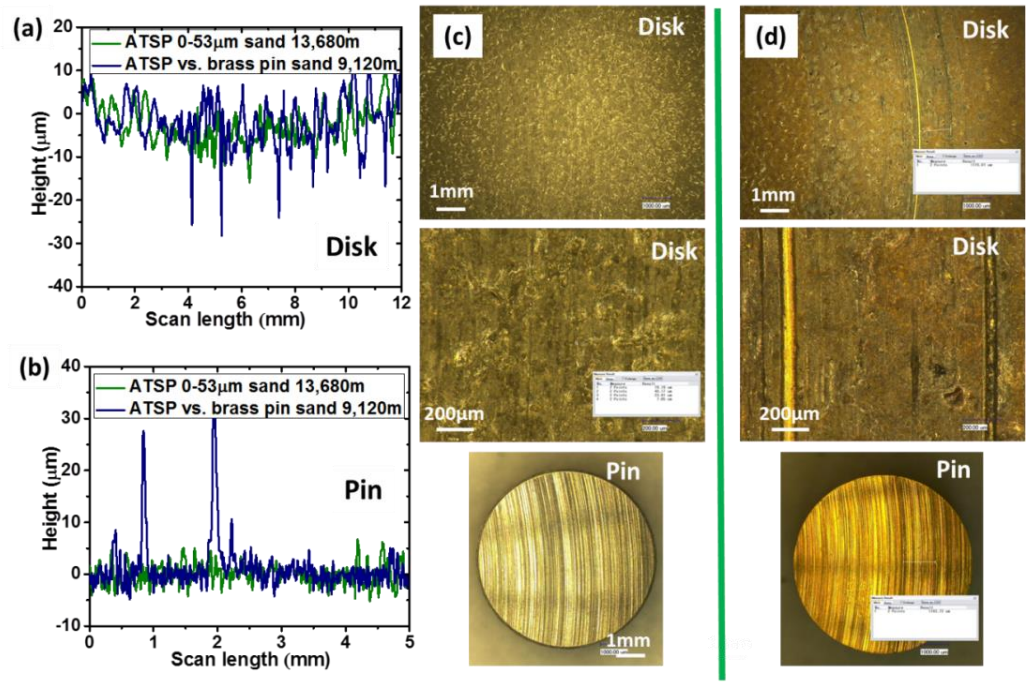

Figure 50 ATSP coating vs.4130 pin with 0-53µm sand and brass pin with #140 sand abrasive wear, (a) wear scan on the disk, (b) wear scan on the pin, (c) Optical images of disk and 4130 pin with 0-53µm sand, (d) Optical images of brass disk and pin with #140 sand.

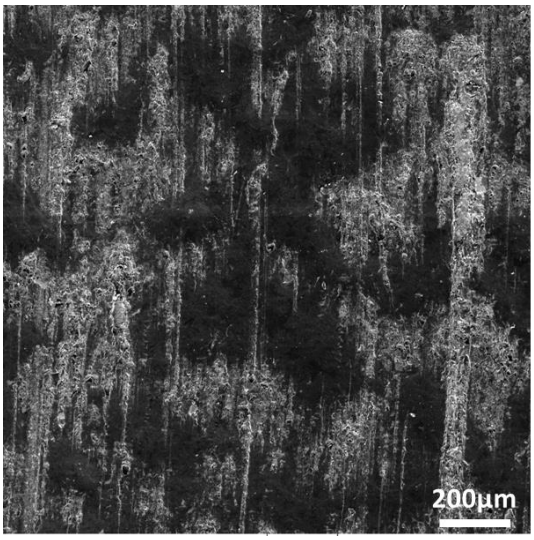

Figure 51 SEM of ATSP coating after 120 min (13,680 m) sieved sand (0-53µm) abrasive wear.

5.3.3 Abrasive wear of PEEK based coatings

A 30 min (3,420 m) experiment without sand particles and 60 min (6,840 m) experiment with sand particles were also carried out with the PEEK BASED coating. **Figure 52** shows the in situ COF vs. distance and the resulting wear scans after the experiments. As in the case of ATSP coatings under sand abrasive conditions, PEEK BASED also exhibited some deep scratch groves as shown in **Figure 52(b)**. Under submerged conditions without sand, PEEK BASED exhibited high wear rate of 5.8×10^{-6} mm^3/Nm, which is almost as high as the starve lubrication condition [87]. This high wear rate was due to the mixed lubrication condition, in which case the steel pin surface was still able to contact the PEEK BASED coating surface and caused abrasive wear even under submerged conditions, as shown in **Figure 53(a)**. However, after adding the

sand, the wear rate of PEEK BASED coating was decreased to $2.1x10^{-6}$ mm^3/Nm. By adding the sand, the COF increased by 9.4%, from 0.0373 to 0.0408; but the wear rate decreased by 64%. Contrary to what was measured for the ATSP coating and to what was anticipated, abrasive sand for PEEK BASED coating had positive effects for its tribological performance because the sand also acted as solid lubricant. Based on the results of **Figure 53**, where the SEM image of PEEK coating after experiments with/without sand is shown, it is concluded that in both conditions the surface exhibited abrasive wear. It is interesting to notice that the abrasive chips or flakes produced in the absence of sand were larger than the ones produced during the experiments with sand. The smaller wear particles in the sand condition resulted in a lower wear rate, compared with the 'no sand' condition.

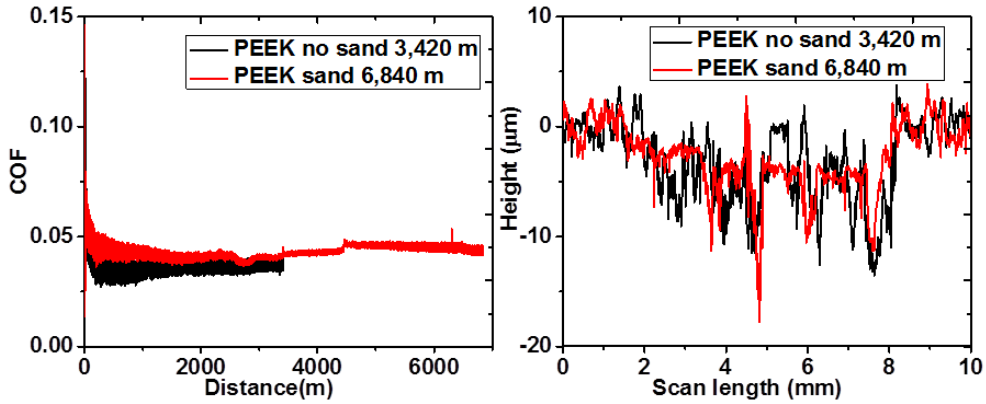

Figure 52 PEEK BASED coating (a) in situ COF vs. sliding distance, and (b) wear scans.

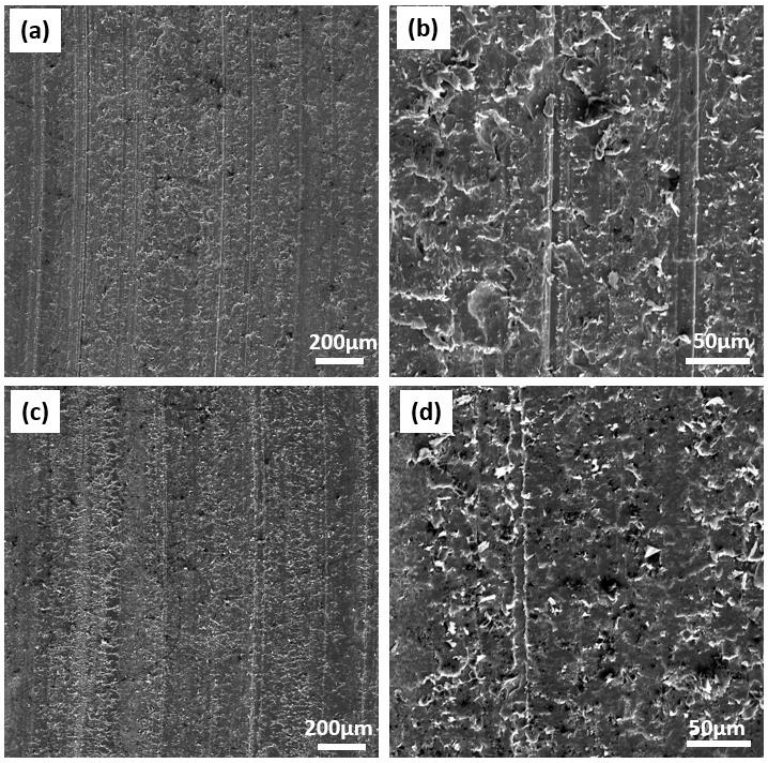

Figure 53 SEM images of the tested PEEK BASED coating, (a, b) 30 min without sand particles, (c, d) 60 min with sand particles.

Figure 54 summarizes the COF vs. wear rate for all surfaces involved in this research work. The lower COF of PEEK BASED coating compared to ATSP coating was due to the lower roughness of the PEEK BASED coating. The same was also found in the case of C18200 substrate. The wear rate of ATSP coating with smaller sand size is higher than in the case of the larger #140 sand; this was because given the same weight percentage of sand, the sand with smaller particle size (0-53µm) can disperse in the lubricant and penetrate through the contact surfaces easier compared to the #140 sand particles (submicron to 300 µm). Among the three disk surfaces under sand abrasive

conditions, ATSP coating exhibited the lowest wear rate but highest COF; PEEK BASED exhibited the lowest COF but highest wear rate; C18200 showed intermediate COF and wear rate values. Despite the fact that no improvement of the smoothness of ATSP coating was applied (e.g., through improved coating deposition method or mechanical polishing), the high COF (due to high roughness) of ATSP coating did not suppress its good functionality. Therefore, ATSP coating is a promising candidate for sand abrasive conditions especially with smaller sand particle size conditions. It seems, though, that even in the case of large sand particle sizes, ATSP coating can be functional as it presents a stable COF and only some penetration scratches.

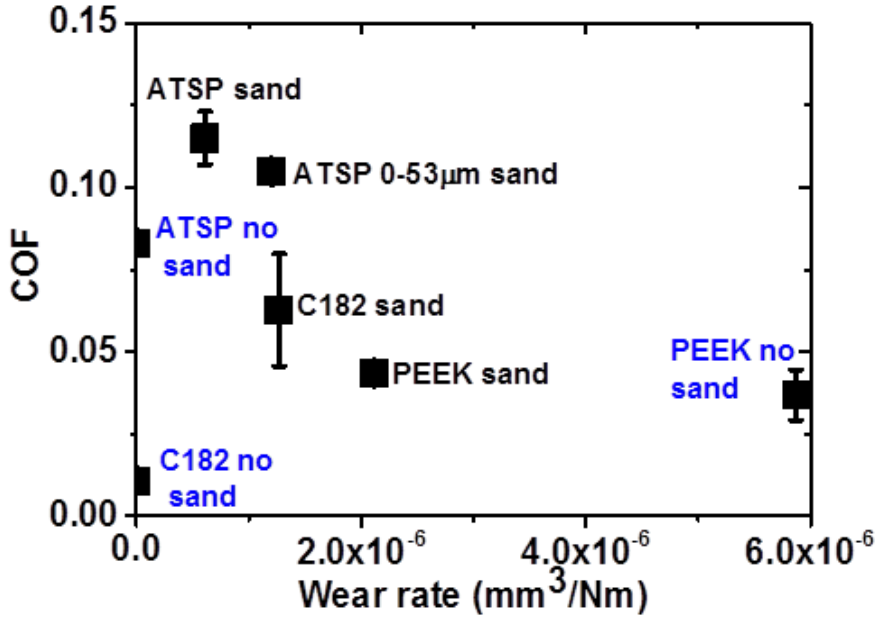

Figure 54 Summary plot of COF vs. wear rate.

5.4 Micro-scratch experiments

In addition to abrasive wear experiments presented above, micro-scratch experiments were also performed to further investigate the tribological behavior of ATSP and PEEK coatings. Micro-scratch experiments were performed using the "high-load" transducer of Hysitron TI Premier. In this set up, a diamond conospherical probe with a tip radius of 4.3 µm was used. The load function is a ramp load that applies a linearly increasing normal force, while it is moving laterally for a set distance. During the scratching process, the transducer records the in situ normal displacement and the lateral (friction) force of the probe. The recorded normal displacement has both elastic and plastic deformations and is called in situ displacement in the present study. A post-scan or retrace using a light force is used to detect the residual depth.

The same load function was applied to test both specimens. The maximum normal load was 400 mN, the lateral scratch distance was 400 µm and the loading time was 30 s. The raw (in situ) data obtained includes normal and lateral forces, and normal and lateral displacements as a function of time. In the present study, what is reported is the extracted normal displacement as a function of normal load and the retrace steps that provide information for the in situ and residual depths, respectively, as shown in **Figure 55**.

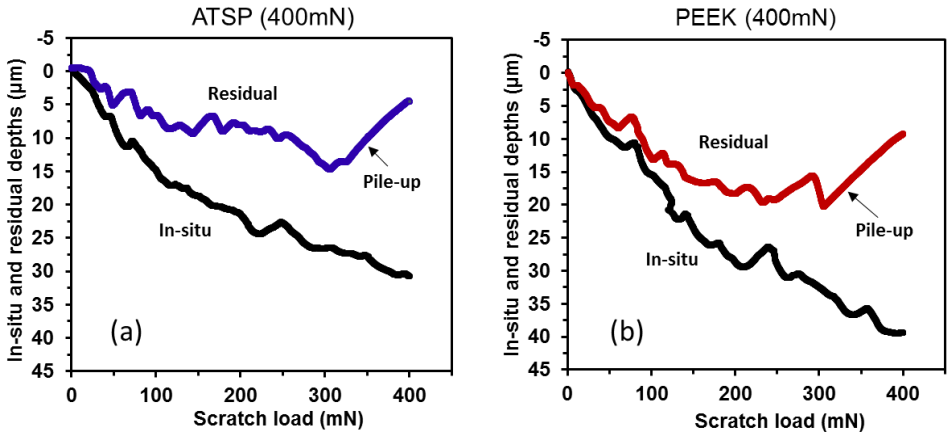

Figure 55 In situ and residual depths from micro-scratch experiments on (a) ATSP and (b) PEEK coatings, using a ramp load with a max force of 400 mN and a scratch distance of 400 µm.

Comparing **Figure 55(a)** and **(b)**, we can draw the following conclusions. First, ATSP shows smaller in situ scratch depth than PEEK under the same scratch load. At the point of 400 mN, ATSP experiences an in situ scratch depth of ~30 µm, which is 25% less than that of PEEK (~40 µm). Second, ATSP shows smaller residual depths, i.e., exhibits higher recovery. In both cases, the maximum residual depth occurs at a load of about 300 mN, with ~15 µm and ~20 µm for the ATSP and PEEK coatings, respectively. It is important to notice that the residual depth curves lift up after the load of about 300 mN. This is because when retracing the scratch, the probe swept some of pile-up debris back to the path. In this discussion of the residual depths, we neglect the abnormal part due to pile-up. Therefore, under the same loading condition, ATSP has smaller in situ and residual depths than PEEK, implying ATSP has larger recovery.

The recovery rate is an important and straightforward parameter to compare materials' resistance to plastic deformation or damage. The parameter is calculated by dividing the elastic recovery with the in situ scratch depth. It varies from 0 to 1 or 100% (percentile scale). The larger the elastic recovery rate, the stronger the material's resistance to plastic deformation. **Figure 56** shows the elastic recovery rates of the two samples according to the data in **Figure 55**. The ATSP and PEEK coatings exhibit elastic recovery rates of 57.3% and 32.7%, respectively. The 25% higher elastic recovery rate of the ATSP coating makes it more scratch resistant compared to PEEK coating. These results are in agreement with the tribological behavior of ATSP coating under sand abrasive conditions in the above reported pin-on-disk experiments.

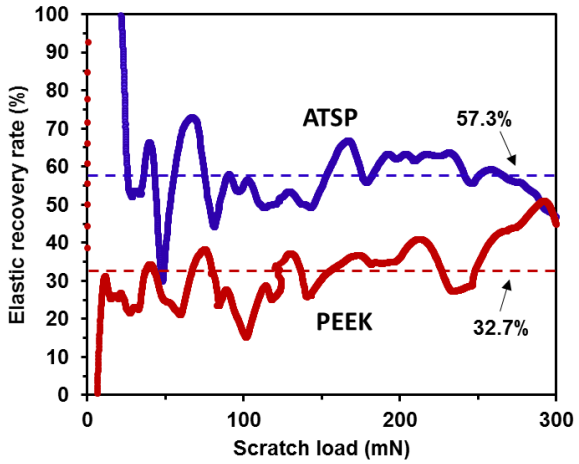

Figure 56 Percent elastic recovery rates of ATSP (57.3%±7.6%) and PEEK (32.7%±8.0%) obtained from the micro-scratch experiments.

5.5 XPS analysis of the tribo-layer formed on the ATSP based coating

Figure 57(a) and **(b)** present the C1s and O1s XPS core level spectra obtained from inside the wear track (black layer) of the ATSP-based coating and outside the wear track (for comparison purposes). The major peak at 284.6 eV corresponds to C-C bond whereas there is a contribution at 286 eV corresponding to C-O bonding environment. In the O1s core level spectrum, the peak at 532 eV corresponds to C-O, which shifts to 533 eV (C=O bond) in the tribo-layer, which is sufficiently reduced. In a similar manner, outside the wear track there is a C1s peak at 289 eV corresponding to ketones groups (C=O). This peak is vanished in the case of the black tribo-layer formed. It is postulated that the C=O groups have been exhausted during the sliding experiment and formed the carbon black layer which help to maintain the contact with low wear and low friction. In addition, in both C1s and O1s cases it is observed that the peaks intensity is lower in the black tribo-layer (following the tribo-contact) which also supports the fact that the active species in the sliding interface have been used to smoothen the contact and at the same time led to the formation of the active (black) tribo-layer. These C-O containing functional groups are originating from the fragmentation of the ATSP coating, the chemical formula of which is shown in **Figure 57(c)**. During sliding and due to the mechanical load exerted on the surface, polymeric bonds break giving rise to short-chained fragments that can improve the adhesion with the metallic substrate due to their polar functional groups. The mobility of these chains is facilitated because of their small

size (smaller than the original ATSP) and the temperature that is developed in the sliding interface.

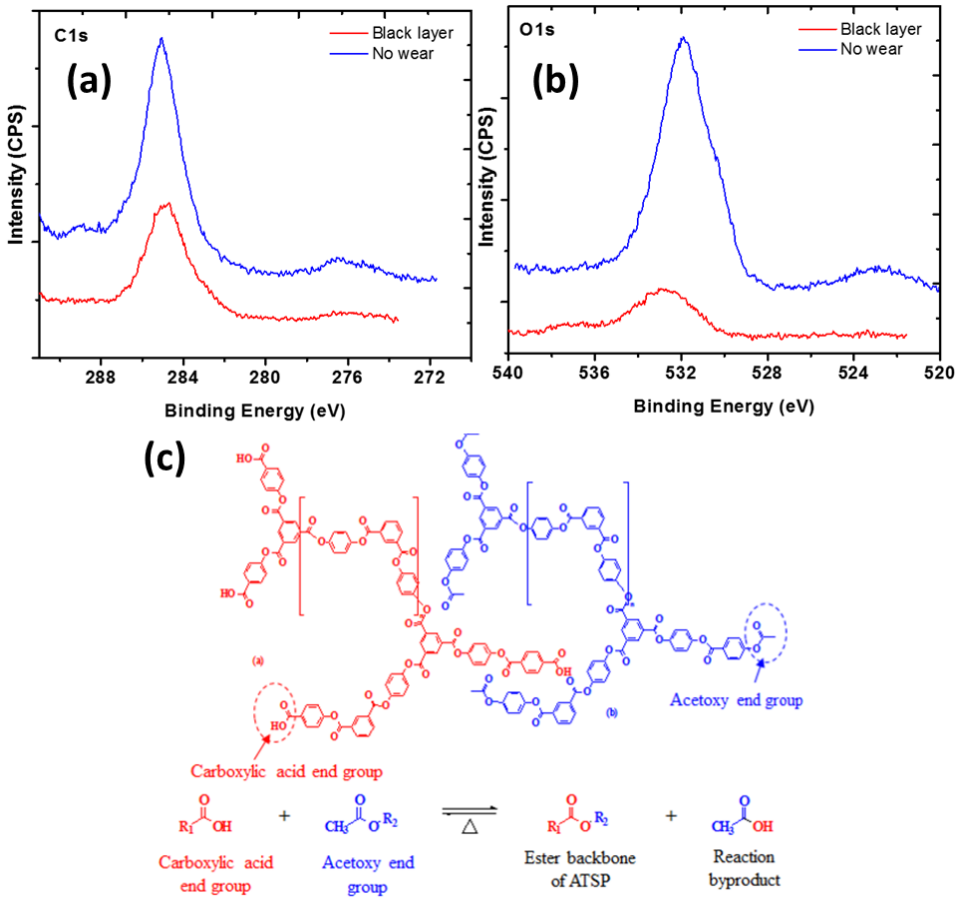

Figure 57 C1s (a) and O1s (b) XPS core level spectra obtained inside the wear track with black tribo-layer and outside wear track on the ATSP-based coating, (c) chemical formula of the ATSP coating.

5.6 Conclusion

Sand abrasive wear experiments were carried out over thin (~30 microns) high load bearing polymeric ATSP-based and PEEK-based coatings. ATSP-based coating showed excellent abrasive wear resistance. These experiments showed that ATSP-based coatings are effective in mitigating friction and wear under aggressive contaminated lubricated conditions, as is the case, for example, in hydrodynamic plain bearings used in ESPs. The following conclusions could be drawn:

a) Without abrasive sand particles in the lubricant, both bare substrate C18200 Chromium copper and ATSP coating exhibited zero wear; while under abrasive sand conditions, ATSP coating showed superior wear resistance (wear rate of 6.1×10^{-7} mm^3/Nm) compared with bare substrate material, which is somewhat counterintuitive.

b) Large sand particles could penetrate the coating, even though its superior tribological performance is still retained. Smaller sand particles only cause minor scratches on the coating.

c) The COF of ATSP coatings remained stable around 0.115 even though there were some deep scratches on the ATSP coating due to the large sand particles.

d) Abrasive sand worked as a solid lubricant causing a beneficial effect in the PEEK based coating case, with a decreasing wear rate form 5.8×10^{-6}

mm^3/Nm under clean lubrication to $2.1x10^{-6}$ mm^3/Nm in the presence of sand.

e) Large scratch recovery rate of ATSP coatings (57.3%) and XPS analysis of the beneficial tribo-layer explained why ATSP coatings exhibited excellent tribological performance and how this is affected by the functional groups present on the coating surface.

6. HIGH TEMPERATURE AND HIGH PRESSURE TRIBOLOGICAL EXPERIMENTS OF ADVANCED POLYMERIC COATINGS IN DRILLING FLUID FOR OIL AND GAS DRILLING APPLICATIONS

Extended reach drilling (ERD) wells enable reaching large areas of reservoir offshore from drilling stations onshore, or islands, and longer total depth (TD) allows larger areas to be reached. However, the friction force encountered between the drilling pipe or string and wall, and the strength of the drilling string set a limitation of TD. Based on the knowledge from chapter 2-5, ATSP based coatings can endure extreme temperature, high load and abrasive conditions; thus, in this chapter, ATSP based coating was used for friction reduction purposes for drilling applications, which combine all the extreme conditions mentioned above. Three types of experiment were carried out, namely temperature effects (75, 125 and 175°C), Stribeck analysis (at 75°C), and wear studies (at 75°C). All experiments were performed at a 3.45 MPa chamber pressure and oil-based drilling fluid. Experimental results showed that the ATSP coatings reduce the COF at different temperatures (~ 58% reduction) and at the boundary lubrication regime (~ 43.7% reduction at speeds lower than 0.95 m/s), compared with bare O1 tool steel material. The wear studies showed the ATSP based coating exhibited very low wear rates, which was of the same order as the base O1 tool steel material. The wear mechanism of the coating and tool steel was investigated using SEM and EDS.

6.1 Introduction

Due to cost-effectiveness and environmental benefits, ERD has become a commonly used technique for the oil and gas industry to access reservoirs. ERD wells have achieved great depths/lengths with TD over 10 km being used around the world [130-132]. With longer TD, more area of the reservoir can be exposed; however, TD is limited because of the higher torque and drag caused by the sliding friction between the drilling string and borehole wall [130-136]. There are techniques to reduce the torque and drag, including well-path design, light weight string components, hole cleaning, co-polymer beads, mechanical friction reduction tools and lubricants [132]. Out of these methods, lubrication method (reduced COF) is the simplest, most predictable and, sometimes, most cost-effective method [137, 138].

Considering the tribology for the drilling system, as shown schematically in **Figure 58**, without the drill bit part, there are three items involved: the drilling fluid, the drill string and the borehole wall. To reduce the COF, we can modify these three items in the system. For the drilling fluid, its main functions are to: (1) carry cuttings from beneath the drill bit and transport them back to the surface; (2) cool and clean the drilling bit; and (3) reduce the friction between the drill string and borehole wall [135, 139]. Both water-based drilling fluids and oil-based drilling fluids have received great attention from the engineering and research communities and a lot of efforts have been attempted trying to understand and improve their lubricity performance [130, 132, 134, 135, 137-143]. However, there is limited tribological research on modifying the drilling

or borehole wall [144, 145]. Danks's [144] work was focused on the wear resistance of hard coatings without considering the COF by extreme load scratch testing; Bangaru [145] used chemical vapor deposited (CVD) DLC coatings to reduce the COF to a very low value of 0.05. However, the CVD deposition method is expensive and not practical to coat the very long (km) and large diameter drill strings. Thus, other cost-effective coatings should also be investigated.

Polymeric materials have good resistance to temperature, corrosion, galling and seizure, low friction, moderate wear resistance, self-lubricating properties, low noise emission and low production cost [19, 97, 98, 103, 108, 117]. Thus, they are very good for tribological applications. In oil and gas industry, the severe corrosion on the steels [146-149] could be largely prohibited if there are polymer coatings deposited on the steel surfaces. In general, as polymers are soft materials, especially for thin polymeric coatings, their wear resistance is a concern. In our previous research, advanced high bearing ATSP-based polymeric coatings showed extremely low wear rate (4.15×10^{-8} mm^3/Nm) in simulating extreme working conditions of tilting pad bearings and compressor conditions [45, 87], high temperature capability [88] and excellent three-body abrasive wear resistance [150]. In the present work, we report on ATSP as a cost-effective coating to reduce the COF for oil&gas drilling applications.

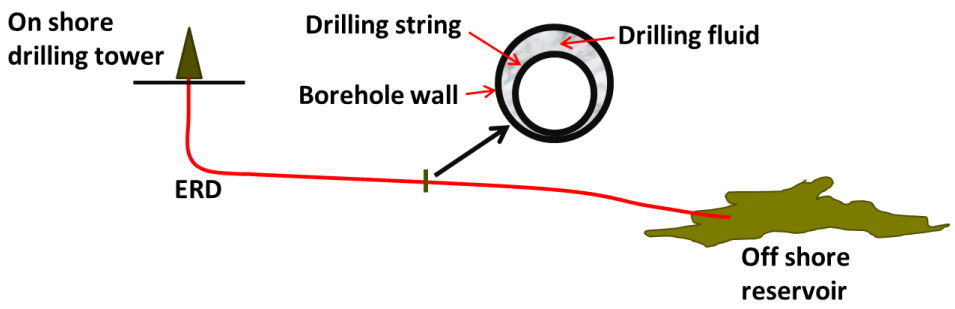

Figure 58 Schematic of ERD

The tribological performance of drilling fluids used in our study is affected by numerous parameters, such as temperature, environmental pressure, sliding speed, and fluid composition [137, 138, 140]. For example, in the Gulf of Mexico area, the operating temperatures can reach higher than 195°C in the bore hole [151]. Because temperature has strong effects on the drilling fluid [137], significant efforts have been tried to take temperature into account for drilling fluid development. However, due to fluid evaporation (especially water in the drilling fluid) at high temperatures, most experiments are carried out at less than 100°C [137, 138, 140, 143, 152, 153]. In this work, we constructed a specialized tribometer that has a high-pressure chamber (up to 13.8MPa), and a controlled temperature up to 200^{o}C. Specifically, in this work, we carried out experiments up to 175°C at a 3.45 MPa (500 psi) chamber pressure, which is able to suppress the evaporation and improve the boiling point of water up to 242°C.

Extreme abrasive conditions, combined with high temperature and high environmental pressure that is encountered in drilling fluid applications is much more

severe than standard or simplified methods used to investigate the micro scale abrasive resistance of polymers, such as applying low sliding speed and small sand size [117, 124-126]. In this work, three different types of experiments, namely temperature effects, Stribeck curve analysis, and wear experiments, were carried out under combined high temperature and high pressure conditions with drilling fluid for both ATSP coatings and bare O1 tool steel substrates. Temperature effects study was to investigate the influence of temperature up to 175°C for the drilling system; Stribeck curve analysis was to capture the speed effect at a wild range from static condition to dynamic condition at speed of 1.9m/s that may happen in field for the drilling string; while the wear experiments were to compare the were resistance of the ATSP coating and bare substrate material in constant conditions (same load, speed and temperature).

6.2 Experimental conditions and samples

6.2.1 Specialized drilling fluid tribometer (DFT)

As shown in **Figure 59(a)**, the DFT (a modification of UPHT as in chapter 5) has a pressurized chamber with pressures up to 13.8 MPa, which enable this tribometer to simulate high pressure environment (1380m sea water pressure) in down hole. The DFT can also do experiments at high temperature up to 250°C for submerged lubrication achieved by a heating plate at the bottom of the secondary drilling fluid chamber, as shown in **Figure 59(b-d). Figure 59(d)** is the cross section schematic of the secondary

chamber which shows the pin-on-disk experimental configuration. The pin sits on a self-align pin holder and there is a view widow to check the alignment between the disk and pin before drilling fluid to be filled in the chamber. The cover on top of the secondary chamber is to prevent the splash of drilling fluid due to high speed rotation. And the hood inside the secondary chamber is to decrease the exposed area of drilling fluid thus can decrease the evaporation of the fluid at high temperature. The tribometer has oscillation (up to 60 Hertz) and unidirectional rotation (different speeds up to 2000rpm), a closed-loop load control system with normal load up to 1120N, and the capability to measure in situ: friction, normal load & near contact temperature.

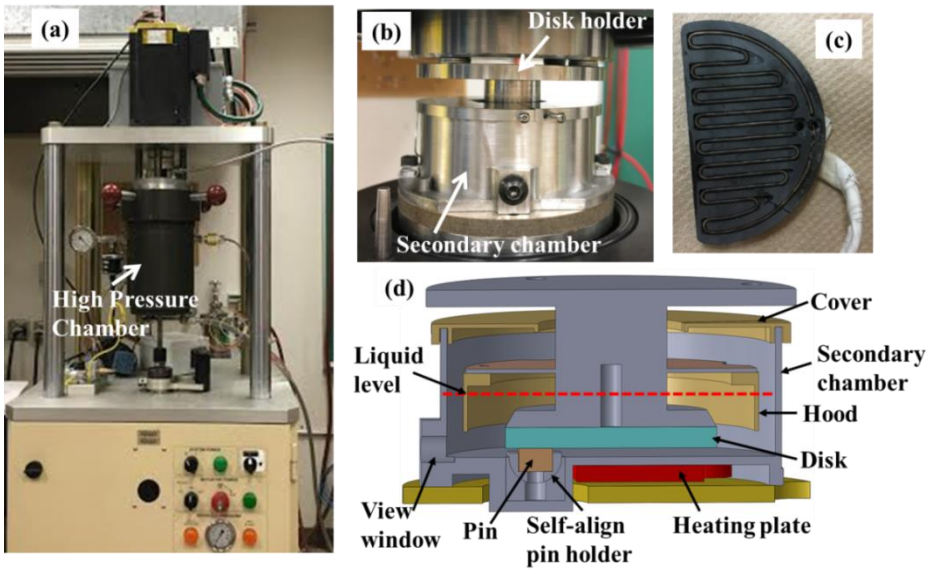

Figure 59 DFT (a) picture of the DFT, (b) picture of opened chamber, (c) heating plate and (d) schematic drawing of the secondary chamber

The tribometer is capable of operating at different speeds, and thus can perform Stribek curve analysis, which relates the measured COF (μ) versus νη/N, as shown schematically in **Figure 60**. Where, ν is the relative velocity, η is the bulk fluid viscosity and N is the contact pressure. Referring to the Stribek curve, there are three lubrication regimes: (1) boundary, (2) mixed or starved, and (3) hydrodynamic (full film) lubrication regimes [137]. At the beginning of the Stribek curve, there is the highest point of the COF, which is the static COF. For most material interfaces, static friction is the largest resistance force before the two contacting surfaces start relative movement. In the boundary lubrication regime, there is presence of minute lubricant; however the two relative surfaces experience significant asperity contact. In the full film hydrodynamic

regime, the two relative surfaces are separated by the fluid film and the internal fluid friction alone determines the COF. Lastly, in the mixed lubrication regime, there is the coexistence of boundary and hydrodynamic lubrication and the fluid film thickness is similar to the contact surface roughness [137] (compared to the boundary lubrication regime, more contact load is now supported by the fluid).

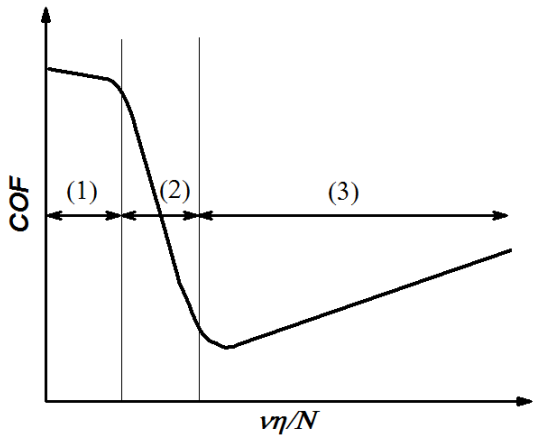

Figure 60 Schematic of the Stribeck curve, (1) boundary, (2) mixed, and (3) hydrodynamic lubrication

6.2.2 Samples

The samples used in the study include a "hair-thin" ATSP coating on bare SAE O1 tool steel disk, bare O1 tool steel disk and curved pins made out of SAE O1 tool steel, as shown in **Figure 61**. The O1 tool steel is commonly used for the ASTM D2714 and D3704 block-on-ring tests. The ATSP coating which is about 35 μm thickness was applied using electrostatic spray deposition method of a powder mixture with 95wt. % of

ATSP and 5wt. % of PTFE, followed by a 30 min curing process at a temperature of 270 °C in convective air. The diameter of the disk is 50.8 mm and the diameter of the wear track is 36.31 mm. The diameter of curvature of the pin is 35 mm and the length of the pin is 8 mm, these dimensions would produce a reasonable initial Herzian contact stress, 153MPa at 89.6N normal force, compared with real application contact stress. The surface roughness of the ATSP coating, bare O1 steel disk and pin were 3.2 μm RMS, 0.2 μm RMS and 0.1μm RMS, respectively, as measured by 5 mm long line scans using a Tencor P6 profilometer.

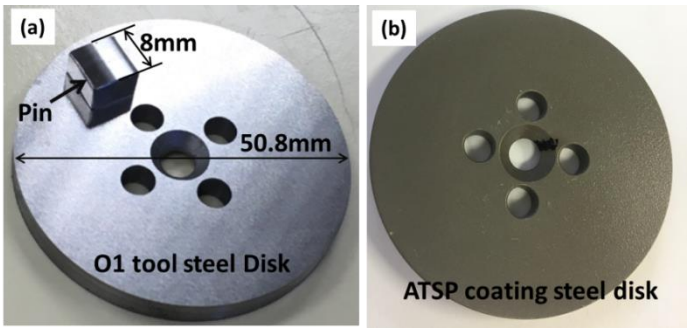

Figure 61 Photographs of samples, (a) O1 tool steel disk and pin, (b) ATSP coating on O1 tool steel

The oil-based drilling fluid (M-I SWACO drilling fluid) is full of abrasive particles, with size from less than 1 micron to 300 microns in diameter, and the main contents of the mud are straight run petroleum, distilled hydro-treated petroleum, barite, calcium carbonate, mica and silica sand, as shown in **Table 8**; the weight percentage of all solids is about 59%, measured by heat evaporation of all the fluid. Both the bare O1

steel disk and pin were ultrasonically cleaned at 50°C for 10 min in acetone before experiments, and then dried by a regular air blower before experiments; while the ATSP coatings were cleaned by isopropanol with the same process.

Table 8 Contents of plain mud.

composition	Weight % Range
Barite	30-60
Distillates, Petroleum	10-30
Calcium Carbonate	5-10
Calcium Chloride	1-5
Silica, Crystalline, quartz	1-5
Mica	1-5

6.2.3 Experimental conditions

Three different types of experiments were carried out, namely temperature effects experiments, Stribeck analysis, and wear experiments. The experimental conditions are summarized in **Table 9**. The high chamber pressure of 3.45 MPa (500 psi) simulates the underground borehole high environmental pressure and also suppress the evaporation of drilling fluid at high temperatures.

Table 9 Experimental conditions in drilling mud

Experiment type	Description
Temperature effects	75 °C, 125 °C and 175 °C; 200 rpm (0.38 m/s), 89.6 N.
Stribeck (speed) analysis	75 °C; 89.6 N; 1000 rpm (1.9 m/s), 750 rpm (1.425 m/s), 500 rpm (0.95 m/s), 200 rpm (0.38 m/s), 100 rpm (0.1 m/s), 44 rpm (0.084 m/s), 3 rpm (0.006 m/s), and oscillation movement to obtain both kinetic COF at different speeds and the static COF.
Wear experiments	75 °C; 89.6 N; 500 rpm (0.95 m/s); 1 hour duration (3420 m)

6.2.2.1 Experimental protocol for temperature experiments

As shown in **Figure 62**, x axis is the time and y axis is for three different parameters: temperature, load and speed. In the temperature effects study of one pair of disk and pin, the first stage of the experiment is performed at room temperature and was treated as a run-in period. After that, there were four different heating up temperature stages, namely 25°C, 75°C, 125°C and 175°C. At each temperature stage, the speed was 200 rpm (0.38 m/s) and the load was 89.6 N. Each experimental stage needed about 6 min; and between each experimental stage, the disk and pin were disconnected, and the speed and load were zero.

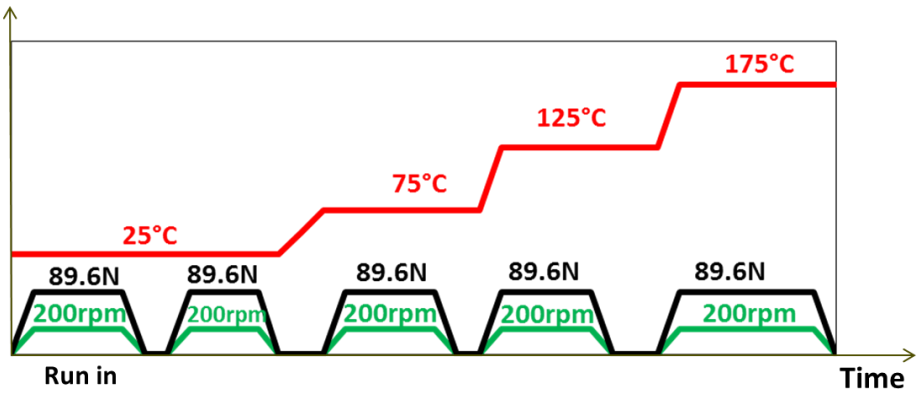

Figure 62 Experimental protocol for temperature effect experiments

6.2.3.1 Experimental protocol for Stribeck experiments

Figure 63 shows the experimental protocol for the Stribek curve analysis: the temperature was set to 75°C and the load to 89.6 N; Eight (8) different speed stages, namely 1000 rpm (1.9 m/s), 750 rpm (1.425 m/s), 500 rpm (0.95 m/s), 200 rpm (0.38 m/s), 100 rpm (0.1 m/s), 44 rpm (0.084 m/s), 3 rpm (0.006 m/s), and oscillation movement were performed to obtain both the kinetic COF at different speeds and the static COF. Note that with the oscillation movement, when we switched the sliding direction, the COF showed a peak value, and we treated this peak COF as the static COF. The whole process was repeated five times and the first time was treated as a run-in period, and it was not counted in the analysis.

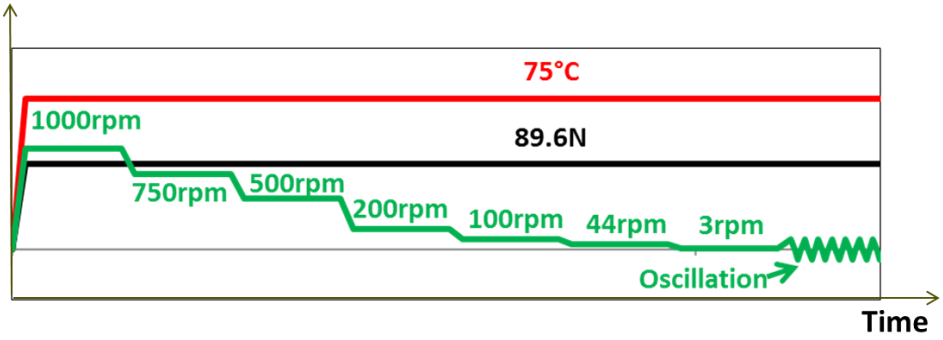

Figure 63 Experimental protocol for Striveck curve analysis

6.2.3.2 Experimental protocol for wear experiments

This is the simplest protocol, where the normal load and sliding speed are kept constant for a pre-determined duration. Specifically, the temperature was set to 75°C, the load to 89.6 N, the speed to 500 rpm and the total duration was one hour, resulting 3420 m sliding distance. During the experiments, the in situ friction coefficient was measured, and at the completion of each experiment, the wear was also measured, and thus enable the calculation of the wear coefficient.

6.3 Tribological experimental results

6.3.1 Temperature effects

Figure 64 shows the experimental results of the temperature effects. From **Figure 64(a)**, for tool steel, the COF increased from room temperature to 75°C and then

decreased. This increasing trend is consistent with tribological studies of drilling fluids at temperature below 100 °C [137, 152]. The decreasing trend at higher temperatures cannot be compared with literature values, since there is no relevant higher temperature tribological studies under drilling fluid conditions. For the ATSP coating, the COF was constant at temperatures below 125°C, and at temperatures higher than 125°C, the COF decreased. At temperatures below 125°C, the COF for the ATSP coating was expected to change with temperature in accordance with viscosity changes of the drilling fluid/lubricant. According to Zhao's rheological study of oil-based drilling fluids at high temperature and high pressure conditions, the viscosity of the drilling fluids exhibited a significant change when temperature increased from room temperature to 121.1°C [154]. Thus, the COF between the contacting surfaces in drilling fluid at different temperatures should also change, assuming that friction is due to shearing of the fluid. In the current study, operation is in the boundary lubrication regime, with a sliding speed of 0.38 m/s, and the abrasive particles in the drilling fluid and the toughness of the ATSP coating play an important role in determining the COF, and the viscosity of the lubricant plays a secondary role. At higher temperatures of 150°C and 175°C, the ATSP coating became softer and the abrasive resistance was less, thus the COF decreased. Compared with bare tool steel, the COF of ATSP coating was 58% lower, at different temperature stages.

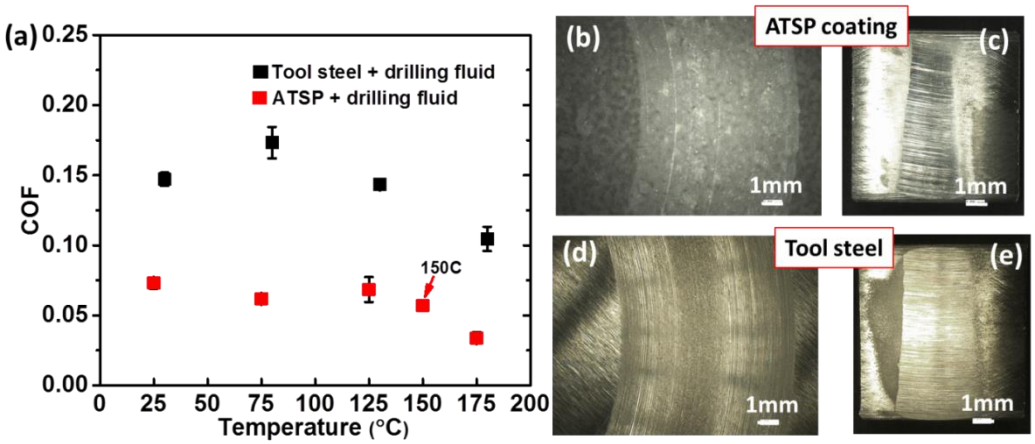

Figure 64 Experimental results of temperature effects: (a) COF at different temperatures. Optical microscopy images of (b) ATSP coating disk, and (c) pin, after experiments, (d) tool steel disk, and (e) pin after experiments.

In general, the friction force between two sliding solids could be attributed to adhesion and deformation surface effects. In the current case of submerged abrasive conditions at low speeds, the friction arises from abrasive scratch (deformation) resistance between the two contacting surfaces. Since the polymeric coating has lower elastic modulus and shear strength, compared to steel, the scratch resistance on the polymeric coating is lower. Thus, the ATSP coating had a much lower COF compared with bare tool steel. In addition to the significant COF reduction by the ATSP coating, the other important finding is that ATSP coating did not wear out under this high temperature and severe abrasive conditions. The optical microscopic images shown in **Figure 64(b-e)** show the samples after the highest temperature of 175°C experiments. Abrasive scratches are very clear on the ATSP coating, bare tool steel disk and the pins.

However, the ATSP coating was not penetrated during the experiment. Further analysis using SEM/EDS techniques and discussion of the wear mechanisms is presented in Sec 6.4

6.3.2 Wear experiments

Figure 65(a) shows the in situ COF vs. time for the 1 hour duration experiments. Note that the pin and disk were disengaged and engaged every 20 mins to ensure better coverage of the drilling fluid between the contacting surfaces. Thus, at the position of 20 min and 40 min, there appears some noise in the COF value, due to stopping and restarting the experiment. The COF of the ATSP coating was constant during the experimental process, and the variation of the COF was also small. For the tool steel, its COF was decreasing through the experimental process; it had a high initial COF and decreased to a value that was very similar to that of the ATSP coating. This decreasing trend was due to the wear on the pin, which switched the line contact to a planar (nominally flat) contact. With smaller contact area during the initial period, higher contact stresses caused sever scratches on the contacting surfaces, resulting in higher COF. Also, the vibration of the tool steel COF was much higher compared with the ATSP coating. Thus, the ATSP coating was superior for vibration absorption and enabled smoother operation, compared with bare tool steel in this third body abrasive drilling fluid condition.

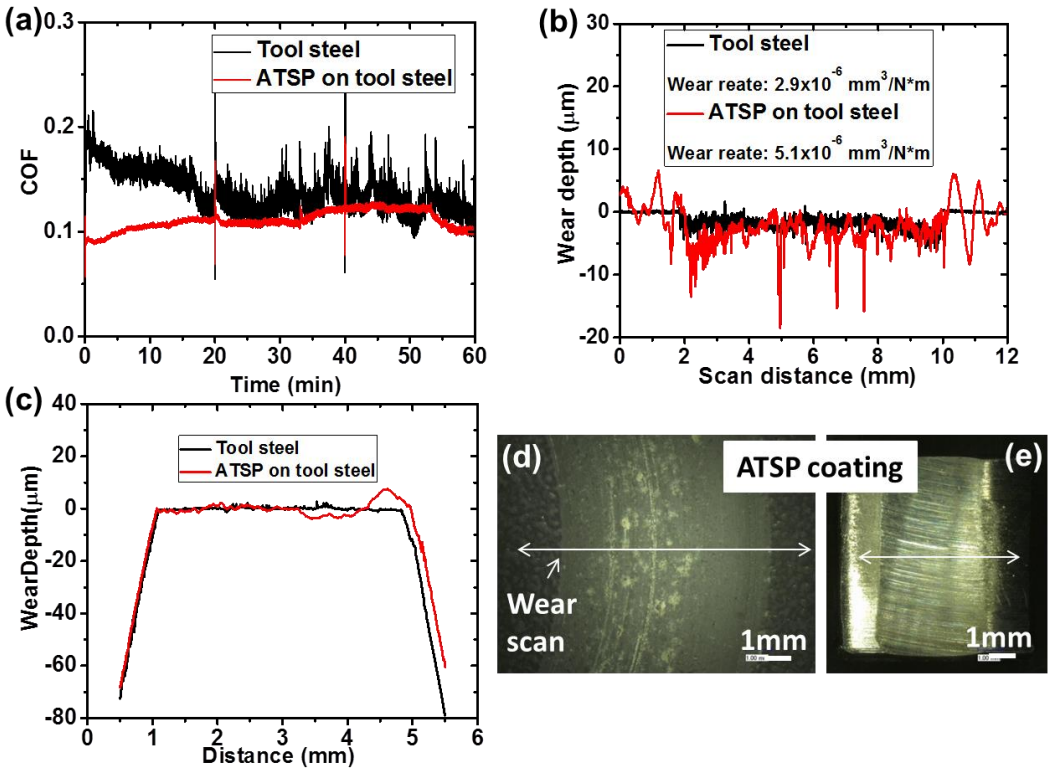

Figure 65 Experimental wear results: (a) COF vs. time, wear scans on the (b) disks and (c) pins, optical microscopic images of (d) ATSP coating disk and (e) pin after experiments.

Figure 65(b-c) show typical wear scans on the worn disks and pins after the wear experiments. The positions of the line scans are shown in the optical images of the disk and pin in **Figure 65(d-e)**. From **Figure 65(b)** and **Figure 65(d)**, the hair-thin ATSP coating was still in good condition (and not penetrated) after the 1 hour-long severe abrasive experiment, even though some deep scratches on the coating are evident. Although there were deep scratches on the ATSP coating surface, the COF was not substantially affected. The formation of these deep scratches also showed in other three

body abrasive experiments on the ATSP coating [150]. The wear rate of ATSP coating was 5.1×10^{-6} mm^3/Nm, which was of the same order of the wear rate for bare tool steel disk (2.9×10^{-6} mm^3/Nm). As shown in **Figure 65(c)** the curved pins also experienced wear, including the steel pin that was in contact with the much softer polymeric ATSP coating. Since ATSP is much softer and has less abrasive scratch resistance than tool steel, we would expect less wear on the pin which contacted with ATSP coating. However, the abrasive particles are readily embedded on the polymeric coating surfaces and formed partial two-body abrasive wear [3], which had higher wear rate, compared with three-body abrasive wear [129].

6.3.3 Stribeck curve analysis

During typical operation, the drilling string starts the rotation from stationary position, to its normal operating speed. For a drilling pipe with diameter of 340 mm, the relative sliding speed at the contacting point is 1.78 m/s at a rotational speed of 100 rpm. In this Stribeck curve analysis, the speed was varied from static (0 m/s) to 1.9 m/s, which covered the whole operating sliding speed in the field. **Figure 66** shows the experimental results of the Stribeck curve analysis. Specifically, **Figure 66(a)** shows the Stribeck curve for the ATSP coating and the bare tool steel. Note the first point of the Stribeck curve was taken as the static COF arrived by the oscillation movement. Except at speeds of 0.95 m/s (500 rpm) and 1.425 m/s (750 rpm), the COF of ATSP coating was lower than bare tool steel. Specially, at speeds of 0.0057 m/s (3 rpm), 0.0836 m/s (44

rpm) and the static condition, the COF for the ATSP coating was only 50% of the value for the bare tool steel. In addition, the tool steel had large variation of static COF, which was due to the bigger particles could randomly engage between the contact surfaces and result unstable contact conditions. While for ATSP coating, the COF was mainly determined by the mechanical property of the coating, thus producing very constant COF. If considering the friction resistance only for the drilling string, application of ATSP coating could reduce the max friction resistance torque by 50% and would be greatly beneficial for ERD to reach larger area in a typical reservoir. **Figure 66(b-c)** show optical micro images of the ATSP coating and pin after the experiments, showing that the ATSP coating survived after 5 repetitions of the Stribeck curve experiments without penetration.

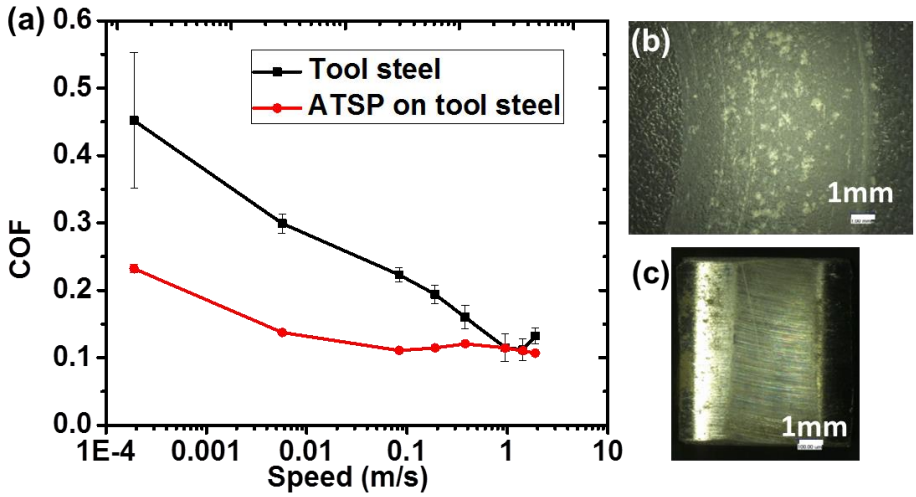

Figure 66 Experimental results of Stribeck curve analysis, (a) COF vs. sliding speed. Optical micro images of (b) ATSP coating with (c) pin after experiments.

6.4 SEM/EDS analysis

Figure 67 shows the SEM images of the ATSP coatings after experiments at different temperatures. Specifically, **Figure 67(a-c)** after one hour wear experiments at 75°C, **Figure 67(d-f)** after the temperature effect experiments that were stopped after 125°C and **Figure 67(g-i)** after the temperature effect experiments that were stopped after 175°C. All cases showed abrasive wear groves, which were due to the abrasive particles in the drilling fluid. At the same time, there were particles embedded on the coating surface at all temperatures. Comparing the surfaces after the temperature effects experiments of 125°C and 175°C, the higher temperature had much more particles on the surfaces. This was because, at higher temperature, the polymer is softer and has better embeddability property.

The SEM/EDS analysis in **Figure 68** shows that the particles embedded in the coating surfaces were solids that came from the drilling fluid, including barite and silica sand. These hard particles embedded on the coating and could sustain the load and protect the coating from severe wear. Meanwhile, the coating itself had small abrasive resistance and worked as solid lubricant, thus the COF was much lower, compared with bare tool steel, especially at higher temperatures such as 175°C. **Figure 68(d),** there are some voids or holes on the surface, and these holes were formed after the embedded particles released from the surface because of the sliding contact with the pin.

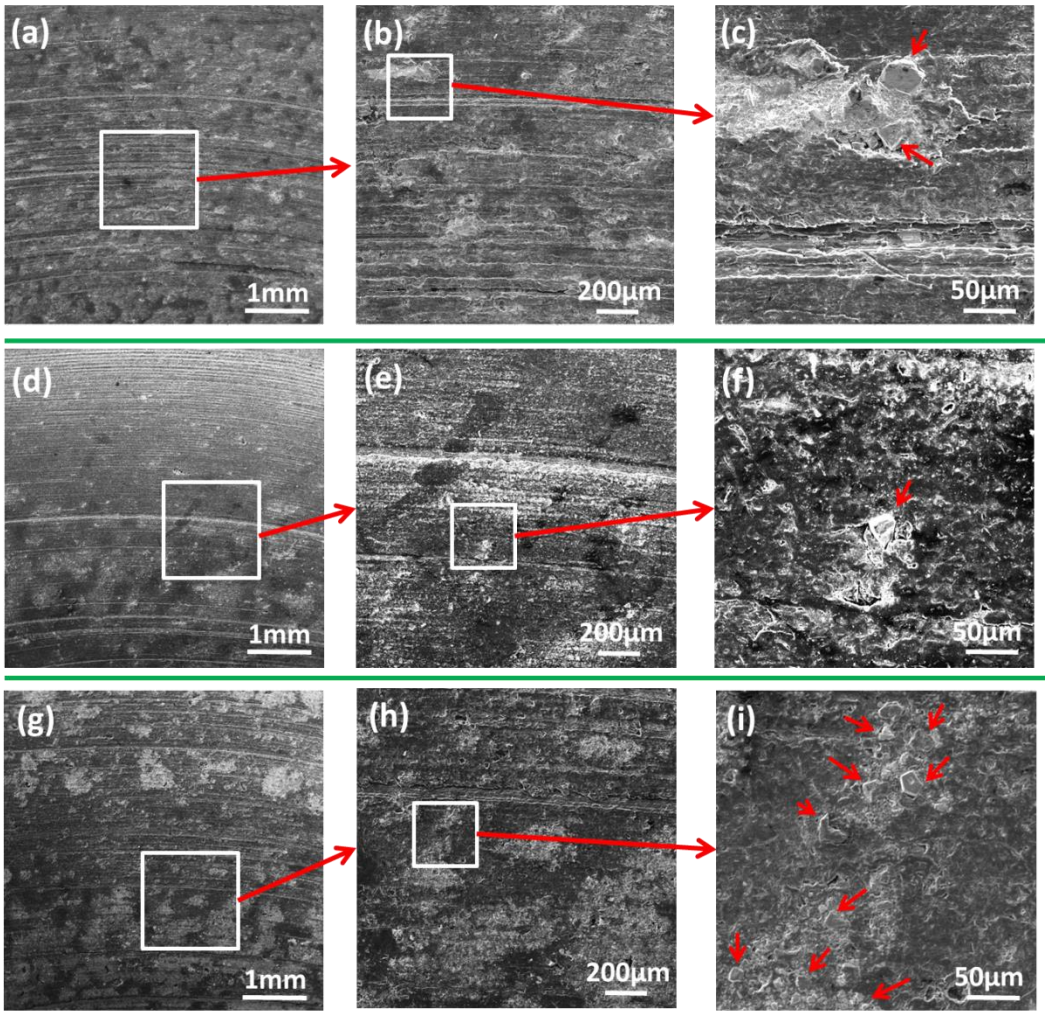

Figure 67 SEM images of ATSP after different temperature experiments, (a, b, c) one hour wear test at 75°C, (d, e, f) temperature effects experiments stopped after 125°C, (g, h, i) temperature effects experiments after 175°C

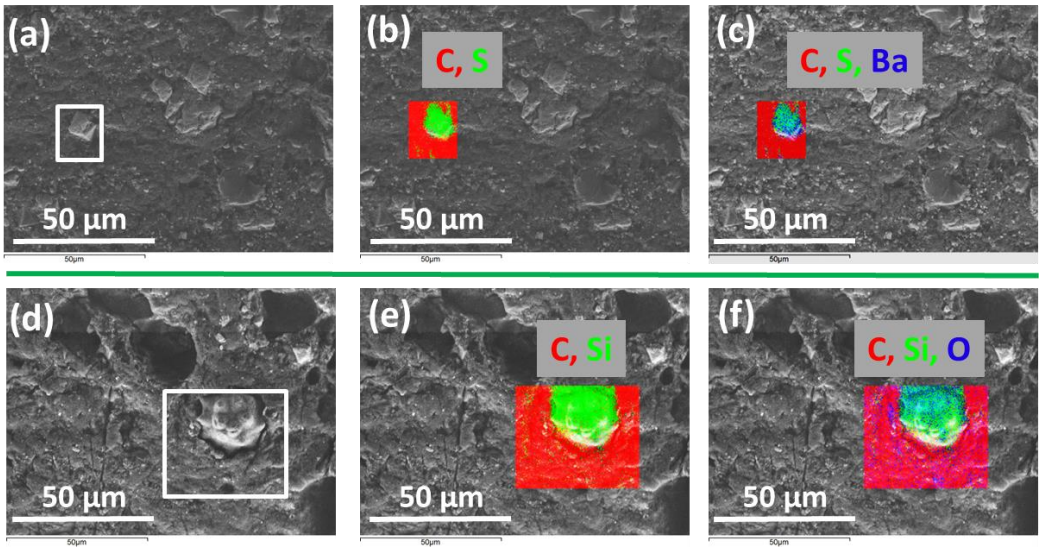

Figure 68 SEM/EDS of ATSP after 175°C temperature effects experiments: (a, b, c) particle source of $BaSO_4$, which is barite particle, (d, e, f) particle source of SiO_2, which is silica sand.

The Optical and SEM images of the wear track on bear tool steel disk after 175°C temperature effects experiments are shown in **Figure 69**. From **Figure 69(a-b)**, the center section of the wear track has a different appearance, compared with the inner and outer parts of the wear track. The center section shows a rough surface and no much abrasive wear groves. Examining closely **Figure 69(c)** for the center section, the surface is full of voids/holes and just few abrasive scratches. The inner and outer parts show clear abrasive wear scratches. Under higher magnification in **Figure 69(d)**, the surface shows abrasive scratches and few voids/holes that were polished by the sliding.

Figure 70 shows the formation mechanism of the voids/holes on the wear track. As shown in the schematic of **Figure 70(a)**, there is the local stream (turbulence) on the

downstream of the sliding direction and this local stream would be stronger in the middle part than the inner and outer sides of the wear track due to the difference effects from the main flow of drilling fluid. Both the inner and outer sides are near the two edges of the pin and the local stream is weakened by the main flow of drilling fluid with opposite direction in the container. The particles in the drilling fluid were brought into the near contact region by this local current (stronger in the middle part), with the pressure and movement from the disk, the particles would erode both the disk and pin as shown in **Figure 69(c)** and **Figure 70(c)**. This erosion wear due to particle impingement combined with abrasive sliding wear as in the middle section of wear track is similar to the real application of the drilling string[155, 156]. As for the case of the ATSP coatings, because of the deformation of the polymer coating, the erosion wear on the pin is not as severe as in the case of the bare tool steel. Thus, the improved embeddability property of the ATSP coating improves the erosion resistance under drilling fluid conditions.

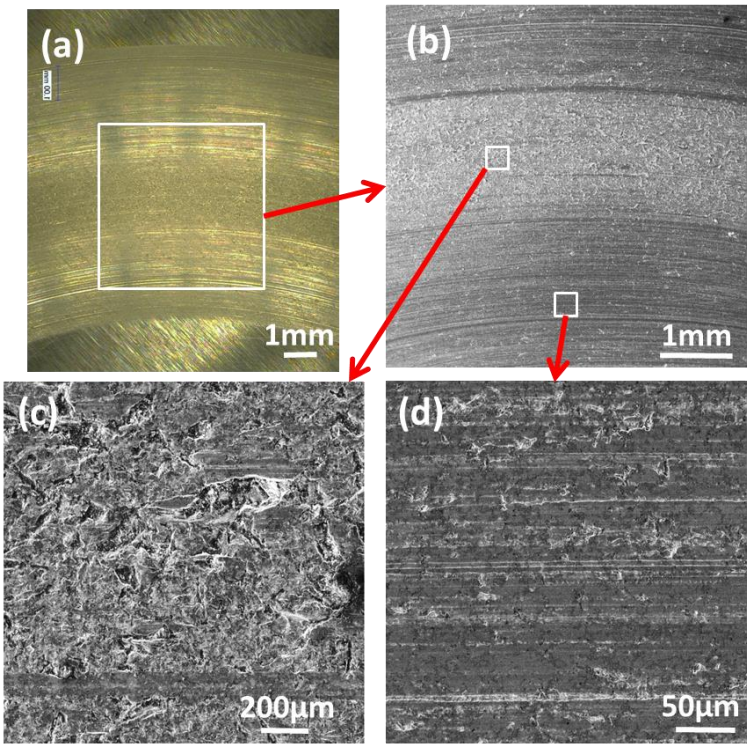

Figure 69 Tool steel disk after 175°C temperature effects experiments. (a) Optical image and (b) SEM image of wear track on tool steel. (c) erosion and abrasive wear in the middle part on wear track, (d) abrasive wear in the boundary part of wear track

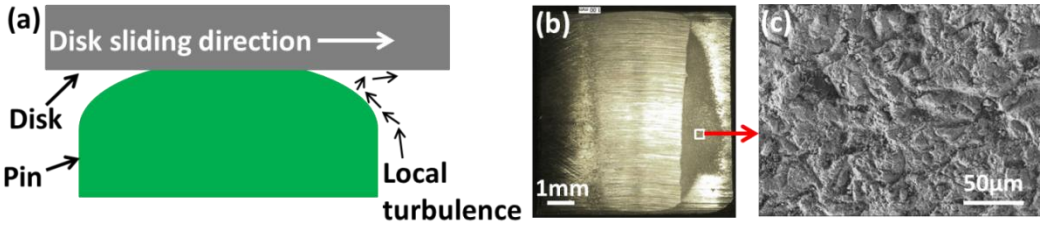

Figure 70 Erosion wear, (a) local turbulence on the downstream sliding direction, (b) optical image and (c) SEM image of steel pin contacted with tool steel after 175°C temperature effects experiments.

6.5 Conclusion

A special tribometer was built and used to perform high temperature and high pressure experiments simulate ERD wells drilling conditions. This work proves the capability of thin polymeric coatings under extreme working conditions. Based on the results the following conclusions could be made:

a) ATSP coatings reduced the COF of bare tool steel by 58% at different temperatures up to 175°C;
b) ATSP coatings exhibited excellent wear resistance with wear rates that were in the same order of bare tool steel in the presence of drilling fluid;
c) From Stribeck analysis, the ATSP coatings had much lower COF in the boundary lubrication regime, compared with bare tool steel;
d) The solid particles from the drilling fluid were readily embedded on the soft ATSP coating and the embedded particles could sustain load and protect the coating;
e) Both abrasive wear and erosion wear occured in the current curved pin-on-disk experiments due to the local current on the downstream direction. ATSP coating could reduce the erosion wear because of its soft and deformable property.

7. ACQUIRING TEMPERATURE EFFECTS ON MECHANICAL PROPERTIES AND FRICTION PERFORMANCE OF VISCOELASTIC POLYMER COATINGS BY HIGH TEMPERATURE NANOINDENTATION[4]

Traditionally, the friction force between two solids is attributed to adhesion and deformation effects. Adhesion involves the shearing between the real contact surfaces and deformation is due to the hard material's asperities plowing on the softer material. In chapter, a model that relates the COF with the viscosity and elasticity of a viscoelastic material is proposed. Two advanced polymeric coatings are selected for this study, namely ATSP and PEEK based coatings. High temperature nanoindentation experiments were conducted on these two coatings at the same elevated temperatures as macro-scale ball-on-disk tribological experiments at different temperatures (room, 100°C, 180°C and 260°C) in chapter 2. Hardness was directly measured from the indentation experiments and viscosity with elastic modulus were obtained by curve fitting of the nanoindentation's unloading curve by a quadratic Maxwell model. The two coatings showed decreasing hardness, elastic modulus and viscosity trends, with increasing temperature. The ATSP coating exhibited a higher indentation recovery rate

[4] Reprinted with permission from "A phenomenological elevated temperature friction model for viscoelastic polymer coatings based on nanoindentation" by Lan P., Zhang, Y., Dai, W. and Polycarpou, A.A., Tribology International, In press (2017), Copyright 2017 by Elsevier.

and hardness compared to the PEEK coating, thus the ATSP material exhibited much better wear resistance. Substituting the viscosity and elastic modulus terms, a model is proposed that shows reasonable COF prediction for the two coatings at higher temperatures, but below the glass transition temperature.

7.1 Introduction

Viscoelastic materials exhibit both viscous and elastic properties. Viscous materials include liquids such as water and lubricants, and elastic materials include steels and other hard material at room temperature. While polymers usually show viscoelastic performance, metals at high temperature also exhibit viscoelasticity. For a pure viscous liquid, as shown in **Figure 71**, the liquid is placed between two parallel plates with distance h_1. If the bottom plate is fixed while the top plate is moving at a sliding speed v_1, there is a resistance force F_1 encountered on the top plate due to the viscosity of the liquid, given as

$$\boldsymbol{F_1 = A_1\,\eta_1\,(\frac{v_1}{h_1})} \qquad (4)$$

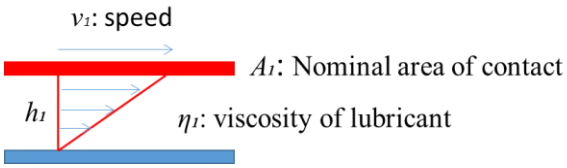

Figure 71 Sliding for pure liquid.

An elastic material exhibits a linear relationship between its stress and strain, as shown schematically in **Figure 72(a)**. For a viscoelastic material, due to its viscous effect, there is a hysteresis loop after one cycle of loading and unloading between the stress and strain, as shown in **Figure 72(b)**. The area enclosed by the hysteresis loop is the energy loss for one loading and unloading cycle.

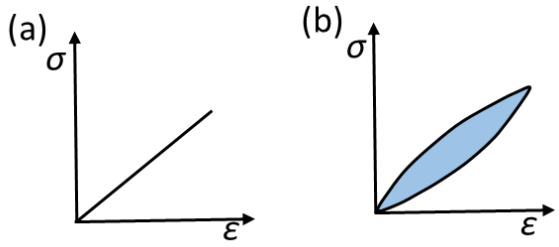

Figure 72 Schematics of stress-strain relationships for (a) elastic material, and (b) viscoelastic material.

The friction force between two solids could be attributed to adhesion and deformation effects. The adhesion force involves the shearing between the real contact surfaces, and the deformation force is due to the hard material's asperities plowing on

the softer material. Chang *et al.* [157] and Kogut and Etsion [158] proposed mathematical models for calculating the friction force and friction coefficient between nominally flat solid rough surfaces. Their models take into account elastic, plastic, geometric, and force parameters of contacting and sliding solids. Researchers have also suggested that polymer lubricants at high shear rates could be considered as pure liquid and calculated friction coefficients based on continuum mechanics theory by taking into account slip lengths, bonding ratio and shear thinning [159, 160]. With regards to viscoelastic materials, Greenwood, Tabor and other researchers attempted to correlate friction and viscoelastic properties of rubber and polymers [161-167]. To decrease the shearing force between a hard slider and rubber, good lubrication was supplied between the surfaces, in which case the friction force would largely depend on the deformation of the rubber; And the deformation of the rubber has a strong relationship with its viscoelastic properties [161, 162]. Due to the contribution from shearing of the lubricant film, the correlation between the friction force and its viscoelastic property could not be well defined [167].

Tabor and others investigated viscoelastic rolling friction and they found that the rolling resistance was primarily due to elastic hysteresis losses in the rubber, and a relationship was proposed between the viscoelasticity and rolling friction [162-167]. Ludema and Tabor [167] found a good relationship between sliding friction at various speeds and temperatures, and the viscoelastic properties of the rubber by sliding a hard slider on rubber, under different experimental conditions. Their results showed that the

correlation between the sliding friction and the various viscoelastic properties was not strong below the glass transition temperature of the polymers. To the best of the authors' knowledge, the works reported in the literature relate friction with viscoelasticity based on experimental data, and there is no model that directly relates the friction force with the viscoelastic term. In this work, motivated by the resistance force of pure liquid (Eq. **(4)**), we propose a direct relationship between the friction force and the viscous term of the viscoelastic polymers.

7.2 Background and model development

7.2.1 Friction coefficient model (COF)

To study the mechanical properties of polymers, Maxwell and Voigt elements are typically used to model viscoelastic polymers [168-171], as shown in **Figure 73**. In each model, there is a spring and a damper, where the damper is dissipating energy once there is motion. **Figure 74** shows a pin-on-disk sliding configuration: a square steel pin with width d, mass m, normal load W and driving force F sliding on a polymer disk at speed v. The real contact area between the pin and disk A_r is proportional to the load W [172-175], based on the assumption of a statistical height distribution of the asperities. Greenwood and Williamson's contact model assumes that the asperities of the surface have spherical summits and their height has a Gaussian probability density function above a reference plane. Under these assumptions, both real contact area and load

depend on the separation of the two contact surfaces in similar ways, thus their ratio is almost constant [175]. The surface morphology has an important effect on the tribological performance of contacting surfaces [17, 176, 177]. According to reference [174], for surface asperity heights (z) distribution with an exponential function ($\psi = 17e^{-3z/\sigma_1}$), which is an approximate function for Gaussian distribution, the real contact area is obtained as

$$\boldsymbol{A_r = \frac{\sqrt{3\pi}}{\sqrt{\sigma_1/R}}\frac{W}{E^*}} \quad (5)$$

Where E^* is the composite modulus, σ_1 is the standard deviation of asperity heights, and R is the average radius of curvature of asperity summits. Let $k' = \frac{\sqrt{3\pi}}{\sqrt{\sigma_1/R}}$, then k' is a dimensionless geometry factor that is determined by the surface roughness properties and Eq. **(5)** can be written as

$$\boldsymbol{A_r = k'\frac{1}{E^*}W} \quad (6)$$

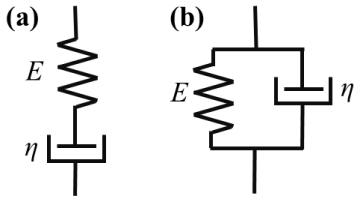

Figure 73 Viscoelastic mechanical elements, (a) Maxwell model and (b) Voigt model.

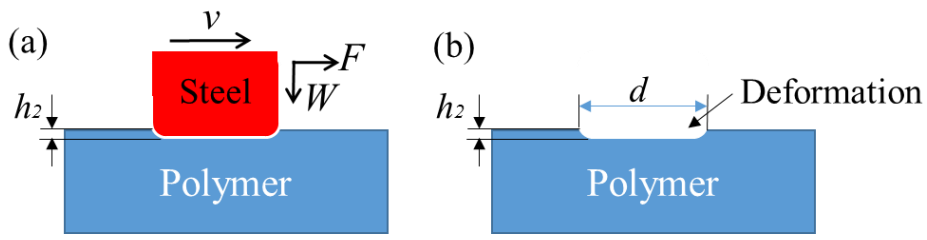

Figure 74 Pin-on-disk sliding: (a) square steel block sliding on polymer, (b) normal direction deformation.

Assuming the polymer is isotropic, and then both normal and lateral directions have an energy dissipation damper component with the same viscosity η. For the normal direction, the energy cost is due to the hysteresis loop energy loss E_{normal}, which is the same as in previously published research [161-167]. The quadratic Maxwell model is widely used to obtain the viscous-elastic-plastic properties of polymers [169, 178, 179]. In the quadratic model, each force component is proportional to the second power of the displacement or velocity, as shown in **Figure 75** (b). For a quadratic model in the lateral direction, within the real contact region, the shear velocity on the polymer is v, so, the resistance force due to polymers' viscosity is

$$\boldsymbol{F_v = \eta\,(A_r\,\rho)\,v^2 W} \qquad (7)$$

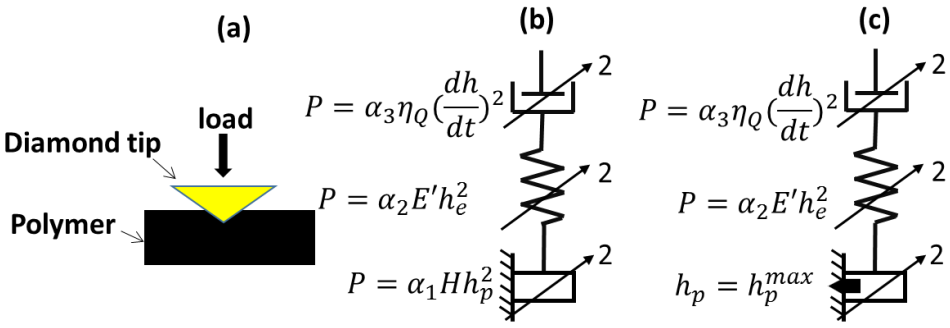

Figure 75 Nanoindentation models for polymers: (a) schematic of nanoindentation, (b) loading and (c) unloading Maxwell models, adapted from Ref. [169].

Where ρ is the density of the viscosity damper, which is determined by the standard techniques to measure viscosity: larger area used in characterization of viscosity would cause larger resistance force and ρ would be smaller. Substituting Eq. **(6)** in Eq. **(7)**, we obtain

$$\boldsymbol{F_v = \eta\, \rho\, k'\, W\, \frac{1}{E^*}\, v^2} \qquad (8)$$

Let $k = \rho\, k'$ with units of m^{-2} to obtain the simplified relationship

$$\boldsymbol{F_v = \eta\, k\, W\, \frac{1}{E^*}\, v^2} \qquad (9)$$

Considering the pin and disk configuration depicted in **Figure 74**, as a whole system, the kinetic and potential energies are constant, with the kinetic energy being $\frac{1}{2}mv^2$ and the potential energy being Ed', where E and d' are the polymer's elastic modulus and its overall deformation, respectively. Within sliding distance d, the energy input E_i is

$$\boldsymbol{E_i = F\,d} \quad (10)$$

Energy cost E_c is due to both normal and lateral dampers in the polymer, that is

$$\boldsymbol{E_c = E_{normal} + F_v\,d} \quad (11)$$

Within the system, the friction force F_μ is equal to the driving force F. Due to energy conservation, energy input and cost should be equal to each other. Then, from Eqs. (**9**), (**10**) and (**11**)we have:

$$\boldsymbol{F_\mu\,d = E_{normal} + \eta\,k\,W\,\frac{1}{E^*}\,v^2\,d} \quad (12)$$

Then, the friction force is solved as

$$\boldsymbol{F_\mu = \frac{E_{normal}}{d} + \eta\,k\,W\,\frac{1}{E^*}\,v^2} \quad (13)$$

And the coefficient of friction (COF) is

$$\boldsymbol{COF = \frac{F_\mu}{W} = \mu_1 + \eta\,k\,\frac{1}{E^*}\,v^2} \quad (14)$$

Where $\mu_1 = \frac{E_{normal}}{W\,d}$ is the COF part due to normal hysteresis losses.

For μ_1 in Eq. (**14**), the sliding distance is the same as the pin's width d and the normal displacement of the pin is h_2, as shown in **Figure 74** (b). Then, the work done by the normal force in the normal direction is $E'_{normal} = W\,h_2$. The normal hysteresis loss energy E_{normal} is less than E'_{normal}, so that we have:

$$\boldsymbol{\mu_1 = \frac{E_{normal}}{W\,d} < \frac{E'_{normal}}{W\,d} = \frac{h_2}{d}} \quad (15)$$

For practical cases with a flat pin on disk, h_2 is typically much smaller than d ($h_2 << d$), and we have

$$\boldsymbol{COF \approx k \frac{\eta}{E^*} v^2} \quad (16)$$

In Eq. (**16**), k is determined by the surface roughness parameters, and the damper density, and viscoelastic terms η and E^* are temperature and time dependent parameters. Specifically, the temperature is the flash temperature T_f at the contact area and this flash temperature is related to the normal load W, sliding speed v and the body temperature T_b of the two contacting parts [180]. Then Eq. (**16**) can be rewritten as

$$\boldsymbol{COF \approx k \frac{\eta}{E^*}(W, v, T_b) v^2} \quad (17)$$

Eq. **(17)** shows that viscous and elastic parameters are important and complicated terms to determine the COF for sliding polymers. Thus, it is important to study these two properties of viscoelastic polymers.

7.2.2 Nanoindentation

Nanoindentation is a widely-used technique to measure the mechanical properties of materials, especially solid thin films. In nanoindentation experiments, a rigid probe is pressed into the sample to be measured, and the transducer records the in situ force and displacement responses. According to the Oliver-Pharr method, the elastic modulus can be obtained from the slope of the initial portion of the unloading curve and the hardness can be calculated by dividing the maximum indentation load with the contact area [181].

Using the Finite Element Method in conjunction with nanoindentation experiments, it is also feasible to extract elastic and plastic properties of the tested samples by fitting experimental loading-unloading curves [182]. However, these traditional methods typically assume that the materials behave as elastic-plastic materials and do not take into account any viscoelastic properties. One reason is that many solid materials such as metals and ceramics exhibit minimum viscoelastic behavior at room temperature. For polymer materials, viscoelasticity is very important. Oyen and Cook developed a series of linear analytical models for load-displacement relations of indentation experiments [169], as shown in **Figure 75**. In the model, P is resistance force of the probe, H is hardness, α_1, α_2 and α_3 are geometry terms; h is the displacement of the tip (h_e is elastic displacement and h_p is plastic displacement); η_Q is the quadratic viscosity, and E' is the reduced elastic modulus. The proposed viscous-elastic-plastic (VEP) model demonstrated its capability of characterizing elastic modulus, hardness and viscosity of polymers. Gayle and Cook presented an improved model consisting of two quadratic viscoelastic Kelvin-like elements and a quadratic plastic element in series [170].

7.3 Nanoindentation and mechanical model

7.3.1 Instrumentation

The present experiments were performed on a high temperature nanomechanical instrument (TI Premier, Bruker). The indenter was a diamond Berkovich probe with a tip radius of 300 nm. The stage is enclosed with insulator materials to ensure thermal stability. Inert gas (95% Ar, 5% Hydrogen) was introduced to the stage to prevent damage of the diamond probe due to oxidation at high temperatures. Before performing high temperature nanoindentation experiments, the sample was heated for about 15 minutes to make sure the sample reaches the desired temperature.

7.3.2 Load function

During nanoindentation, polymers exhibit time-dependent viscoelastic creep, especially at higher temperatures. Standard nanoindentation experiments are based on the assumption that the deformation during initial unloading is purely elastic, and the elastic modulus is calculated by curve fitting the slope of the initial unloading curve [181, 183]. To minimize creep effects, researchers have developed a trapezoidal loading function that holds the peak load for a length of time and then unloads [10, 181, 184, 185], as shown in **Figure 76**. By varying the peak holding time, the polymers showed stable indentation modulus after 2 seconds holding period at ambient temperature [10, 181] and at elevated temperature up to 200 °C. In this work, we applied the trapezoidal

loading function with 5 s peek holding time and 5 s for loading/unloading for all experiments, as shown in **Figure 76**, with t_1=5 s, t_2=10 s and t_3=15 s. Different peak loads were used and all the indentation depths were within 10% of the coatings' thickness, thus minimizing substrate effects.

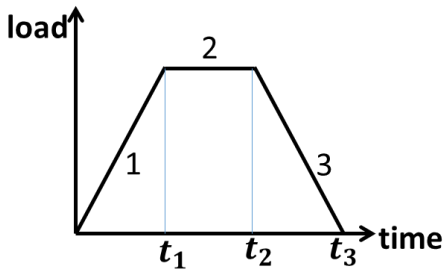

Figure 76 Nanoindentation trapezoidal loading curve.

7.3.3 Nanoindentation mechanical model

Figure 75 shows the quadratic Maxwell model that describes viscous-elastic-plastic polymers. The material properties such as hardness (resistance to plastic deformation), elastic modulus and viscous term inferred from fits of the model to the loading/unloading response were in agreement with measurements reported in the literature [170]. From the load function of **Figure 76**, during the loading part (0- t_1), the polymer has three deformation elements; these are plastic deformation, elastic deformation and viscous deformation, as shown in **Figure 75(b)**; while in the unloading part (t_2- t_3), the plastic deformation is suppressed and we assume there is only elastic and

viscous deformation, as shown in **Figure 75(c)** [169]. Based on this assumption, the unloading curve gives the displacement solution [169]:

$$\boldsymbol{h^{unload}(t) = \dot{P}_A^{\,1/2}\left[\frac{t_2^{3/2}-(2t_2-t)^{3/2}}{3/2(\alpha_3\eta_Q)^{1/2}} + \frac{(2t_2-t)^{1/2}-t_2^{1/2}}{(\alpha_2 E')^{1/2}}\right] + h(t_2)} \qquad (18)$$

$\dot{P}_A$ is unloading rate and $h(t_2)$ is the displacement at time t_2.

7.3.4 Coatings and high temperature nanoindentation

Two advanced polymeric coatings that exhibited excellent tribological performance for bearing applications from previous study [24, 45, 87, 88, 186] were selected for this work: an ATSP and a PEEK based coatings, which were the same coatings as described chapter 2 to 4 and were deposited on C182 chromium copper disks by EDS. The polymeric coatings have thicknesses of 30±5 μm and 35±5 μm, and a root-mean-square (Rq) roughness of 3.3 μm and 1.9 μm for ATSP and PEEK coatings, respectively. The glass transition temperature T_g for ATSP is 240-285°C [12] and T_g for the PEEK based coatings is significantly lower at about 140°C [61].

Nanoindentation experiments were performed at room temperature, 100°C, 180°C and 260°C, which are the same temperature conditions as the macro-scale ball-on-disk tribological experiments [88]. The same temperatures were used in order to correlate the tribological performance at the macro-scale with the micro/ nanomechanical properties obtained using indentation experiments of the two viscoelastic polymeric coatings. **Figure 77** shows the COF and wear results for both

ATSP and PEEK coatings under 5 N normal load and 0.139 m/s sliding speed at different temperatures. For the ATSP coatings, the COF decreased first with increasing temperature, from 0.21 at 25ºC to 0.11 at 180ºC, and then slightly increased to 0.12 at 260ºC. For the PEEK coatings, the COF monotonically decreased with increasing temperature, from 0.22 at 25ºC to 0.093 at 260ºC. In regards to wear resistance, the ATSP coating showed 'zero wear' (immeasurable) under all temperature conditions. For the PEEK coating, the wear rate decreased until the temperature reached 180ºC and then increased at the temperature of 260ºC [88]. The current study is to explain the complex tribological performance of the two coatings at elevated temperatures using two different properties (which are more readily obtained): (a) solid mechanical properties of hardness from nanoindenation measurements and (b) viscous and elastic terms of the viscoelastic material obtained through curve fitting using Eq. **(18)**.

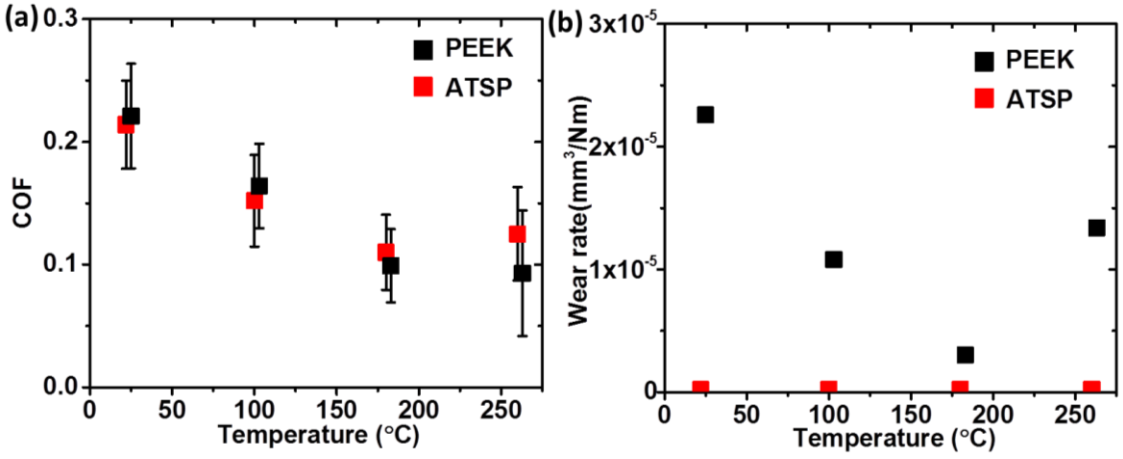

Figure 77 High temperature ball-on-disk tribological experiments for ATSP and PEEK coatings: (a) COF vs. temperature (b) wear rate vs. temperature [88].

7.4 Results

7.4.1 Hardness and elastic modulus results from nanoindentation experiments

Temperature effects on friction are usually explained by the mechanical characteristics of polymers, measured at the same temperature, and for some polymers, there is a correlation of the COF with the hardness and shear strength [3]. **Figure 78** shows the hardness of ATSP and PTFE coatings obtained from nanoindentation measurements. **Figure 79** and **Figure 80** show the load-displacement curves for ATSP and PEEK coatings, respectively. The indentation depth values are in the range from few hundred nanometers to 3 microns, which are within 10% of the thickness of the coatings. The hardness decreases as the temperature increases. Comparing the load-displacement curves of ATSP and PEEK in **Figure 79** and **Figure 80** (similar maximum indentation depth), ATSP coating shows shallower residual depth, which means ATSP coating has a higher elastic recovery. This is also found from the microscratch experiments for these two coatings .

With mechanical properties such as hardness, it is reasonable to conclude that the decreasing trend of the COF is due to the softening of the polymeric coating at elevated temperatures [60, 88]. The wear resistance of ATSP coating is much better than PEEK coating, and the reason could be from the higher hardness (shown in **Figure 78**) and higher recovery rate of ATSP coating. The above analysis of the COF is in agreement with the literature; however it is qualitative in nature. In this work, we propose a

quantitative model that predicts high temperature tribology properties from high temperature nanoindentation experiments.

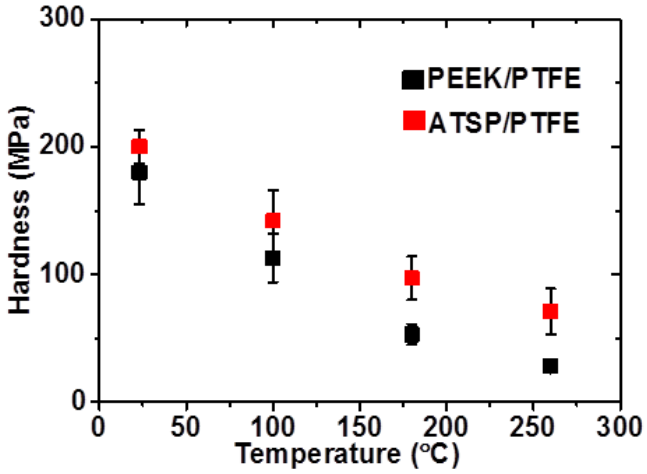

Figure 78 Nanoindentation experimental results of hardness for ATSP and PEEK coatings at different temperatures.

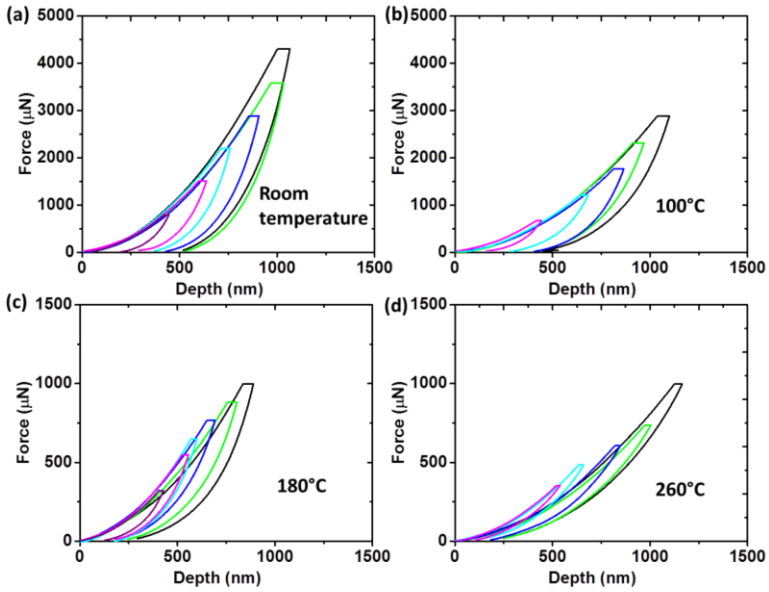

Figure 79 Nanoindentation load-displacement curves of ATSP coating at different temperatures, (a) room temperature, (b) 100°C, (c) 180°C and (d) 260°C.

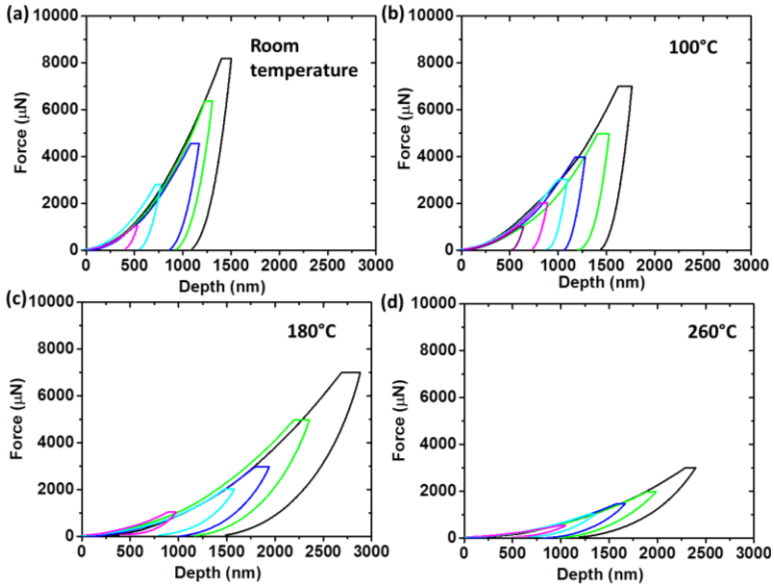

Figure 80 Nanoindentation load-displacement curves of PEEK coating at different temperatures, (a) room temperature, (b) 100°C, (c) 180°C and (d) 260°C.

7.4.2 Viscous and elastic properties

7.4.2.1 Viscous and elastic results

The plastic deformation of the unloading curve is suppressed by the trapezoidal loading function and the viscous term can be obtained by curve fitting Eq. **(18)** by the unloading data from the nanoindentation experiments. **Table 10** lists the curve fitting results from the nanoindentation unloading data of ATSP and PEEK coatings, as shown in **Figure 81**. The R-square value, in **Table 10**, is an indicator that evaluates the goodness of a model that fits the data, with a value of one being a perfect fit. All R-square values in **Table 10** are very close to one and the fitting curves shown in **Figure 81** are very well aligned with the unloading experimental data. This indicates that the quadratic Maxwell model solution of Eq. **(18)** is suitable for the coatings' viscoelastic models.

Table 10 Curve fitting viscous & elastic terms in Eq. **(18)** for ATSP and PEEK coatings.

Temperature (°C)	ATSP coating			PEEK coating		
	Viscous term $\alpha_3\eta_Q$ (Pa S2)	Elastic term $\alpha_2 E'$ (GPa)	R-square	Viscous term $\alpha_3\eta_Q$ (Pa S2)	Elastic term $\alpha_2 E'$ (GPa)	R-square
25	$3.05\pm0.03 \times10^{12}$	7.16±0.02	0.9996	$6.08\pm0.54 \times10^{14}$	45.1 ±0.2	0.9994
100	$1.40\pm0.01 \times10^{12}$	4.03 ±0.01	0.9997	$1.69\pm0.09 \times10^{14}$	47.7 ±0.3	0.9991
180	$5.25\pm0.05 \times10^{11}$	1.51 ±0.004	0.9995	$6.04\pm0.05 \times10^{11}$	2.04 ±0.01	0.9997
260	$7.44\pm0.41 \times10^{11}$	0.483±0.004	0.9997	$1.4\pm0.01 \times10^{12}$	1.37±0.002	0.9999

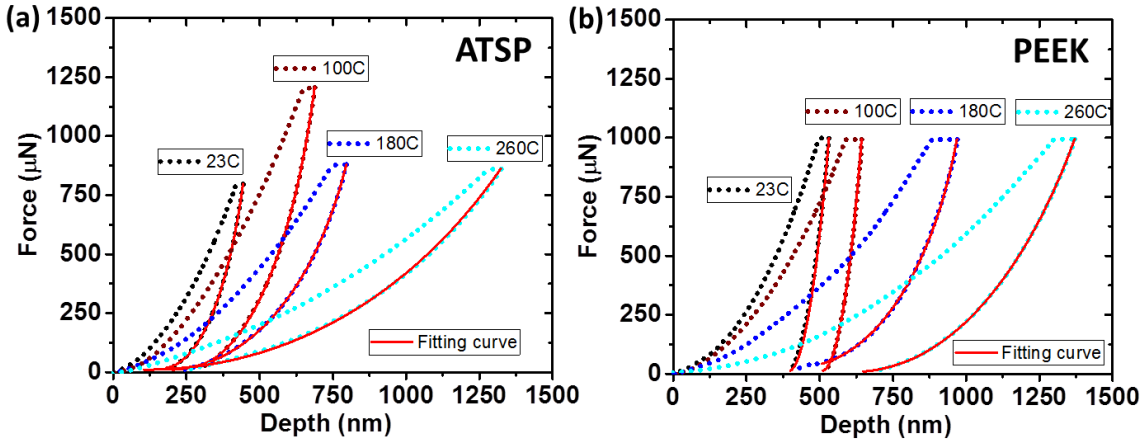

Figure 81 Curve fitting of nanoindentation unloading experimental data for (a) ATSP and (b) PEEK coatings.

To evaluate the robustness of the viscous and elastic terms obtained from the indentation experiments in **Figure 81**, the values listed in **Table 10** are substituted for different indentation load/depth experiments reported in **Figure 79** and **Figure 80** (that were not used to obtain the fitting coefficients). The fitting plots with the experimental data are shown in **Figure 82** and **Figure 83**, where all the fitting curves are aligned very well with the nanoindentation experimental data. This shows that the obtained viscous and elastic terms are characteristic of these polymeric materials, and describe their viscoelastic behavior well.

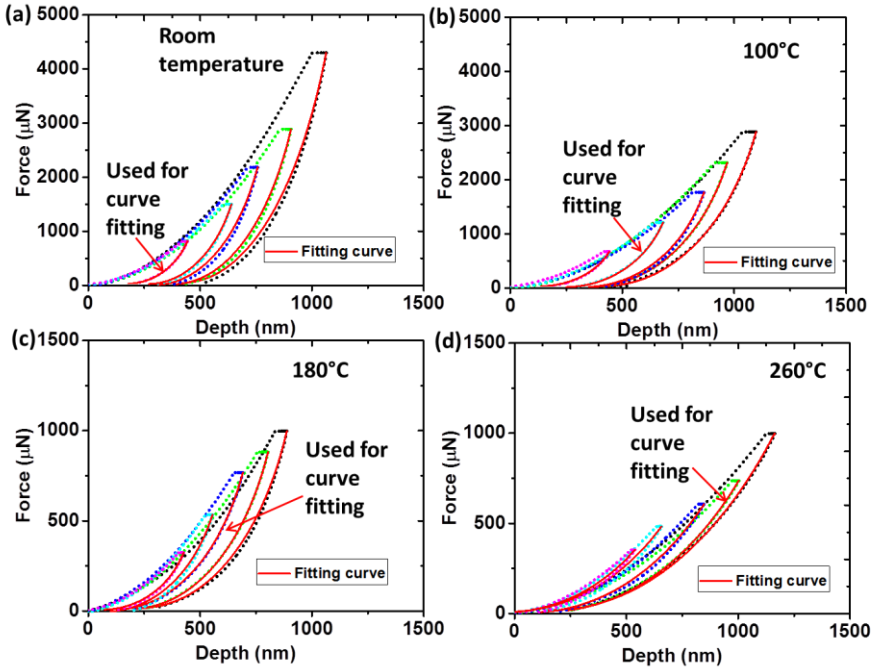

Figure 82 Load-unload nanoindentation curves compared to model predictions, Eq. **(18)** at different temperatures (ATSP coating): (a) room temperature, (b) 100°C, (c) 180°C and (d) 260°C.

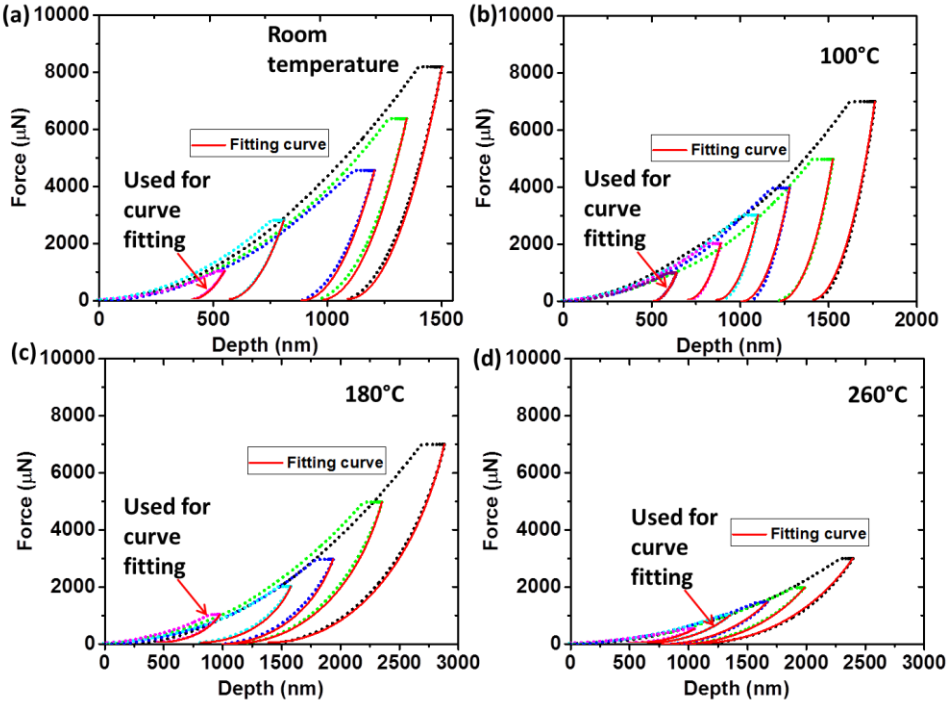

Figure 83 Load-unload nanoindentation curves compared to model predictions, Eq. **(18)** at different temperatures (PEEK coating): (a) room temperature, (b) 100°C, (c) 180°C and (d) 260°C.

Since the values in **Table 10** fit well the rest of the indention experiments, the average viscous and elastic values were acquired by performing the curve fitting for the other indentation data. The average data is shown in **Table 11** and the plots are shown in **Figure 84**. For all curve fittings, the R-square value is higher than 0.995. Note that for ATSP coating, in general, its viscosity and elastic modulus are decreasing uniformly; while for the PEEK coating, there is a significant drop from 100°C to 180°C, which is

due to the glass transition temperature of this coating (140°C). For both coatings, the viscosity increases at 260°C, compared to180°C.

Table 11 Average viscous and elastic terms of ATSP and PEEK coatings.

	ATSP coating		PEEK coating	
Temperature (°C)	Viscous term $\alpha_3\eta_Q$ (Pa S2)	Elastic term α_2E' (GPa)	Viscous term $\alpha_3\eta_Q$ (Pa S2)	Elastic term α_2E' (GPa)
25	$3.01\pm0.39\times10^{12}$	7.88±0.45	$5.11\pm1.34\times10^{14}$	39.65±4.21
100	$1.48\pm0.26\times10^{12}$	4.17±0.37	$3.33\pm0.98\times10^{14}$	54.52±8.88
180	$0.75\pm0.15\times10^{12}$	1.86±0.24	$0.86\pm0.16\times10^{12}$	2.06±0.16
260	$1.12\pm0.23\times10^{12}$	0.86±0.16	$1.14\pm0.38\times10^{12}$	1.27±0.08

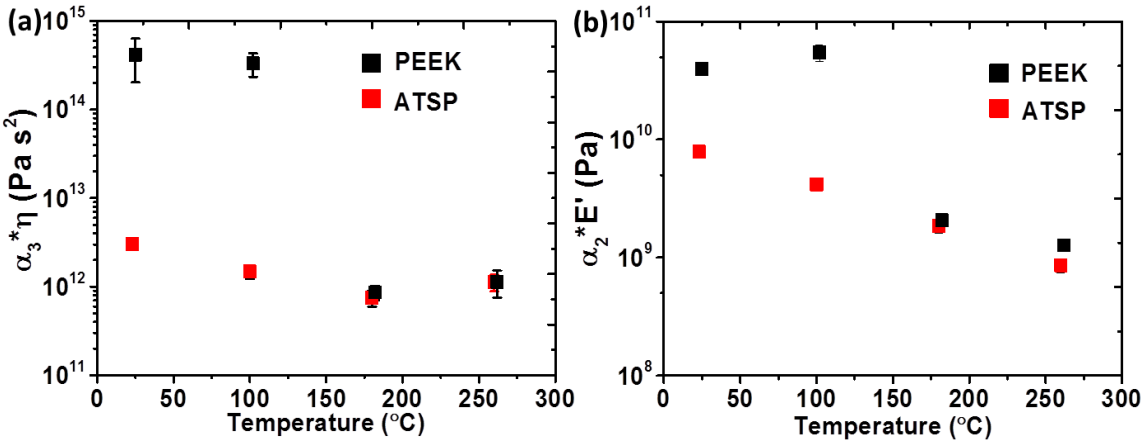

Figure 84 Average values of the viscous and elastic terms of ATSP and PEEK coatings, (a) results of the viscous term $\alpha_3\eta$, (b) results of the elastic modulus term $\alpha_2 E'$.

7.4.2.2 Relationship between COF and viscosity

From Eq. (**16**), we can predict the COF from the viscous and elastic terms of the viscoelastic polymeric materials. In Eq. (**16**), the velocity is fixed for all experiments at 0.139 m/s; while both elastic modulus and viscosity are dependent on the temperature. At higher temperatures, the polymers soften and the elastic modulus decreases. Thus, the viscosity of the polymers decreases, due to the decrease of the elastic modulus, and the COF may only change slightly. **Table 12** and **Figure 85** summarize the predicted COF and the measured COF at elevated temperatures. To explain the prediction process, take the room temperature and 100°C for ATSP, for example: Based on Eq. **(16)** and COF at room temperature, we have

$$k\,v^2 \approx \frac{COF_{room}}{\frac{\eta_{room}}{E^*_{room}}}$$

The *COF* at 100°C is:

$$COF_{100℃} \approx \frac{\eta_{100℃}}{E^*_{100℃}} \frac{COF_{room}}{\frac{\eta_{room}}{E^*_{room}}}$$

E^* is propotional with E', and substituting the elastic term ($\alpha_2 E'$) and viscous term ($\alpha_3 \eta_Q$) values from **Table 11**:

$$COF_{100℃} = \frac{\alpha_3 \eta_{100℃}}{\alpha_2 E_{100℃}} \frac{COF_{room}}{\frac{\alpha_3 \eta_{\mathrm{room}}}{\alpha_2 E_{room}}} = 0.19$$

Note that this prediction is not considering the normal load, velocity and flash temperature effects on the elastic modulus and viscosity as shown in Eq. **(17)**.

Table 12 Measured and predicted COF of ATSP and PEEK coatings.

Coating	ATSP coating				PEEK coating			
Temperature	25°C	100°C	180°C	260°C	25°C	100°C	180°C	260°C
Measured COF	0.21	0.15	0.11	0.1	0.22	0.16	0.1	0.09
Prediction COF	---	0.19	0.22	0.72	---	0.13	0.01	0.02

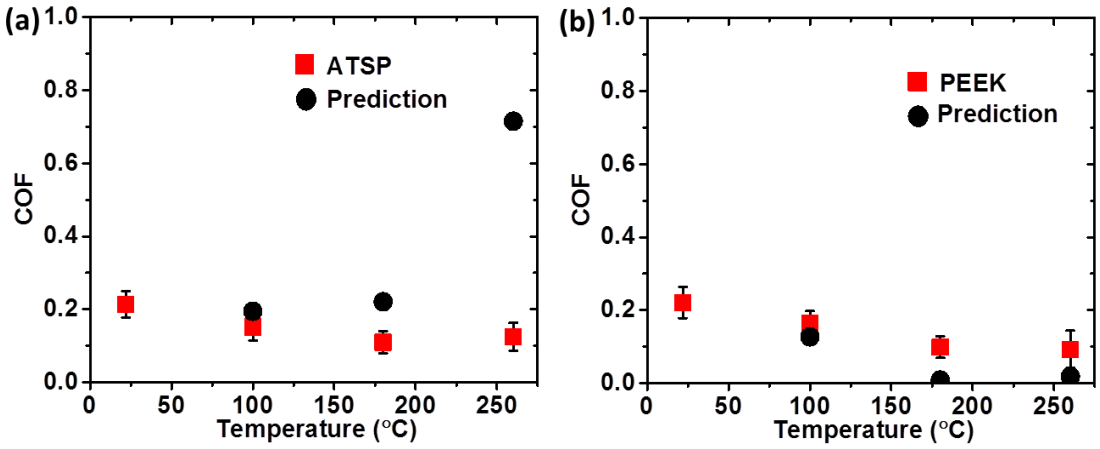

Figure 85 Measured and predicted COF for (a) ATSP and (b) PEEK coatings.

From **Table 12** and **Figure 85**, the COF prediction is very good for PEEK at all temperatures, whereas for ATSP it deviates substantially at the highest temperature of 260 °C. Note that when the tribological experiments were performed at temperatures lower than the glass transition temperature T_g, the predicted COF is excellent. When the temperature is equal or higher than T_g, the prediction is not appropriate any more. There are several reasons for this discrepancy: (a) the viscous and elastic properties are measured at the polymers' body temperature, not the flash temperature that directly affects the contact surface mechanical properties; (b) the velocity and load effects on the flash temperature are not considered; (c) the surface roughness may change when temperature changes and each experiment may have different surface roughness even for the same coating; (d) at higher temperatures, because of low elastic modulus, the pin could have large normal displacement, in which case the normal direction hysteresis loss

becomes larger; and (e) the viscoelastic performance is also time-dependent, so the values in Table 3 may have different time parameters compared with the experiments.

7.5 Conclusion

In this work a viscoelastic friction model given by Eq. (**16**) that relates the COF with viscous and elastic parameters of tribological viscoelastic coating materials is proposed. In addition, nanoindentation was carried out for viscoelastic ATSP and PEEK coatings at elevated temperatures. Mechanical properties such as hardness, viscosity and elastic modulus were obtained from the indentation data and by curve fitting of the nanoindentation's unloading curves. The following conclusions could be drawn:

1) The hardness decreases when temperature increases for both ATSP and PEEK coatings;
2) ATSP coating has higher hardness and higher indentation recovery rates, compared with PEEK coating at all temperatures, and thus ATSP exhibited better wear resistance;
3) The quadratic Maxwell model fits the nanoindenation model very well; the viscosity and elastic modulus obtained from curve fitting showed reasonable decreasing trends when temperature increased, and PEEK coating showed a phase change from 100°C to 180°C since its viscoelastic parameters had a significant drop; and

4) The limitations of the model were discussed and include additional complications due to contact pressure, speed and flash temperature effects.

8. CONCLUSION AND FUTURE WORK

To study the capability and limitation of the polymer coatings, the tribological performance of three different advanced coatings (PTFE-, PEEK- and ATSP based coatings) is studied by using the extreme conditions such as high temperature, cryogenic temperature, high load, high chamber pressure, and sand abrasion, and so on. To explain the friction performance for polymers at high temperature, a new friction model is also proposed in this dissertation.

8.1 Main conclusions

Because polymers have the advantages for tribological applications, extensive research has been done for the polymers, especially for polymers in bulk format. However, compared with bulk format, polymers in coating format have superior such as high load capability, low surface temperature and dimension accuracy due to the thin thickness. Based on the research done in this dissertation, several conclusions can be archived as bellow:

1) For dry sliding conditions at cryogenic and high temperatures, ATSP based coating exhibited “zero wear” as measured using wear scans under 5N normal force from temperature -160ºC up to 260ºC. SEM analysis showed the wear of the ATSP coatings at high temperature was mainly from burnishing of the asperity peeks of the coating and the failure mechanism of

the ATSP coating under this case was due to cracks formed by elastic fatigue. At cryogenic temperatures, SEM images showed the micro cracks on the peaks of the coatings, which was because of the extreme high contact pressure on these peaks.

2) In the case of PEEK based coatings of dry sliding conditions, in the high temperature range, with increasing of the operating temperature, the abrasive wear became less important and the adhesive wear became more predominant. At 180ºC, the steel ball contacting with PEEK based coating formed a transfer layer that helped decrease both COF and the wear rate of the coating. Different with high temperature range, PEEK coatings in cryogenic conditions showed 'zero wear', this was because the molecular in the polymer had less mobility and became tougher at low temperature.
3) In dry sliding condition, in general, the COF was decreasing when temperature increased from -160 ºC to 260 ºC; but for ATSP coating, its COF at -100°C showed a peak value. In cryogenic temperatures, ATSP coating had smaller COF compared with PEEK coating. While in high temperatures, the COF of the two coatings was similar. Both ATSP and PEEK based coatings showed that increasing the load/pressure could result in decreasing of the COF at all different temperatures. In addition, higher contact pressure at -160ºC for ATSP coating could facilitate the development of transfer layer.

4) In simulating of extreme working conditions of tilting pad bearing, all coatings improved the load capability compared to the substrate materials. All coatings showed preferable COF and excellent wear resistance. Especially, for life experiments (155.5 Km) of ATSP on C932, the coating showed an extremely low wear rate of $4.15x10^{-8}$ mm^3/Nm. SEM analysis demonstrated that due to adhesive wear, ATSP coating formed porous surfaces, which was good for improving the lubrication condition. PEEK and PTFE coatings' wear came from both abrasive and adhesive wear.
5) ATSP coating had superior wear resistance (wear rate of $6.1x10^{-7}$ mm^3/Nm) compared with bare substrate material C18200 Chromium copper in third-body sand abrasive wear condition; large sand particles could penetrate the coating, even though its superior tribological performance is still retained. In case of PEEK coating, the abrasive sand worked as a solid lubricant causing improvement of wear resistance. ATSP coatings' large scratch recovery rate of (57.3%) explained why ATSP coatings exhibited excellent tribological performance.
6) In simulating of drilling string working conditions of high temperature, high contact pressure and high environment pressure, ATSP coatings had tremendous COF reduction (58%) compared with bare tool steel at boundary lubrication condition of 75°C and at different temperatures up to 175°C. Because of the soft and deformable property of ATSP coating, the solid

particles from the drilling fluid were readily embedded on the soft ATSP coating and the embedded particles could sustain load and protect the coating, resulting excellent wear resistance of ATSP coating.

7) High temperature nanoindentation shows that the hardness, elastic modulus and viscosity decrease when temperature increases for both ATSP and PEEK coatings; ATSP coating has higher hardness and higher indentation recovery rates compared with PEEK coating at all temperatures, and thus ATSP exhibited better wear resistance.
8) By inserting the viscoelastic parameters achieved from high temperature nanoindentation, the viscoelastic friction model shows reasonable COF prediction for both ATSP and PEEK coatings at higher temperatures, but below the glass transition temperature.

8.2 Future work

From the tribological study at extreme temperatures in chapters 2 and 3, ATSP based coating exhibited “zero wear” with 5 N from -160°C to 260°C. However, there were cracks seen on the peaks of the coating at cryogenic temperatures due to very high contact pressures. To obtain a clear wear volume without cracks at cryogenic temperatures, lower contact stress and longer duration tests should be carried out on smoother ATSP coating samples. Instead of ball on disk configuration with high contact

stress, lower contact stress can be achieved by a curve pin on disk or flat pin on disk configuration. Thus, uniform wear rate can be achieved and be able to compare with other relevant materials.

ATSP coatings exhibited extremely low wear rates ($4.15x10^{-8}$ mm^3/Nm) in boundary lubrication regime, simulating tilting pad bearings in harsh conditions. This ATSP coating also showed excellent abrasive wear resistance and temperature capability up to 260°C. These pin on disk experimental configurations are more severe compared with industrial applications, however, it is very necessary to apply the ATSP based coating on an actual thrust bearing to understand their thermo-elasto-hydrodynamic performance simulating realistic downhole applications. Since ATSP has extremely low wear rate and can sustain high temperature, in the future, the ATSP surfaces may also be micro-textured for hydrodynamic bearings that has been proven to effectively improve film thickness and load capability, and also reduce the friction coefficient and pad temperature [187, 188]

Finally, with the quadratic Maxwell model, viscoelastic parameters acquired by high temperature nanoindentation showed reasonable values, which should also be cross validated by the viscoelastic parameters acquired through other methods such dynamic mechanical analysis. The proposed viscoelastic friction model showed reasonable COF prediction for both ATSP and PEEK coatings at higher temperatures but lower than T_g. To further investigate its effectiveness, systematic macro tribological experiments with lower sliding speed, lower contact stress and smother coating surface should be carried

out; thus can minimize the error due to the differences of surface morphology, gap between body temperature and contact flash temperature.

REFERENCES

[1] Zhang S. State-of-the-art of polymer tribology. Tribology International. 1998;31:49-60.

[2] Rymuza Z. Tribology of polymers. Archives of Civil and Mechanical Engineering. 2007;7:177-84.

[3] Myshkin N, Petrokovets M, Kovalev A. Tribology of polymers: adhesion, friction, wear, and mass-transfer. Tribology International. 2006;38:910-21.

[4] Nunez EE, Yeo SM, Polychronopoulou K, Polycarpou AA. Tribological study of high bearing blended polymer-based coatings for air-conditioning and refrigeration compressors. Surface and Coatings Technology. 2011;205:2994-3005.

[5] Demas NG, Polycarpou AA. Tribological performance of PTFE-based coatings for air-conditioning compressors. Surface and Coatings Technology. 2008;203:307-16.

[6] Dascalescu D, Polychronopoulou K, Polycarpou A. The significance of tribochemistry on the performance of PTFE-based coatings in CO_2 refrigerant environment. Surface and Coatings Technology. 2009;204:319-29.

[7] Cirino M, Pipes R, Friedrich K. The abrasive wear behaviour of continuous fibre polymer composites. Journal of Materials Science. 1987;22:2481-92.

[8] Cenna A, Allen S, Page N, Dastoor P. A polyethylene-reinforced polymer composite abraded by bulk solids. Wear. 2001;249:663-71.

[9] Startsev OV, Krotov AS, Startseva LT. Interlayer shear strength of polymer composite materials during long term climatic ageing. Polymer Degradation and Stability. 1999;63:183-6.

[10] Yeo SM, Polycarpou AA. Micromechanical properties of polymeric coatings. Tribology International. 2013;60:198-208.

[11] Zhang G, Liao H, Li H, Mateus C, Bordes J-M, Coddet C. On dry sliding friction and wear behaviour of PEEK and PEEK/SiC-composite coatings. Wear. 2006;260:594-600.

[12] Schroeder R, Torres F, Binder C, Klein A, de Mello J. Failure mode in sliding wear of PEEK based composites. Wear. 2013;301:717-26.

[13] Barletta M. Dry sliding wear response of some industrial powder coatings. Tribology International. 2011;44:1236-50.

[14] Demas NG, Zhang J, Polycarpou AA, Economy J. Tribological characterization of aromatic thermosetting copolyester–PTFE blends in air conditioning compressor environment. Tribology Letters. 2008;29:253-8.

[15] Bahadur S. The development of transfer layers and their role in polymer tribology. Wear. 2000;245:92-9.

[16] Zhai W, Shi X, Yang K, Huang Y, Zhou L, Lu W. Mechanical and tribological behaviors of the tribo-layer with nanocrystalline structure during sliding contact: Experiments and model assessment. Composites Part B: Engineering. 2017;108:354-63.

[17] Nunez EE, Polycarpou AA. The effect of surface roughness on the transfer of polymer films under unlubricated testing conditions. Wear. 2015;326:74-83.

[18] Yeo SM, Polycarpou AA. Fretting experiments of advanced polymeric coatings and the effect of transfer films on their tribological behavior. Tribology International. 2014;79:16-25.

[19] Holmberg K, Mathews A. Coatings tribology: a concept, critical aspects and future directions. Thin Solid Films. 1994;253:173-8.

[20] Zhang H, Zhou L-y, Eger C, Zhang Z. Abrasive wear of transparent polymer coatings: considered in terms of morphology and surface modification of nanoparticles. Composites Science and Technology. 2013;88:151-7.

[21] Ebert D, Bhushan B. Transparent, superhydrophobic, and wear-resistant coatings on glass and polymer substrates using SiO_2, ZnO, and ITO nanoparticles. Langmuir. 2012;28:11391-9.

[22] Zhang J, Demas NG, Polycarpou AA, Economy J. A new family of low wear, low coefficient of friction polymer blend based on polytetrafluoroethylene and an aromatic thermosetting polyester. Polymers for Advanced Technologies. 2008;19:1105-12.

[23] Cannaday ML, Polycarpou AA. Tribology of unfilled and filled polymeric surfaces in refrigerant environment for compressor applications. Tribology Letters. 2005;19:249-62.

[24] Zhang J, Polycarpou AA, Economy J. An improved tribological polymer-coating system for metal surfaces. Tribology Letters. 2010;38:355-65.

[25] Burris DL, Sawyer WG. A low friction and ultra low wear rate PEEK/PTFE composite. Wear. 2006;261:410-8.

[26] Burris DL, Sawyer WG. Tribological behavior of PEEK components with compositionally graded PEEK/PTFE surfaces. Wear. 2007;262:220-4.

[27] McElwain SE, Blanchet TA, Schadler LS, Sawyer WG. Effect of particle size on the wear resistance of alumina-filled PTFE micro-and nanocomposites. Tribology Transactions. 2008;51:247-53.

[28] Burris DL, Sawyer WG. Improved wear resistance in alumina-PTFE nanocomposites with irregular shaped nanoparticles. Wear. 2006;260:915-8.

[29] Golchin A, Friedrich K, Noll A, Prakash B. Influence of counter surface topography on the tribological behavior of carbon-filled PPS composites in water. Tribology International. 2015;88:209-17.

[30] Almajid A, Friedrich K, Floeck J, Burkhart T. Surface damage characteristics and specific wear rates of a new continuous carbon fiber (CF)/polyetheretherketone (PEEK) composite under sliding and rolling contact conditions. Applied Composite Materials. 2011;18:211-30.

[31] Sharma S, Padenko E, Bijwe J, Wetzel B, Friedrich K. Erosive and sliding wear of polybenzimidazole at elevated temperatures. Journal of Materials Science. 2016;51:262-70.

[32] Yeo SM, Polycarpou AA. Tribological performance of PTFE-and PEEK-based coatings under oil-less compressor conditions. Wear. 2012;296:638-47.

[33] Zhai W, Lu W, Zhang P, Zhou M, Liu X, Zhou L. Microstructure, mechanical and tribological properties of nickel-aluminium bronze alloys developed via gas-atomization and spark plasma sintering. Materials Science and Engineering: A. 2017;707:325-36.

[34] Zhai W, Shi X, Yang K, Huang Y, Zhou L, Lu W. Tribological Behaviors of Ni3Al Intermetallics with MoO_3 Multilayer Ribbon Crystal Prepared by Spark Plasma Sintering. Acta Metallurgica Sinica (English Letters). 2017;30:576-84.

[35] Zhou M, Lu W, Liu X, Zhai W, Zhang P, Zhang G. Fretting wear properties of plasma-sprayed Ti_3SiC_2 coatings with oxidative crack-healing feature. Tribology International. 2018;118:196-207.

[36] Trezona R, Pickles M, Hutchings I. A full factorial investigation of the erosion durability of automotive clearcoats. Tribology International. 2000;33:559-71.

[37] Masuko M, Ikushima F, Aoki S, Suzuki A. Preliminary study on the tribology of an organic-molecule-coated touch panel display surface. Tribology International. 2013;65:314-25.

[38] Kessman A, Huckaby D, Snyder C, Kukureka S, Cairns D. Tribology of water and oil repellent sol–gel coatings for optical applications. Wear. 2009;267:614-8.

[39] Zhang H, Tang L, Zhou L, Eger C, Zhang Z. Comparative study on the optical, surface mechanical and wear resistant properties of transparent coatings filled with pyrogenic and colloidal silica nanoparticles. Composites Science and Technology. 2011;71:471-9.

[40] Khanjani J, Pazokifard S, Zohuriaan-Mehr MJ. Improving dirt pickup resistance in waterborne coatings using latex blends of acrylic/PDMS polymers. Progress in Organic Coatings. 2017;102:151-66.

[41] Corcione CE, De Simone N, Santarelli ML, Frigione M. Protective properties and durability characteristics of experimental and commercial organic coatings for the preservation of porous stone. Progress in Organic Coatings. 2017;103:193-203.

[42] Belhadjamor M, El Mansori M, Belghith S, Mezlini S. Anti-fingerprint properties of engineering surfaces: a review. Surface Engineering. 2016:1-32.

[43] Liu H, Leng Y, Tang J, Wang S, Xie D, Sun H, et al. Tribological performance of ultra-high-molecular-weight polyethylene sliding against DLC-coated and nitrogen ion implanted CoCrMo alloy measured in a hip joint simulator. Surface and Coatings Technology. 2012;206:4907-14.

[44] Song J, Liu Y, Liao Z, Wang S, Tyagi R, Liu W. Wear studies on ZrO_2-filled PEEK as coating bearing materials for artificial cervical discs of Ti6Al4V. Materials Science and Engineering: C. 2016;69:985-94.

[45] Akram MW, Meyer JL, Polycarpou AA. Tribological interactions of advanced polymeric coatings with polyalkylene glycol lubricant and r1234yf refrigerant. Tribology International. 2016;97:200-11.

[46] Zhang D, Ho JK, Dong G, Zhang H, Hua M. Tribological properties of Tin-based Babbitt bearing alloy with polyurethane coating under dry and starved lubrication conditions. Tribology International. 2015;90:22-31.

[47] Heshmat H, Hryniewicz P, Walton Ii JF, Willis JP, Jahanmir S, DellaCorte C. Low-friction wear-resistant coatings for high-temperature foil bearings. Tribology International. 2006;38:1059-75.

[48] Gee M, Nunn J, Muniz-Piniella A, Orkney L. Micro-tribology experiments on engineering coatings. Wear. 2011;271:2673-80.

[49] Al-Kawaz A, Rubin A, Badi N, Blanck C, Jacomine L, Janowska I, et al. Tribological and mechanical investigation of acrylic-based nanocomposite coatings reinforced with PMMA-grafted-MWCNT. Materials Chemistry and Physics. 2016;175:206-14.

[50] Lin L-Y, Kim D-E. Tribological properties of polymer/silica composite coatings for microsystems applications. Tribology International. 2011;44:1926-31.

[51] Rudermann Y, Iost A, Bigerelle M. Scratch tests to contribute designing performance maps of multilayer polymeric coatings. Tribology International. 2011;44:585-91.

[52] Shi S-C, Wu J-Y, Huang T-F, Peng Y-Q. Improving the tribological performance of biopolymer coating with MoS_2 additive. Surface and Coatings Technology. 2016;303:250-5.

[53] Yamane M, Stolarski TA, Tobe S. Wear and friction mechanism of PTFE reservoirs embedded into thermal sprayed metallic coatings. Wear. 2007;263:1364-74.

[54] Frich D, Goranov K, Schneggenburger L, Economy J. Novel high-temperature aromatic copolyester thermosets: synthesis, characterization, and physical properties. Macromolecules. 1996;29:7734-9.

[55] Huang Y, Economy J. Wear properties of UHMWPE/aromatic thermosetting copolyester blends in unlubricated sliding. Wear. 2007;262:943-8.

[56] Vandevier JG, Ben Application of Electrical Submersible Pumping Systems in High Temperature Geothermal Environments. Geothermal Resource Council Transactions. 2009;33:649–52.

[57] Economy J, Polycarpou A, Meyer J. Polymer coating system for improved tribological performance. United States Patent, US9534138; 2017.

[58] Ebnesajjad S, Morgan RA. 4 - Manufacturing and Properties of Low-Molecular-Weight Fluoropolymer Additives. Fluoropolymer Additives. Oxford: William Andrew Publishing; 2012. p. 37-52.

[59] Fusaro RL. Tribological properties of polymer films and solid bodies in a vacuum environment. Annual meeting of the American Society of Lubrication Engineers, Anaheim, CA, USA, 1987.

[60] Samad MA, Sinha SK. Dry sliding and boundary lubrication performance of a UHMWPE/CNTs nanocomposite coating on steel substrates at elevated temperatures. Wear. 2011;270:395-402.

[61] Koike H, Kida K, Santos EC, Rozwadowska J, Kashima Y, Kanemasu K. Self-lubrication of PEEK polymer bearings in rolling contact fatigue under radial loads. Tribology International. 2012;49:30-8.

[62] Rae P, Dattelbaum D. The properties of poly (tetrafluoroethylene)(PTFE) in compression. Polymer. 2004;45:7615-25.

[63] D'Amore A, Pompo A, Nicolais L. Viscoelastic effects in poly (ether ether ketone)(PEEK) and PEEK-based composites. Composites Science and Technology. 1991;41:303-25.

[64] Lancaster J. Accelerated wear testing of PTFE composite bearing materials. Tribology International. 1979;12:65-75.

[65] Barletta M, Lusvarghi L, Mantini FP, Rubino G. Epoxy-based thermosetting powder coatings: surface appearance, scratch adhesion and wear resistance. Surface and Coatings Technology. 2007;201:7479-504.

[66] Pelletier H, Mendibide C, Riche A. Mechanical characterization of polymeric films using depth-sensing instrument: Correlation between viscoelastic-plastic properties and scratch resistance. Progress in Organic Coatings. 2008;62:162-78.

[67] Theiler G, Hübner W, Gradt T, Klein P. Friction and wear of carbon fibre filled polymer composites at room and low temperatures. Materialwissenschaft und Werkstofftechnik. 2004;35:683-9.

[68] Bozet J-L. Modelling of friction and wear for designing cryogenic valves. Tribology International. 2001;34:207-15.

[69] McCook N, Burris D, Dickrell P, Sawyer W. Cryogenic friction behavior of PTFE based solid lubricant composites. Tribology Letters. 2005;20:109-13.

[70] Burris DL. Investigation of the tribological behavior of polytetrafluoroethylene at cryogenic temperatures. Tribology Transactions. 2008;51:92-100.

[71] Ostrovskaya YL, Strel'nitskij V, Kuleba V, Gamulya G. Friction and wear behaviour of hard and superhard coatings at cryogenic temperatures. Tribology International. 2001;34:255-63.

[72] Theiler G, Gradt T. Polymer composites for tribological applications in hydrogen environment. Proc 2 International Conference on Hydrogen Safety, San Sebastian, Spain, 2007.

[73] Wang Q, Zheng F, Wang T. Tribological properties of polymers PI, PTFE and PEEK at cryogenic temperature in vacuum. Cryogenics. 2016;75:19-25.

[74] Veenstra T, Venhorst G, Burger J, Holland H, ter Brake H, Sirbi A, et al. Development of a stainless steel check valve for cryogenic applications. Cryogenics. 2007;47:121-6.

[75] Hübner W, Gradt T, Schneider T, Börner H. Tribological behaviour of materials at cryogenic temperatures. Wear. 1998;216:150-9.

[76] Gradt T, Börner H, Schneider T. Low temperature tribometers and the behaviour of ADLC coatings in cryogenic environment. Tribology International. 2001;34:225-30.

[77] Theiler G, Hübner W, Gradt T, Klein P, Friedrich K. Friction and wear of PTFE composites at cryogenic temperatures. Tribology International. 2002;35:449-58.

[78] Gradt T, Schneider T, Hübner W, Börner H. Friction and wear at low temperatures. International Journal of Hydrogen Energy. 1998;23:397-403.

[79] Ostrovskaya YL, Yukhno T, Gamulya G, Vvedenskij YV, Kuleba V. Low temperature tribology at the B. Verkin Institute for Low Temperature Physics & Engineering (historical review). Tribology International. 2001;34:265-76.

[80] Gamulya G, Lebedeva I, Vvedensky YV, Yukhno T. Secondary structure formation and wear mechanisms for solid lubricant coatings under friction in vacuum. Wear. 1994;171:143-8.

[81] Gamulya G, Ostrovskaya YL, Ostapenko I, Presnyakova G, Strel'Nitskij V. Friction behaviour and wear resistance of diamond-like carbon films under cryogenic temperatures. Diamond and Related Materials. 1994;3:1381-4.

[82] Yukhno T, Vvedensky YV, Sentyurikhina L. Low temperature investigations on frictional behaviour and wear resistance of solid lubricant coatings. Tribology International. 2001;34:293-8.

[83] Gamulya G, Kopteva T, Lebedeva I, Sentyurikhina L. Effect of low temperatures on the wear mechanism of solid lubricant coatings in vacuum. Wear. 1993;160:351-9.

[84] McLaren K, Tabor D. Visco-elastic properties and the friction of solids: friction of polymers: influence of speed and temperature. Nature. 1963;197:856-8.

[85] Babuska T, Pitenis A, Jones M, Nation B, Sawyer W, Argibay N. Temperature-dependent friction and wear behavior of PTFE and MoS_2. Tribology Letters. 2016;63:1-7.

[86] Barry PR, Chiu PY, Perry SS, Sawyer WG, Sinnott SB, Phillpot SR. Effect of temperature on the friction and wear of PTFE by atomic-level simulation. Tribology Letters. 2015;58:50.

[87] Lan P, Meyer JL, Vaezian B, Polycarpou AA. Advanced polymeric coatings for tilting pad bearings with application in the oil and gas industry. Wear. 2016;354:10-20.

[88] Lan P, Meyer JL, Economy J, Polycarpou AA. Unlubricated Tribological Performance of Aromatic Thermosetting Polyester (ATSP) Coatings Under Different Temperature Conditions. Tribology Letters. 2016;61:1-14.

[89] Fu S-Y. Cryogenic Properties of Polymer Materials. Polymers at Cryogenic Temperatures: Springer; 2013. p. 9-39.

[90] Frich D, Hall A, Economy J. Nature of adhesive bonding via interchain transesterification reactions (ITR). Macromolecular Chemistry and Physics. 1998;199:913-21.

[91] Clarke T, Street G. Ultrathin perfluoropolyether films—influence of anchoring and mobility of polymers on the tribological properties. Journal of Tribology. 1996;118:663.

[92] Chang L, Zhang Z, Ye L, Friedrich K. Tribological properties of epoxy nanocomposites: III. Characteristics of Transfer Films. Wear. 2007;262:699-706.

[93] Voort JV, Bahadur S. The growth and bonding of transfer film and the role of CuS and PTFE in the tribological behavior of PEEK. Wear. 1995;181:212-21.

[94] Chang L, Zhang Z, Ye L, Friedrich K. Tribological properties of epoxy nanocomposites. Wear. 2007;5:699-706.

[95] Amamou A, Chouchane M. Nonlinear stability analysis of long hydrodynamic journal bearings using numerical continuation. Mechanism and Machine Theory. 2014;72:17-24.

[96] Wang Q. Seizure failure of journal-bearing conformal contacts. Wear. 1997;210:8-16.

[97] Simmons J, Knox R, Moss W. The development of PTFE (polytetrafluoroethylene)-faced hydrodynamic thrust bearings for hydrogenerator application in the United Kingdom. Proceedings of the Institution of Mechanical Engineers, Part J: Journal of Engineering Tribology. 1998;212:345-52.

[98] Fillon M, Glavatskih S. PTFE-faced centre pivot thrust pad bearings: Factors affecting TEHD performance. Tribology International. 2008;41:1219-25.

[99] Finston L. Monitoring improvements extend electrical submersible pump life. Journal of Petroleum Technology. 2001;53:30.

[100] Denney D. Analysis and Prediction of Electrical-Submersible-Pump Failures. Journal of Petroleum Technology. 2000; 46-47.

[101] Lea J, Wells M, Bearden J, Wilson L, Shepler R. Electrical submersible pumps: On and offshore problems and solutions. International Petroleum Conference and Exhibition of Mexico: Society of Petroleum Engineers; 1994.

[102] Takacs G. Chapter 7 - Monitoring and Troubleshooting. Electrical Submersible Pumps Manual. Boston: Gulf Professional Publishing; 2009. p. 309-41.

[103] Mahieux C. Experimental characterization of the influence of coating materials on the hydrodynamic behavior of thrust bearings: a comparison of Babbitt, PTFE, and PFA. Journal of Tribology. 2005;127:568-74.

[104] Dwyer-Joyce R, Harper P, Pritchard J, Drinkwater B. Oil film measurment in polytetrafluoroethylene-faced thurst pad bearings for hydrogenerator applications. Proceedings of the Institution of Mechanical Engineers, Part A: Journal of Power and Energy. 2006;220:619-28.

[105] Glavatskih SB. Evaluating thermal performance of a PTFE-faced tilting pad thrust bearing. Journal of Tribology. 2003;125:319-24.

[106] McCarthy D, Glavatskih S, Sherrington I. Oil-film thickness and temperature measurements in PTFE and babbitt faced tilting-pad thrust bearings. Proceedings of the Institution of Mechanical Engineers, Part J: Journal of Engineering Tribology. 2005;219:179-85.

[107] Markin D, McCarthy D, Glavatskih S. A FEM approach to simulation of tilting-pad thrust bearing assemblies. Tribology International. 2003;36:807-14.

[108] Ettles C, Knox R, Ferguson J, Horner D. Test results for PTFE-faced thrust pads, with direct comparison against Babbitt-faced pads and correlation with analysis. Journal of Tribology. 2003;125:814-23.

[109] McCarthy D, Glavatskih S. Assessment of polymer composites for hydrodynamic journal‐bearing applications. Lubrication Science. 2009;21:331-41.

[110] Pratt GC. Bearing Materials: Plain Bearings A2 - Buschow, K.H. Jürgen. In: Cahn RW, Flemings MC, Ilschner B, Kramer EJ, Mahajan S, Veyssière P, editors. Encyclopedia of Materials: Science and Technology (Second Edition). Oxford: Elsevier; 2001. p. 488-96.

[111] Xu H, Feng Z, Chen J, Zhou H. Tribological behavior of the carbon fiber reinforced polyphenylene sulfide (PPS) composite coating under dry sliding and water lubrication. Materials Science and Engineering: A. 2006;416:66-73.

[112] Bouyer J, Fillon M. Experimental measurement of the friction torque on hydrodynamic plain journal bearings during start-up. Tribology International. 2011;44:772-81.

[113] Akram MW, Polychronopoulou K, Polycarpou AA. Lubricity of environmentally friendly HFO-1234yf refrigerant. Tribology International. 2013;57:92-100.

[114] Kingsbury I. Equalizing Thrust Bearings, Comprehensive Design Guide. http://www.kingsbury.com/pdf/catalog-eqh.pdf. Accessed on 07/30/2017.

[115] Nobili L, Magagnin L. DLC coatings for hydraulic applications. Transactions of Nonferrous Metals Society of China. 2009;19:810-3.

[116] Ge F, Zhu P, Meng F, Xue Q, Huang F. Achieving very low wear rates in binary transition-metal nitrides: The case of magnetron sputtered dense and highly oriented VN coatings. Surface and Coatings Technology. 2014;248:81-90.

[117] Shipway P, Ngao N. Microscale abrasive wear of polymeric materials. Wear. 2003;255:742-50.

[118] Thomsen K, Klit P. A study on compliant layers and its influence on dynamic response of a hydrodynamic journal bearing. Tribology International. 2011;44:1872-7.

[119] Simmons GF, Varela AC, Santos IF, Glavatskih S. Dynamic characteristics of polymer faced tilting pad journal bearings. Tribology International. 2014;74:20-7.

[120] Wodtke M, Wasilczuk M. Evaluation of apparent Young′ s modulus of the composite polymer layers used as sliding surfaces in hydrodynamic thrust bearings. Tribology International. 2016;97:244-52.

[121] Pratt G. Bearing materials: plain bearings. Encyclopedia of materials: Science and Technology. 2008:488-96.

[122] Unal H, Sen U, Mimaroglu A. Abrasive wear behaviour of polymeric materials. Materials & Design. 2005;26:705-10.

[123] Harsha A. An investigation on low stress abrasive wear characteristics of high performance engineering thermoplastic polymers. Wear. 2011;271:942-51.

[124] Rutherford K, Trezona R, Ramamurthy A, Hutchings I. The abrasive and erosive wear of polymeric paint films. Wear. 1997;203:325-34.

[125] Trezona R, Hutchings I. Three-body abrasive wear testing of soft materials. Wear. 1999;233:209-21.

[126] Bello J, Wood R. Micro-abrasion of filled and unfilled polyamide 11 coatings. Wear. 2005;258:294-302.

[127] Demas NG, Polycarpou AA. Ultra high pressure tribometer for testing CO_2 refrigerant at chamber pressures up to 2000 psi to simulate compressor conditions. Tribology Transactions. 2006;49:291-6.

[128] Penberthy Jr W, Shaughnessy C. Sand Control, 1, 11-17. Richardson, Texas: Monograph Series, Society of Petroleum Engineers; 1992.

[129] Zum Gahr K-H. Wear by hard particles. Tribology International. 1998;31:587-96.

[130] Schamp JH, Estes BL, Keller SR. Torque reduction techniques in ERD Wells. IADC/SPE Drilling Conference: Society of Petroleum Engineers; 2006.

[131] Gupta VP, Sanford SR, Mathis RS, DiPippo EK, Egan MJ. Case history of a challenging thin oil column extended reach drilling (ERD) development at Sakhalin. SPE/IADC Drilling Conference: Society of Petroleum Engineers; 2013.

[132] McCormick JE, Evans CD, Le J, Chiu T. The practice and evolution of torque and drag reduction: theory and field results. International Petroleum Technology Conference: International Petroleum Technology Conference; 2011.

[133] Cameron C. Drilling fluids design and management for extended reach drilling. SPE/IADC Middle East Drilling Technology Conference: Society of Petroleum Engineers; 2001.

[134] Briscoe B, Cann P, Delfino A, Maitland G. Lubrication With Water-Based Clay Suspensions. World Tribology Congress III: American Society of Mechanical Engineers; 2005. p. 529-30.

[135] Zhang HJ, Ke M, Panamarathupalayam B, Patel A. Lubricants and Drag Reducers for Oilfield Applications-Chemistry, Performance, and Environmental Impact. SPE International Symposium on Oilfield Chemistry: Society of Petroleum Engineers; 2013.

[136] Aarrestad TV. Torque and drag-two factors in extended-reach drilling. Journal of Petroleum Technology. 1994;46:800-3.

[137] Livescu S, Craig SH, Watkins T. Challenging the Industry"s Understanding of the Mechanical Friction Reduction for Coiled Tubing Operations. SPE Annual Technical Conference and Exhibition: Society of Petroleum Engineers; 2014.

[138] Apaleke AS, Al-Majed AA, Hossain ME. Drilling fluid: State of the art and future trend. North Africa Technical Conference and Exhibition: Society of Petroleum Engineers; 2012.

[139] Hossain ME, Al-Majed AA. Fundamentals of sustainable drilling engineering: John Wiley & Sons, Inc., Hoboken, NJ, USA.; 2015.

[140] Holand J, Kvamme SA, Omland TH, Saasen A, Taugbol K, Jamth J. Lubricant enabled completion of ERD well. SPE/IADC Drilling Conference: Society of Petroleum Engineers; 2007.

[141] Livescu S, Craig S, Watkins T. Smaller Coiled Tubing Diameter Achievable by the Use of Lubricants. International Petroleum Technology Conference: International Petroleum Technology Conference; 2014.

[142] Slater K, Amer A. New Automated Lubricity Tester Evaluates Fluid Additives, Systems and Their Application. Offshore Mediterranean Conference and Exhibition: Offshore Mediterranean Conference; 2013.

[143] Xiao H, Liu S, Chen Y, Han D, Wang D. Impacts of polypropylene glycol (PPG) additive and pH on tribological properties of water-based drilling mud for steel-steel contact. Tribology International. 2017;110:318-25.

[144] Danks D, Jones D, Chowdhary H, Naaykens B. Extreme load scratch testing. Wear. 2015;332:1200-5.

[145] Bangaru N-RV, Ozekcin A, Jin H-W, Biediger EAO, Bailey JR, Gupta V, et al. Ultra-low friction coatings for drill stem assemblies. United States Patent; US8220563 ; 2012.

[146] Guo Y, Meng T, Wang D, Tan H, He R. Experimental research on the corrosion of X series pipeline steels under alternating current interference. Engineering Failure Analysis. 2017;78:87-98.

[147] Guo Y-B, Liu C, Wang D-G, Liu S-H. Effects of alternating current interference on corrosion of X60 pipeline steel. Petroleum Science. 2015;12:316-24.

[148] Ning J, Zheng Y, Brown B, Young D, Nesic S. The Role of Pyrite in Localized H_2S Corrosion of Mild Steel. CORROSION 2017: NACE International Conference; 2017.

[149] Zheng Y, Ning J, Brown B, Nešić S. Advancement in Predictive Modeling of Mild Steel Corrosion in CO_2-and H_2S-Containing Environments. Corrosion. 2016;72:679-91.

[150] Lan P, Polychronopoulou K, Zhang Y, Polycarpou AA. Three-body abrasive wear by (silica) sand of advanced polymeric coatings for tilting pad bearings. Wear. 2017;382–383:40-50.

[151] Close F, McCavitt RD, Smith B. Deepwater Gulf of Mexico development challenges overview. SPE North Africa Technical Conference & Exhibition: Society of Petroleum Engineers; 2008.

[152] Kaarstad E, Aadnoy BS, Fjelde T. A study of temperature dependent friction in wellbore fluids. SPE/IADC Drilling Conference and Exhibition: Society of Petroleum Engineers; 2009.

[153] Xiao H, Liu S, Guo Y, Wang D, Chen Y. Effects of Microscale Particles as Antiwear Additives in Water-Based Slurries with Abrasives. Tribology Transactions. 2016;59:323-9.

[154] Zhao S-y, Yan J-n, Shu Y, Zhang H-x. Rheological properties of oil-based drilling fluids at high temperature and high pressure. Journal of Central South University of Technology. 2008;15:457-61.

[155] Zhu X, Liu S, Tong H, Huang X, Li J. Experimental and numerical study of drill pipe erosion wear in gas drilling. Engineering Failure Analysis. 2012;26:370-80.

[156] Zhu H, Lin Y, Zeng D, Zhou Y, Xie J, Wu Y. Numerical analysis of flow erosion on drill pipe in gas drilling. Engineering Failure Analysis. 2012;22:83-91.

[157] Chang W-R, Etsion I, Bogy D. Static friction coefficient model for metallic rough surfaces. Journal of Tribology. 1988;110:57-63.

[158] Kogut L, Etsion I. A static friction model for elastic-plastic contacting rough surfaces. Journal of Tribology. 2004;126:34-40.

[159] Vakis AI, Eriten M, Polycarpou AA. Modeling bearing and shear forces in molecularly thin lubricants. Tribology Letters. 2011;41:573-86.

[160] Zhang Y, Polycarpou AA. A single asperity sliding contact model for molecularly thin lubricant. Microsystem Technologies. 2016:1-9.

[161] Greenwood J, Tabor D. The friction of hard sliders on lubricated rubber: the importance of deformation losses. Proceedings of the Physical Society. 1958;71:989.

[162] Bueche A, Flom D. Surface friction and dynamic mechanical properties of polymers. Wear. 1959;2:168-82.

[163] Flom D. Rolling friction of polymeric materials. II. Thermoplastics. Journal of Applied Physics. 1961;32:1426-36.

[164] McLaren K, Tabor D. Visco-elastic properties and the friction of solids: friction of polymers: influence of speed and temperature. Nature. 1963;197:856-8.

[165] Eldredge K, Tabor D. The mechanism of rolling friction. I. The plastic range. Proceedings of the Royal Society of London A: Mathematical, Physical and Engineering Sciences: The Royal Society; 1955. p. 181-98.

[166] Tabor D. The mechanism of rolling friction. II. The elastic range. Proceedings of the Royal Society of London A: Mathematical, Physical and Engineering Sciences: The Royal Society; 1955. p. 198-220.

[167] Ludema K, Tabor D. The friction and visco-elastic properties of polymeric solids. Wear. 1966;9:329-48.

[168] Aklonis J. Mechanical properties of polymers. J Chem Educ. 1981;58:892.

[169] Oyen ML, Cook RF. Load–displacement behavior during sharp indentation of viscous–elastic–plastic materials. Journal of Materials Research. 2003;18:139-50.

[170] Gayle AJ, Cook RF. Mapping viscoelastic and plastic properties of polymers and polymer-nanotube composites using instrumented indentation. Journal of Materials Research. 2016;31:2347-60.

[171] Cheng L, Xia X, Yu W, Scriven L, Gerberich W. Flat ‐ punch indentation of viscoelastic material. Journal of Polymer Science Part B: Polymer Physics. 2000;38:10-22.

[172] Greenwood J, Tripp J. The contact of two nominally flat rough surfaces. Proceedings of the Institution of Mechanical Engineers. 1970;185:625-33.

[173] Bush A, Gibson R, Thomas T. The elastic contact of a rough surface. Wear. 1975;35:87-111.

[174] Polycarpou AA, Etsion I. Analytical approximations in modeling contacting rough surfaces. Journal of Tribology. 1999;121:234-9.

[175] Greenwood J, Williamson J. Contact of nominally flat surfaces. Proceedings of the Royal Society of London A: Mathematical, Physical and Engineering Sciences: The Royal Society; 1966. p. 300-19.

[176] Lu W, Zhang P, Liu X, Zhai W, Zhou M, Luo J, et al. Influence of surface topography on torsional fretting wear under flat-on-flat contact. Tribology International. 2017;109:367-72.

[177] Lu W, Zhang G, Liu X, Zhou L, Chen L, Jiang X. Prediction of surface topography at the end of sliding running-in wear based on areal surface parameters. Tribology Transactions. 2014;57:553-60.

[178] Oyen ML, Cook RF, Emerson JA, Moody NR. Indentation responses of time-dependent films on stiff substrates. Journal of Materials Research. 2004;19:2487-97.

[179] Wang Y, Lloyd IK. Time-dependent nanoindentation behavior of high elastic modulus dental resin composites. Journal of Materials Research. 2010;25:529-36.

[180] Ashby M, Abulawi J, Kong H. Temperature maps for frictional heating in dry sliding. Tribology Transactions. 1991;34:577-87.

[181] Oliver WC, Pharr GM. An improved technique for determining hardness and elastic modulus using load and displacement sensing indentation experiments. Journal of Materials Research. 1992;7:1564-83.

[182] Yu N, Polycarpou AA, Conry TF. Tip-radius effect in finite element modeling of sub-50 nm shallow nanoindentation. Thin Solid Films. 2004;450:295-303.

[183] Oliver WC, Pharr GM. Measurement of hardness and elastic modulus by instrumented indentation: Advances in understanding and refinements to methodology. Journal of Materials Research. 2004;19:3-20.

[184] Seltzer R, Kim JK, Mai YW. Elevated temperature nanoindentation behaviour of polyamide 6. Polymer International. 2011;60:1753-61.

[185] Ngan A, Tang B. Viscoelastic effects during unloading in depth-sensing indentation. Journal of Materials Research. 2002;17:2604-10.

[186] Yeo SM, Escobar Nunez E, Polycarpou AA. Tribological Performances of Polymer-Based Coating Materials Designed for Compressor Applications. Advances in Science and Technology: Trans Tech Publ; 2010. p. 33-42.

[187] Morris NJ, Rahmani R, Rahnejat H. A hydrodynamic flow analysis for optimal positioning of surface textures. Proceedings of the Institution of Mechanical Engineers, Part J: Journal of Engineering Tribology. 2017;231:1140-50.

[188] Marian VG, Gabriel D, Knoll G, Filippone S. Theoretical and experimental analysis of a laser textured thrust bearing. Tribology Letters. 2011;44:335.